university of groningen

University Medical Center Groningen

University of Groningen

Excited state charge separation in symmetrical alkenes

Zijlstra, Robert Wiebo Johan

IMPORTANT NOTE: You are advised to consult the publisher's version (publisher's PDF) if you wish to cite from it. Please check the document version below.

Document Version
Publisher's PDF, also known as Version of record

Publication date:
2001

Link to publication in University of Groningen/UMCG research database

Citation for published version (APA):
Zijlstra, R. W. J. (2001). *Excited state charge separation in symmetrical alkenes*. s.n.

Copyright
Other than for strictly personal use, it is not permitted to download or to forward/distribute the text or part of it without the consent of the author(s) and/or copyright holder(s), unless the work is under an open content license (like Creative Commons).

The publication may also be distributed here under the terms of Article 25fa of the Dutch Copyright Act, indicated by the “Taverne” license. More information can be found on the University of Groningen website: https://www.rug.nl/library/open-access/self-archiving-pure/taverne-amendment.

Take-down policy
If you believe that this document breaches copyright please contact us providing details, and we will remove access to the work immediately and investigate your claim.

Downloaded from the University of Groningen/UMCG research database (Pure): http://www.rug.nl/research/portal. For technical reasons the number of authors shown on this cover page is limited to 10 maximum.

Download date: 19-04-2025

Excited State Charge Separation in Symmetrical Alkenes

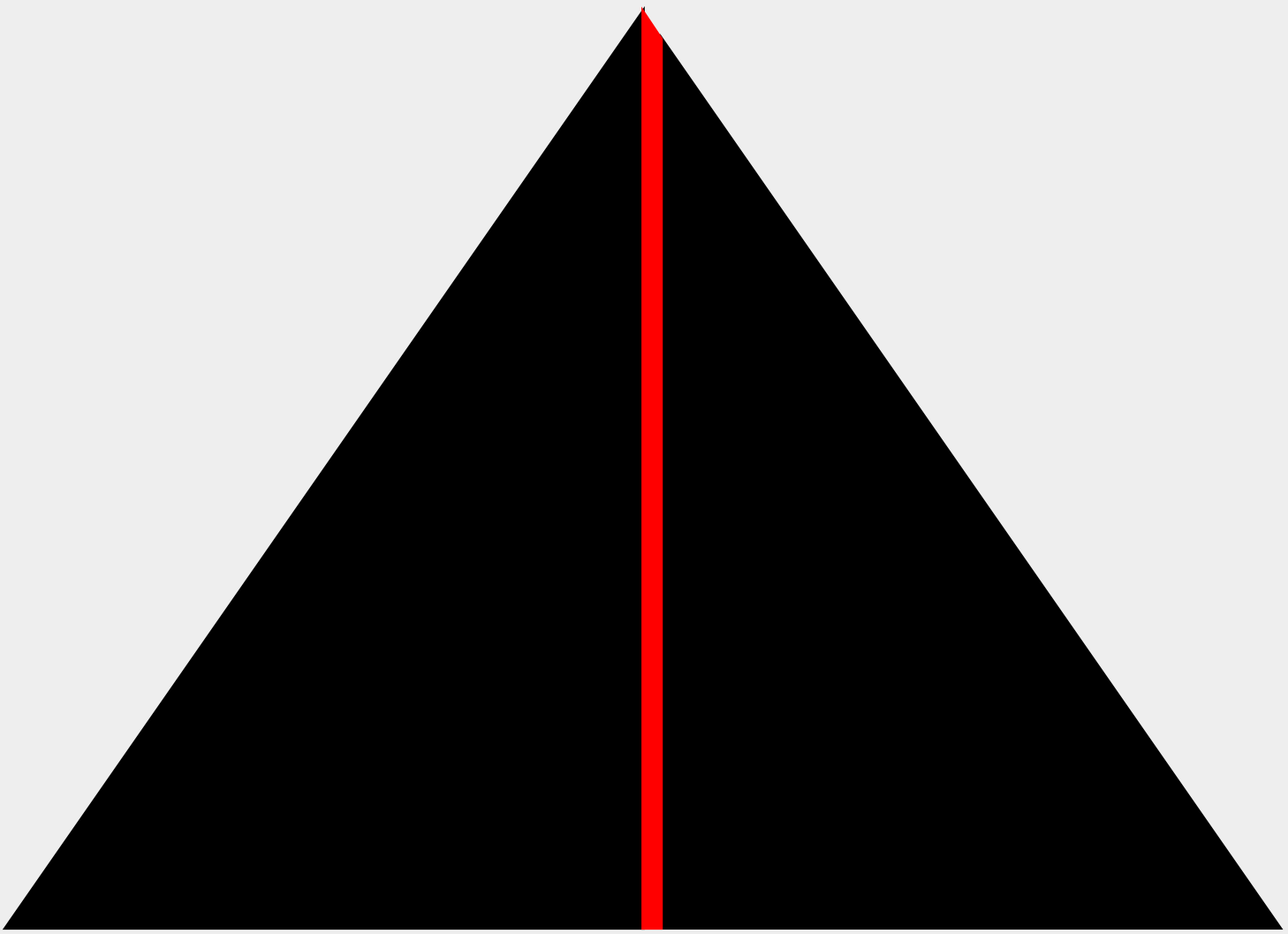

Rob Zijlstra

Front cover design is based on: *Jericho* (1967-1968) by Barnett Newman, acrylic on canvas, Centre Georges Pompidou, Paris (France).

The study described in this thesis was conducted under supervision of and in close collaboration with Dr. Piet Th. van Duijnen at the Department of Chemistry, Theoretical Chemistry (Materials Science Centre) of the University of Groningen, The Netherlands.

RIJKSUNIVERSITEIT GRONINGEN

EXCITED STATE CHARGE SEPARATION IN SYMMETRICAL ALKENES

Proefschrift

ter verkrijging van het doctoraat in de
WISKUNDE en NATUURWETENSCHAPPEN
aan de Rijksuniversiteit Groningen
op gezag van de
Rector Magnificus, dr. D.F.J. Bosscher
in het openbaar te verdedigen op
vrijdag 29 juni 2001
om 14.15 uur

door

Robert Wiebo Johan Zijlstra
geboren op 8 mei 1963
te Leeuwarden

Promotor:	Prof. Dr. B.L. Feringa
Beoordelingscommissie:	Prof. Dr. K. Duppen
	Prof. Dr. J.B.F.N. Engberts
	Prof. Dr. J.G. Snijders

Voorwoord

Ongetwijfeld tot verrassing van een enkeling (en niet in het minst mezelf) is het er dan toch van gekomen; mijn proefschrift heeft een definitieve vorm bereikt. Dit is te danken aan een aantal personen, die ik hieronder in deels hiërarchische, deels willekeurige volgorde de revue wil laten passeren.

Allereerst wil ik Piet van Duijnen bedanken voor het aan mij bieden van de gelegenheid om in zijn groep een promotieonderzoek te verrichten. Piet, je eerste woorden na mijn aanstelling waren in de trant van "En nu gaan we een quantumchemicus van je maken", waarop mijn reactie "nou, dat dacht ik niet" ongetwijfeld direct een tweeslachtig gevoel opgeroepen zal hebben... Ik heb met zeer veel genoegen met je samengewerkt en de ruimte die jij je medewerkers biedt heb ik zeer gewaardeerd. Als er al sprake is geweest van een tweeslachtige gevoel dan hoop ik dat de uitvloeisels van onze samenwerking dat naar de positieve kant hebben doen doorslaan.

Daarnaast wil ik mijn promotor Ben Feringa van harte bedanken voor het aandragen van het onderwerp van dit proefschrift en de ondersteuning die ik door de jaren heen heb mogen genieten. Ben, ondanks onze soms botsende karakters hebben we, naast het werk beschreven in dit proefschrift, een groot aantal vruchtbare samenwerkingsprojecten gehad waar ik met plezier en trots op terugkijk.

Speciale dank gaat uit naar Douwe Wiersma en Koos Duppen. Douwe, ik ben je erkentelijk voor het feit dat je mij in de gelegenheid gesteld hebt om de femtoseconde experimenten beschreven in hoofdstuk 5 en 6 in jouw groep te verrichten. Ondanks de initiëel aanwezige scepsis denk ik dat we allebei tevreden kunnen zijn met de uitkomsten van dit werk. Dat is overigens niet in de laatste plaats te danken aan Koos Duppen die mij in de 'spectro-periode' op bijzondere wijze ondersteund heeft. Koos, je deur stond altijd open om crises op de werkvloer te bespreken, en jouw ongebreidelde en soms enigszins onwelkome peptalks hebben (desondanks) hun positieve uitwerking niet gemist !

Daarnaast ben ik Koos en de andere leden van de leescommissie, Jan Engberts en Jaap Snijders, zeer erkentelijk voor de gezwinde correctie van dit proefschrift.

Ria Broer en Coen de Graaf wil ik bedanken voor het bieden van de faciliteiten en ondersteuning bij het verrichten van de Molcas berekeningen uit hoofdstuk 2. Jullie behulpzaamheid en belangstelling voor mijn onderzoek heb ik als bijzonder stimulerend ervaren. Hierbij mag ook Johan Heijnen niet onvermeld blijven; het zonder morren opkrikken van mijn diskquota als ik weer eens mijn account had volgeschreven is door mij zeer gewaardeerd. Daarnaast waren onze veelvuldige bridgediscussies een prettige afwisseling van het wetenschappelijk werk. Nu nog eens een echt systeem leren spelen ...

Het werk in hoofdstuk 3 en 4 had niet gerealiseerd kunnen worden zonder de ondersteuning van Alex de Vries, en kamergenoten Marcel Swart en Ferdinand Grozema. Alex was altijd bereid om HONDRF (en later GAMESS-UK) programmeerklusjes voor mij te verrichten. Je weet niet half hoe blij ik daarmee was ... Naast zijn bijdragen als lid van het DRF team heeft Marcel alle hand en spandiensten verricht om de e-mails uit Eindhoven om te toveren tot documenten voor de leescommissie. Marcel, bedankt! Ferdinand wil ik bijzonder bedanken voor het verrichten van de vele werkzaamheden die bijgedragen hebben aan de totstandkoming van hoofdstuk 4. Daarnaast heb ik bijzonder veel plezier beleefd aan onze samenzweringen op wetenschappelijk gebied en aan onze Snood en Barrack competities.

De pump-probe metingen van hoofdstuk 5 en 6 waren nooit tot stand gekomen zonder de bijzonder kundige ondersteuning van Thomas Steffen. Thomas, jouw revisies van de CPM laser, de hulp bij de finetuning van mijn opstelling alsmede de wetenschappelijke input bij het totstandkomen van het werk beschreven in hoofdstuk 5 en 6 zijn van onschatbare waarde geweest. Mijn dank is groot. Daarnaast wil ik Egbert Lenderink, Mirjam van Burgel, Frank Everdij, Ben Hesp en Foppe de Haan bedanken voor alle hulp die ik van hun ontvangen heb bij het verrichten van mijn dagelijkse werkzaamheden in de kelder. Tevens wil ik Annemarie Schoevaars bedanken voor de synthese van de *para*-gefunctionaliseerde TPEs waaraan ik gemeten heb (zie hoofdstuk 6). Dit heb ik zeer gewaardeerd.

Ook wil ik iedereen in den lande bedanken die mijn verblijf in Groningen tot een zeer aangename periode gemaakt hebben. In het bijzonder noem ik mijn kamergenoten Koos Bijma en Marc Veen, ondanks dat Koos twee toetsen uit het toetsenbord van mijn Mac heeft gebroken tijdens de koffie-flipperpotjes. Gelukkig was je beter in de chemie! Met Marc heb ik veel lol beleefd aan onze vele samenzweringen. Geep en Jan van Esch wil ik bedanken voor het feit dat ze nog tegen me praten ondanks dat ik ze heb blootgesteld aan een helletocht over de Noordzee en Bas Dros bedank ik met name voor de gezamenlijke en genoeglijke eerste schreden op bridgegebied.

En natuurlijk Edwin en Peter, bedankt voor de vele mooie stapavonden en voor het mij willen bijstaan op de dag des oordeels.

Bijna tot slot wil ik mijn familie en in het bijzonder Pieke bedanken voor hun ondersteuning bij het nemen van de vele hobbels in het promotietraject.

My final thoughts have to go to Swati. The main reason why this thesis has finally got there is because of your relentless efforts to persuade me to finish it. Even though I have cursed you for that on more than one occasion, I can't tell you how grateful I am for these efforts and for your presence in my life. Surrey can't come soon enough...

Rob Zijlstra Eindhoven, mei 2001.

Table of Contents

Introduction

1.1. Background and Motivation

Apart from their versatile applicabilities as synthons, alkenes, i.e. organic compounds containing a carbon-carbon double bond, exhibit special dynamic behaviour as a result of this double bond. In their ground states, most alkenes resist rotation around these bonds under ambient conditions, and cis-trans isomerizations on the ground state potential energy surface (PES) prove to be processes associated with high activation barriers. Barriers around 60 kcal.mole^{-1} for thermal cis-trans isomerizations[1] are no exception, thus giving alkenes a high degree of conformational stability at ambient temperatures.

However, upon photo-excitation of an electron from the π molecular orbital (by means of a $\pi^* \leftarrow \pi$ transition) of the alkene, this picture changes drastically. Because this excitation reduces the bond order of the olefinic bond[2], rotation around this bond becomes more facile and exhibits only small or even non-existent activation barriers. In fact, once on their photoexcited potential energy surfaces, alkenes usually quickly depart their planar geometries around the double bond to undergo large conformational changes. This is caused by the aforementioned reduction of the bond order, which allows the release of steric repulsion present between vicinal functional groups attached to the double bond at the planar ground state geometries by rotation around this bond (figure 1.1). This conformational relaxation leads to a (near-) perpendicular orientation of the vicinal groups with respect to each other (orientation of R_1,R_2 with respect to R_3,R_4 in the right structure in figure 1.1).

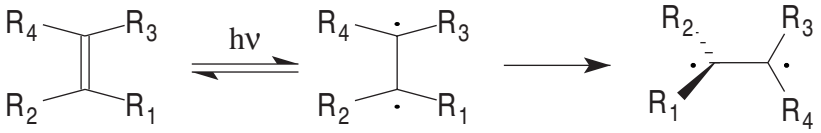

Figure 1.1 Ground state geometry (left structure), vertically excited state geometry (middle structure) and relaxed excited state geometry (right structure) of alkenes.

The excited state dynamic behaviour of alkenes is widely studied, and in particular stilbene has often been used as a model compound to investigate the dynamics of photo-induced cis–trans isomerizations[3, 4].

The bistability of alkenes, i.e. their high conformational integrity on the ground state PES combined with the facile cis-trans (and trans-cis) rearrangements on the photo-excited PES makes them excellent building blocks for the development of molecular devices[5] such as molecular data storage elements, especially when the cis and trans form of the alkene have sufficiently different absorption spectra. A beautiful example of utilizing the alkene bistability can be found in figure 1.2, in which the dynamic behaviour of (3R,3R')-1,1',2,2',3,3',4,4'-octahydro-3,3'-dimethyl-4,4'-biphenanthrylidene on both ground and photo-excited PES is depicted[6]. In this case, the combination of alkene bistability with sterically demanding functional groups and chirality has led to a molecule exhibiting mono-directional relaxation behaviour under controlled conditions.

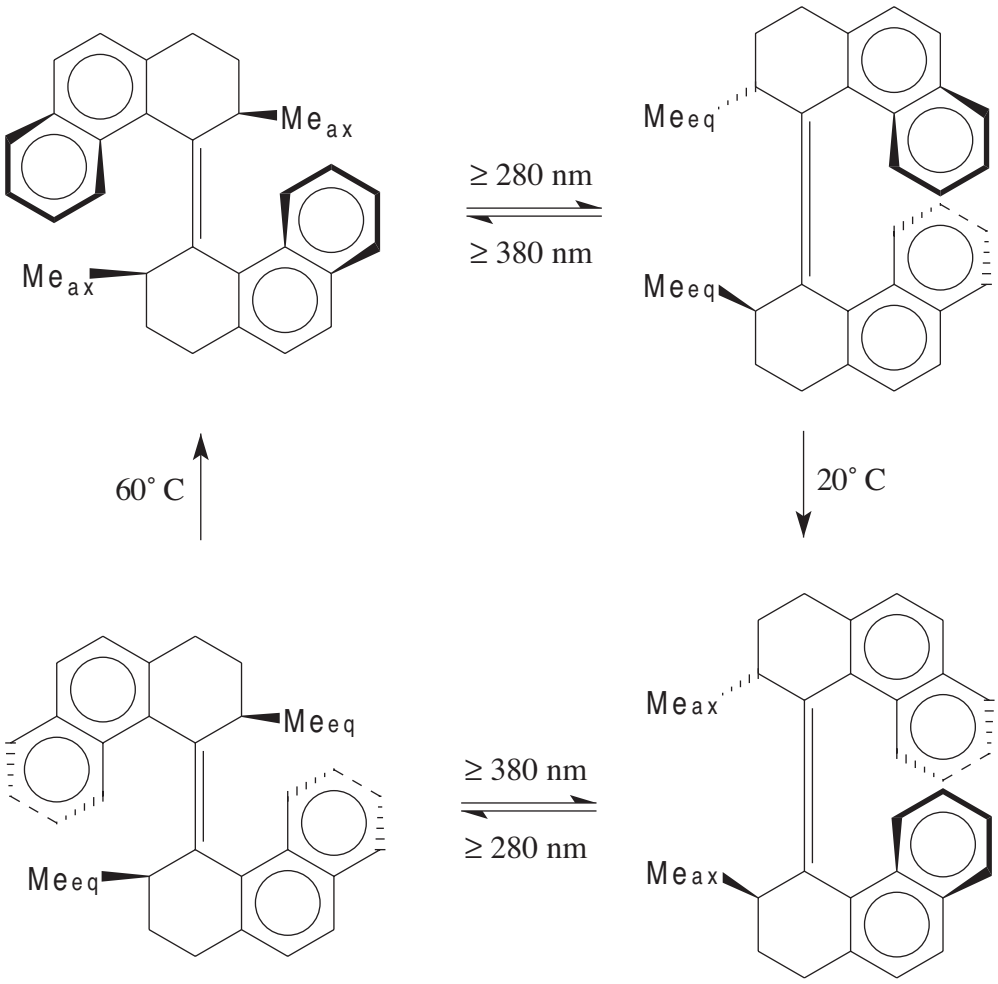

Figure 1.2 Combination of thermally induced and light-induced dynamics of (3R,3R')-1,1',2,2',3,3',4,4'-octahydro-3,3'-dimethyl-4,4'-biphenanthrylidene.

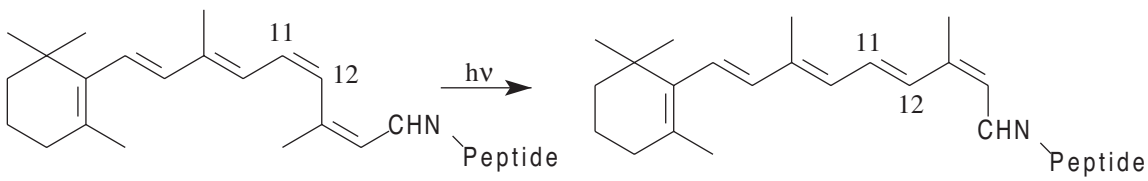

Figure 1.3 Photoinduced cis-trans isomerization of the retinal moiety in rhodopsin.

The bistability of alkenes has also found an important application in nature. By far the most famous example can be found in the process of vision in mammals. A crucial step in this process is the photoexcitation and subsequent cis-trans isomerization of the C_{11}-C_{12} bond in the retinal chromophore of the peptide rhodopsin[7-9] (figure 1.3), which is believed to trigger a series of events ultimately leading to vision.

An interesting feature of the photoinduced relaxation of alkenes is the occurrence of two near-degenerate excited state potential energy surfaces in the vicinity of the perpendicular geometry of alkenes[10-12].

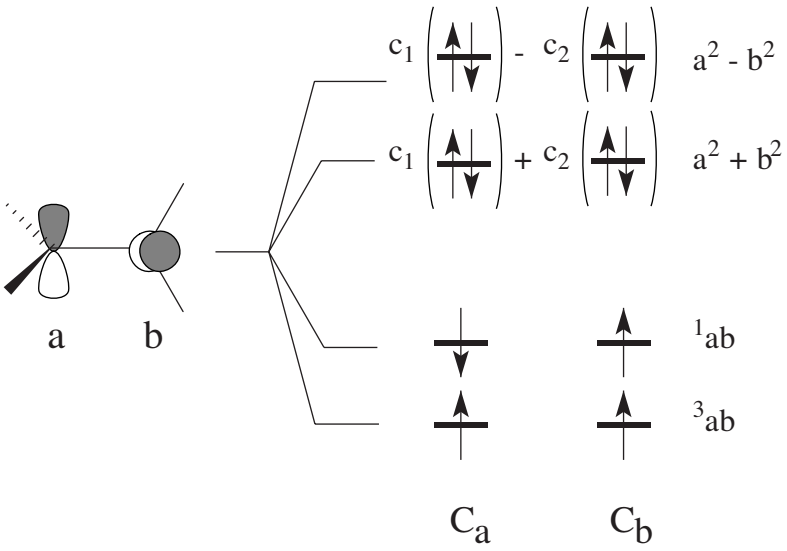

Figure 1.4 Schematic representation (in terms of p-orbital occupation) of the four lowest lying electronic states of ethylene: the lowest energy triplet biradical ("^{3}ab") state, the singlet ("^{1}ab") biradical state and the two near degenerate singlet excited states ($a^2 \pm b^2$). The two singlet excited states consist of two closed shell, ionic determinants (depicted by the doubly occupied p-orbitals) with coefficients c_1 and c_2 ($c_1=c_2$ in symmetrical alkenes).

The main reason for making this an interesting feature lies enclosed in the antisymmetric electronic nature of the two states involved[2, 13, 14]. Figure 1.4 provides an intuitive picture of the shape of the electronic states of interest at the perpendicular geometry of ethylene.

As can be seen in figure 1.4, the two near-degenerate excited states both are linear combinations of two ionic determinants ($a^2 \pm b^2$). In the case of C_2- or D_2-symmetrical alkenes like stilbene and ethylene, respectively, both ionic determinants will have equal weights in the wave function ($c_1=c_2$) due to the molecular symmetry, thus leading to electronic states with zero dipole moments. However, according to quantum theory[13, 15, 16], when these two states become degenerate, any linear combination of the two antisymmetric wave functions becomes equally acceptable. In other words, the symmetrical ($a^2 + b^2$) versus ($a^2 - b^2$) representation of figure 1.4 is as acceptable as the (a^2) versus (b^2) representation for these two respective states. Obviously, since the latter representations are purely ionic, this would provide excited states exhibiting large dipole moments even in intrinsically non-polar alkenes like ethylene, provided a symmetry-lowering perturbation of the wave function is present. This effect has been given the name 'sudden polarization', because it is predicted to occur in a confined region of the PES in the vicinity of the perpendicular geometry only[17].

Theoretical studies on the parent alkene ethylene[18, 19] have suggested that the required symmetry lowering in symmetrical alkenes can be provided by a selective deformation of one half of the alkene, thus facilitating the necessary symmetry breaking of the molecule. However, spectroscopic investigations studying the sudden polarization

behaviour of tetraphenylethylenes in the condensed phase[20-23] show that the solvent has a distinct influence on the sudden polarization behaviour as well.

It has been suggested that the sudden polarization effect also plays a major role in the (cycloaddition) reactions involving non-polar cycloalkenes[24-26], based on the obtained product ratios in these reactions. Less surprisingly, its occurrence has been reported in the photoexcited states of alkenes with intrinsically low symmetry, like push-pull polyenes[27-31]. More interestingly, it has been suggested that the effect may also play an important role in the triggering of the process of vision[32]. In addition, it is not unlikely that the excited state behaviour of chiroptical switches may be influenced by the occurrence of the sudden polarization phenomenon as well.

It must have become obvious to the interested reader that the sudden polarization effect is likely to play an important role in many photon driven processes. Therefore, the work presented in this thesis has focussed on the driving forces behind this effect. To prevent any form of bias caused by structural asymmetries (like in the case of push-pull stilbenes), the studies presented in this thesis have been limited to the investigation of the occurrence of charge separation in intrinsically non-polar D_2-symmetrical alkenes.

1.2 Outline of this Thesis

The content of this thesis is divided into a theoretical part (chapters 2-4) and an experimental part (chapters 5-6). In chapter 2, an extended description of the sudden polarization effect together with an overview of theoretical studies of this topic will be presented. As already mentioned in the previous section, these studies have led to the general assumption that the occurrence of the sudden polarization phenomenon in symmetrical alkenes is driven by an exothermic intramolecular symmetry-lowering perturbation (e.g. a selective pyramidalization of one of the olefinic carbon centers). In chapter 2, the outcome of a theoretical study investigating the correctness of this assumption will be given. In this study, the excited state PES of ethylene and tetramethylethylene at (near-)perpendicular geometries and various pyramidalization angles have been compared. It will be demonstrated that the concept of intramolecular symmetry breaking might not be as generally applicable as previously assumed.

The work reported in chapters 3 and 4 has been dedicated to investigate the possible role of the environment as the symmetry lowering element in the sudden polarization of ethylene. To model the solvent effects on the ethylenic excited states, the Direct Reaction Field (DRF) Model by Van Duijnen et al.[33-35] has been used.

In chapter 3, a general description of this model will be provided. In addition, the outcome of a preliminary study, in which the sudden polarization of the ethylene molecule in various non-symmetrical environments (i.e. a non-symmetrically polarized continuum with a number of different values of ε) has been investigated, will be presented. It will be shown that the environment is indeed capable of inducing the sudden polarization effect, but that the magnitude and stabilization of the polarizated states depends on the applied values of ε.

In chapter 4, the outcome of a DRF study in which the excited state behaviour of ethylene in various solvents has been modeled, will be presented. In this study, the

ethylene molecule has been enveloped by 50 discrete solvent molecules. The results of this study clearly suggest that only polar solvents are capable of effectively inducing and stabilizing the polar excited states, which raises the question whether the occurrence of charge separated states of symmetrical alkenes is largely solvent dependent.

Chapters 5 and 6 have been dedicated to finding an answer to this question by experiment. In chapter 5, the outcome of a study examining the excited state behaviour of tetraphenylethylene (TPE) by means of time-resolved pump-probe spectroscopy[36] will be presented, preceded by an extensive review of previous photoinduced experiments on TPE and a theoretical description of pump-probe spectroscopy. The TPE excited state behaviour has been investigated in various solvents at both femtosecond and picosecond time scales. It will be demonstrated that the TPE excited state twist dynamics are largely solvent dependent, and that the quantum yield of the sudden polarization of the TPE excited states critically depends on solvent polarity. This quantum yield is much smaller in the non-polar solvent cyclohexane than in a number of alcohols, thus providing a positive answer to the question posed on the basis of the results presented in chapter 4.

Finally, in chapter 6 the results of an extended pump-probe study will be presented. In this work, the excited state behaviour of several *p*-substituted TPEs in cyclohexane and ethanol has been investigated to establish the influence of electron directing functional groups on the sudden polarization effect and molecular dynamics of *p*-substituted-TPEs. It will be shown that large effects can be observed, although a clearcut correlation between the electron directing nature of the *p*-substituents and the sudden polarization effect could not be made.

1.3 References

1. S.H. Pine, *Organic Chemistry*, McGraw-Hill Book Company, New York, 1987.
2. R.S. Mulliken, Phys. Rev., **41**, 751-758 (1932).
3. D.H. Waldeck, Chem. Rev., **91**, 415-436 (1991).
4. R.A. McGill, J.K. Rice, A.P. Baranovski, J.C. Owrutsky, A.H. Lowrey, K.K. Stavrev, T. Tamm and M.C. Zerner, Int. J. Quant. Chem. Symp., **30**, 383-394 (1996).
5. B.L. Feringa, R.A. van Delden, N. Koumura and E.M. Geertsema, Chem. Rev., **100**, 1789-1816 (2000).
6. N. Koumura, R.W.J. Zijlstra, R.A. van Delden, N. Harada and B.L. Feringa, Nature, **401**, 152-154 (1999).
7. G. Wald, Science, **162**, 230-239 (1968).
8. Q. Wang, R.W. Schoenlein, L.A. Peteanu, R.A. Mathies and C.V. Shank, Science, **266**, 422-424 (1994).
9. K.C. Hasson, F. Gai and P.A. Anfinrud, Proc. Natl. Acad. Sci. U.S.A., **93**, 15124-15129 (1996).
10. G. Orlandi, P. Palmieri and G. Poggi, J. Am. Chem. Soc., **101**, 3492-3497 (1979).
11. C.M. Meerman-van Benthem, H.J.C. Jacobs and J.J.C. Mulder, Nouv. J. Chim., **2**, 123-127 (1977).
12. M. Merchán and R. González-Luque, J. Chem. Phys., **106**, 1112-1122 (1997).
13. V. Bonacic-Koutecky, J. Cizek, D. Döhnert and J. Koutecky, J. Chem. Phys., **69**, 1169-1176 (1978).
14. M. Persico, J. Am. Chem. Soc., **102**, 7839-7845 (1980).
15. C.E. Wulfman and S. Kumei, Science, **172**, 1061 (1971).
16. A. Szabo and N.S. Ostlund, *Modern Quantum Chemistry*, Macmillan Publishing Co. Inc., New York, 1982.
17. V. Bonacic-Koutecky, P. Bruckmann, P. Hiberty, J. Koutecky, C. Leforestier and L. Salem, Angew. Chem., Int. Ed. Engl., **14**, 575-576 (1975).
18. B.R. Brooks and H.F Schaefer III, J. Am. Chem. Soc., **101**, 307-311 (1979).
19. R.J. Buenker, V. Bonacic-Koutecky and L. Pogliani, J. Chem. Phys., **73**, 1836-1849 (1980).
20. P.F. Barbara, S.D. Rand and P.M. Rentzepis, J. Am. Chem. Soc., **103**, 2156-2162 (1981).
21. J. Ma and M.B. Zimmt, J. Am. Chem. Soc., **114**, 9723-9724 (1992).
22. W. Schuddeboom, S.A. Jonker, J.M. Warman, M.P. de Haas, M.J.W. Vermeulen, W.F. Jager, B. de Lange, B.L. Feringa and R.W. Fessenden, J. Am. Chem. Soc., **115**, 3286-3290 (1993).
23. E. Lenderink, K. Duppen and D.A. Wiersma, J. Phys. Chem., **99**, 8972-8977 (1995).
24. J.A. Marshall, Science, **170**, 137-141 (1970).
25. W.G. Dauben and J.S. Ritscher, J. Am. Chem. Soc., **92**, 2925-2926 (1970).
26. T. Tezuka, O. Kikuchi, K.N. Houk, M.N. Paddon-Row, C.M. Santiago, N.G. Rondan, J.C. Williams Jr. and R.W. Gandour, J. Am. Chem. Soc., **103**, 1367-1371 (1981).

27. E. Gilabert, R. Lapouyade and C. Rullière, Chem. Phys. Lett., **145**, 262-268 (1988).
28. H. Ephardt and P. Fromherz, J. Phys. Chem., **93**, 7717-7725 (1989).
29. I.D.L. Albert and S. Ramasesha, J. Phys. Chem., **94**, 6540-6543 (1990).
30. E. Gilabert, R. Lapouyade and C. Rullière, Chem. Phys. Lett., **185**, 82-87 (1991).
31. R. Lapouyade, K. Cheschka, W. Majenz, W. Rettig, E. Gilabert and C. Rullière, J. Phys. Chem., **96**, 9643-9650 (1992).
32. L. Salem, Acc. Chem. Res., **12**, 87-92 (1979).
33. P. Th. van Duijnen, A.H. Juffer and H.P. Dijkman, J. Mol. Struct. (THEOCHEM), **260**, 195-205 (1992).
34. P. Th. van Duijnen and A.H. de Vries, Int. J. Quant. Chem., **60**, 1111-1132 (1996).
35. A.H. de Vries, *Modelling Condensed-Phase Systems*, Ph.D. thesis, University of Groningen, 1995.
36. Y.J. Yan, L.E. Fried and S. Mukamel, J. Phys. Chem., **93**, 8149-8162 (1989).

Theoretical Descriptions of the Sudden Polarization Effect:

The Intramolecular Driving Force Revisited

2.1 Introduction

As early as 1932, Robert Mulliken published a theoretical description of the quantum chemistry of the double bond[1], in which he described ground and excited states of planar and perpendicular ethylene ($R_{1\text{-}4}$ = H, see figure 2.1) in terms of point group symmetry.

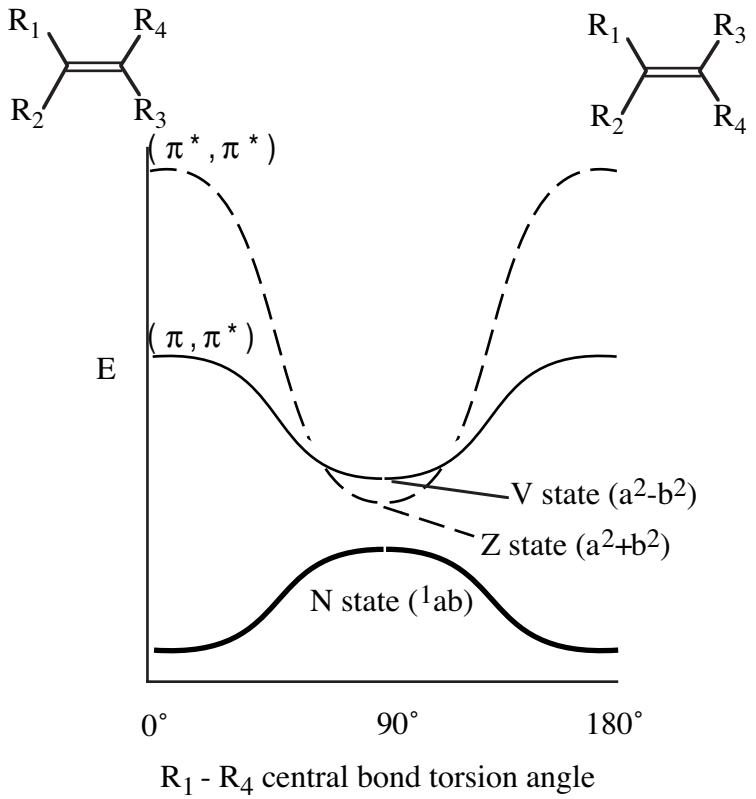

Figure 2.1 Schematic representation of the vacuum potential energy surfaces of the electronic singlet states of interest in (symmetrical) ethylenes.

He predicted the relaxed nuclear geometry of the π,π* state to be (near)-perpendicular, which has distinctive implications for the existing electronic states at this geometry (figure 2.1).

At the perpendicular geometry, the overlap between the two p orbitals at carbon centers a and b is (close to) zero, and as a result the exchange interaction between the electrons occupying these orbitals is small. At this geometry, these two atomic orbitals, which have maximum overlap at planar geometries leading to the formation of the 'closed shell' π molecular orbital, can have occupation numbers between 0 and 2 (with the obvious restriction that the sum of both occupation numbers should be exactly 2).

Mulliken demonstrated that for the perpendicular geometry 4 low lying electronic states exist; a singlet and triplet biradical (^{1}ab (N) and ^{3}ab (B)), being nearly degenerate in energy in which p_x(a) and p_y(b) are singly occupied. Due to the fact that the overlap integral S_{ab} is zero at the perpendicular geometry and the difference in energy between the two states is solely governed by the exchange integral K_{ab}, the ^{3}ab state is predicted to be the slightly more stable state (by an amount of $2K_{ab}$), as dictated by Hund's rule. The other two states were estimated to lie approximately 1 eV higher in energy, 'originating

from the CH_2^+ and CH_2^- fragments'. These can be written as $p_x(a)^2$ and $p_y(b)^2$ and can be interpreted as zwitterionic states.

Due to the fact that in a non-perturbed (i.e. D_2-symmetrical) wave function both zwitterionic solutions are equally acceptable, the correct representation of these upper two states are the symmetrized linear combinations of the two states (equation 2.1):

$$\Psi \sim p_x(a)^2 \pm p_y(b)^2 \qquad \textbf{(2.1)}$$

These states are commonly referred to as the Z and V states; with coefficients $c_1 = c_2 = {}^1/_2\sqrt{2}$. It is tempting to use the term biradical(oid) in order to label the wave functions described by equation 2.1 in situations where $c_1 \approx c_2$, when the wave function basically consists of a linear combination of the two localized (ionic) closed shell determinants a^2 and b^2 rather than of two unpaired electrons. It should be clear, however, that the term 'biradical' is applicable to the ^{1}ab (N) and ^{3}ab (B) states rather than the states described by equation 2.1, since the term biradical is usually associated with electronic states in which two unpaired, weakly interacting electrons are present[2].
A more appropriate nomenclature of these states based on their behaviour is suggested in chapter 5, where the outcome of an experimental study on the photo-induced excited state dynamics of tetraphenylethylene (TPE) is discussed.

The direct consequence of the excited state behaviour as a result of the shape of the wave functions in equation 2.1 stayed unrecognized until the early seventies. In 1970, Marshall reported remarkable and unexpected polar behaviour in the excited states of several cyclohexenes and cycloheptenes[3], molecules exhibiting only a very small dipole moment in their ground state geometries. Wulfman et al. explained this by suggesting that under a perturbation of, for instance, the electric field of a nearby ion c_1 and c_2 can become unequal[4, 5]. In their words, a catastrophic polarization of the near-perpendicular excited states could occur. The occurrence of a 'catastrophic' polarization results in wave function representations for the two excited states for which the two electrons become localized at one half of the molecule, thus forming zwitterionic (or polar) states, which was presented as a possible explanation for the observed excited state polarity by Marshall.

This dramatic polarizability of the excited state has been shown to depend critically on the amount of twisting of the central bond[6-12]. It was demonstrated that this behaviour only exists in (close) vicinity of the perpendicular geometries, since the necessary degeneracy between the Z and V states only exists in this region (figure 2.1). The fact that this behaviour only occurs in a confined region of the excited state potential energy surface (PES) is the main reason why it is often referred to as 'sudden polarization', as suggested by Bonacic-Koutecky[6].

2.2 Theoretical Description of Relevant Methods

In this section, an overview will be given of the computational models for the work presented in this chapter and for studying the sudden polarization effect in general. More extensive descriptions can be found in the documents referred to and references therein.

The calculation of electronic properties of molecular systems are usually based on quantumchemical descriptions of some sort. In such approaches the aim is to find an approximate solution of the Schrödinger equation for the N electrons in the system[13, 14]. This can be done in several ways, but usually the N-electron wave function is expanded in anti-symmetrized products Φ_k of the one-electron functions φ_i (eq. 2.2 and 2.3),

$$\Psi = \sum_k C_k \Phi_k \qquad \textbf{(2.2)}$$

$$\Phi_k = \hat{O}^a (\varphi_p(1)\, \varphi_q(2) .... \ \varphi_s(N)) \qquad \textbf{(2.3)}$$

with Φ_k usually referred to as Slater determinants. A linear combination of Slater determinants that fulfils spin and spatial symmetry constraints is usually referred to as a configuration state function (CSF). The exact solution of the problem is given by the complete (i.e. infinite) expansion of all Slater determinants that can be generated from the one-electron space. Since this solution is unachievable for obvious reasons, approximate solutions to the N-electron problem have to be found.

The simplest and most frequently used approach to approximately solve such an N-electron problem is the Hartree-Fock (HF) or Self Consistent Field (SCF) method; a method aimed to find the orbital solution with the lowest accompanying energy.

In this method the N-electron space is limited to just one Slater determinant, in which case equation 2.2 simplifies to:

$$\Psi = C_0 \Phi^{HF} \qquad \textbf{(2.4)}$$

In HF methods, the electron-electron repulsion is treated in a mean-field way. In many cases, like in the case of organic molecules in their electronic ground state configurations the HF approximation is very reasonable. However, if one is for instance interested in the description of excited states or in calculating the expectation value of an energy with high accuracy, correlated wave functions, in which the various electron-electron repulsions (the so-called electron correlation effects) are explicitly taken into consideration, are required.

In cases where the HF wave function is already a reasonable estimate, an accurate description of the wave function can usually be obtained by employing Configuration Interaction (CI) calculations. An important feature of a CI calculation is that it leaves the reference one-electron functions (orbitals) unchanged, which is why the HF reference wave function needs to be of reasonable quality. Usually, the inclusion of single and double excitations from the reference wave function leads to the retrieval of a large part of the electron correlation effects. This method is known as the Configuration Interaction Singles Doubles (CISD) method:

$$\Psi^{CISD} = C_0 \Phi^{HF} + \sum_{i,\,a} C_i^a \Phi_i^a + \sum_{ij,\,ab} C_{ij}^{ab} \Phi_{ij}^{ab} \qquad \textbf{(2.5)}$$

in which the first sum depicts all configurations generated by single excitations from the HF reference wave function and the second sum depicts all configurations originating

from double excitations. However, in cases where the HF reference provides a qualitatively poor description of the actual wave function, the CISD approach will not yield reliable results and more appropriate methods are needed to accurately describe the wave function.

A better description can be obtained by using the Multiconfigurational SCF (MCSCF) method. This method also includes all nearly degenerate configurations in the reference wave function:

$$\Psi = C_1 \Phi_1 + C_2 \Phi_2 + ... \quad C_i \Phi_i + ... \quad C_m \Phi_m \qquad \textbf{(2.6)}$$

In a MCSCF calculation, the one-electron orbitals are optimized in a SCF type step, thus improving the quality of the reference wave function as well. In such calculations, Ψ can be optimized for a single state, or for a mixture of states. The latter application is commonly reffered to as a state averaged calculation.

An MCSCF wave function can be used as a reference in CI calculations that are capable of including a plurality of reference wave functions. This is particularly useful in cases where the HF method gives a poor description of the N-electron wave function, in which case the CISD method is not the most appropriate method for including electron correlation effects.

Such Multi Reference CI (MRCI) wave functions can be written as an ordering of the external configurations by their number of external electrons:

$$\Psi^{MRCI} = \sum_{m} C_m \Phi_m + \sum_{m,\,a} C_m^a \Phi_m^a + \sum_{m,\,ab} C_m^{ab} \Phi_m^{ab} \qquad \textbf{(2.7)}$$

with m indexing over all configurations in the reference wave function in both equations 2.6 and 2.7. Such CI expansions can yield excellent results, but are quite time consuming, especially if no CSF selection algorithms are applied.

A popular setup of MCSCF wave functions is the so-called Complete Active Space SCF (CASSCF) formalism[15, 16]. In the theoretical summary presented below, the following labels will be used:

- a, b, c,... for secondary (virtual) orbitals
- i, j, k,... for inactive orbitals
- p, q, r and s for general orbitals
- t, u, v,... for active orbitals

The active orbitals are the orbitals which are included in the CAS expansion. Inactive orbitals are the *occupied* orbitals which are excluded from this expansion, whereas secondary (or virtual) orbitals are the *unoccupied* orbitals that are excluded from the CAS. Finally, general orbitals can either be occupied or unoccupied, and can either be active or inactive/secondary orbitals. Within the CASSCF formalism, the orbital space is divided into three subsets:

- the inactive space (i.e. the complete set of inactive orbitals)
- the secondary (or virtual) space (i.e. the complete set of secondary orbitals)

- the active space (i.e. the complete set of active orbitals)

Orbitals in the inactive space stay doubly occupied in all configurations whereas orbitals in the secondary space remain unoccupied. The electrons occupying orbitals in the active space are distributed in all spin and symmetry allowed ways.
In fact, a complete CI is being performed over the active space. This has the additional advantage that, as a result of the completeness of the wave function, orbital rotations (i.e transformations to restore orthogonality) among active orbitals are redundant and can be ignored. This is one of the main reasons why CASSCF wave functions usually converge rapidly.

In CASSCF calculations, the core orbitals are orbitals that typically occupy the inactive space, because they usually have a negligable influence on the correlation energy. It should be emphasized that the CASSCF method is not constructed to provide a good estimate of the electron correlation effects, but to provide an excellent starting point to obtain such estimates with other methods.

A more flexible setup of MCSCF wave functions can be achieved with the Restricted Active Space SCF (RASSCF) approach[17]. This approach embodies five active spaces called RAS1, RAS2 and RAS3 together with an inactive and an external space. The latter two are similar to the inactive and the secondary space in a CAS type description. In the RAS1 space a fixed number of holes is allowed (i.e. the number of electrons allowed to be excited from the RAS1 to either the RAS2 or RAS3) whereas in the RAS3 a fixed number of added electrons (i.e. electrons excited into the RAS3 from either the RAS1 or RAS2) is allowed. Again, in the RAS2 a complete CI expansion is formed. The main advantage of a RASSCF is that it is able to tackle larger systems. Therefore, when practical restrictions prohibit the inclusion of the full orbital set in the active space, it usually provides a better estimate of the electron correlation than a CASSCF approach. However, due to the fact that the wave function is no longer complete in just one active space, the active - active orbital rotations between the three active spaces now have to be included in the method to eliminate the nonorthogonality between the RAS spaces, which was introduced by the orbital optimization steps. As a result, RASSCF type wave functions usually converge much more slowly than CASSCF wave functions due to this inclusion, making RASSCF calculations less accessible.

A way of obtaining an estimate of the correlation energy in a nonvariational manner is by applying Møller-Plessett (MP) perturbation theory[18] on a reference wave function. This theory states that in the case of a dominating RHF wave function, a division of the Hamiltionian can be made:

$$\hat{H} = \hat{H}^{(0)} + \hat{H}^{(1)} \qquad \textbf{(2.8)}$$

In this expression, the zeroth order Hamiltionian is defined as the sum over the one-electron Fock operators:

$$\hat{H}^{(0)} = \sum_{I}^{N} \hat{F}(I) \ , \qquad \hat{F}(I)\ \varphi_i(I) = \varepsilon_i \varphi_i(I) \tag{2.9a}$$

$$\hat{H}^{(0)}\Phi_{HF} = E^{(0)}\Phi_{HF},\ \langle \Phi_{HF} | \hat{H} | \Phi_{HF} \rangle = E^{(0)} + E^{(1)} \tag{2.9b}$$

where I runs over all electrons. In 2.9b, the zeroth order energy is the sum over all occupied orbital energies ε_i, whereas the first order energy is equal to the HF energy.

The application of second order perturbation theory (MP2) provides an estimation of the correlation energy and first order wave function in the following manner:

$$E^{(2)} = -\sum_{i<j} \sum_{a<b} \frac{\left[\langle \varphi_i \varphi_j | \hat{H}^{(1)} | \varphi_a \varphi_b \rangle \right]^2}{\varepsilon_a + \varepsilon_b - \varepsilon_i - \varepsilon_j} \tag{2.10}$$

$$\Psi^{(1)} = \sum_{i<j} \sum_{a<b} C_{ij}^{ab\,(1)} |\Phi_{ij}^{ab}\rangle \text{ with } C_{ij}^{ab\,(1)} = \frac{\langle \varphi_i \varphi_j | \hat{H}^{(1)} | \varphi_a \varphi_b \rangle}{\varepsilon_a + \varepsilon_b - \varepsilon_i - \varepsilon_j} \tag{2.11}$$

The necessary parts of equations 2.10 and 2.11 can be easily obtained from the preceding RHF reference wave function, which makes MP2 an accessible and straightforward method to obtain an estimate of the electron correlation effects. Extending this theory to multiconfigurational wave functions is not possible, because the partitioning of the Hamiltonian (equation 2.8) cannot be made.

To allow the application of perturbation theory to MCSCF wave functions, other methods have to be used. One such method has been developed by Roos and Andersson. The second-order Complete Active Space Perturbation Theory (CASPT2)[19, 20] requires a CASSCF wave function as reference. From this reference it calculates the remaining electron correlation energy and the first-order estimate of the wave function. In this theory, $\hat{H}^{(0)}$ is a sum of Fock-type one-elctron operators which reduces to the MP operator when a single configuration reference is being used;

$$\hat{H}^{(0)} = \sum_{pq} f_{pq} \hat{E}_{pq} \qquad \text{with } f_{pq} = -\left\langle 0 \left| \left[\left[\hat{H}, a_q^{\dagger} \right], a_p \right]_+ \right| 0 \right\rangle \tag{2.12}$$

where $|0\rangle$ is the CASSCF reference function and $\hat{E}_{pq}$ an excitation operator defined as the product of a creation operator $a_q^{\dagger}$ and an annihilation operator a_p.

The first-order wave function $|\Psi^{(1)}\rangle$ can be constructed in a similar fashion as in the Internally Contracted MRCI (ICMRCI) method[21]. It can be expressed as an internally contracted expansion of all configurations connected to single and double excitations from the CASSCF reference wave function:

$$\left| \Psi^{(1)} \right\rangle = \sum_{pqrs} C_{pqrs} \hat{E}_{pq} \hat{E}_{rs} |0\rangle \tag{2.13}$$

The CASPT2 extension to a CASSCF calculation generally provides a very good estimate of electron correlation effects.

A possible breakdown of perturbation theory based on Fock-type operators can occur if states with a similar expectation value of $\hat{H}^{(0)}$ as the reference wave function exist (so-called intruder states). In these cases, energy differences between the states are near zero which will lead to very small energy denominators in the expressions for $E^{(2)}$ and $C^{(1)}$, leading to the aforementioned breakdown. The best way to avoid this behaviour is to include the near-degenerate states in the reference wave function. However, in cases where this reference is already very large, such inclusions might become unfeasible and other techniques have to be considered. A possible solution can be found in applying level shifting techniques[22]. The use of such techniques has not been required in this thesis and will therefore not be described here.

2.3 Theoretical Investigations on the Sudden Polarization Behaviour of (*D2*-Symmetrical) Ethylenes: History and Approach

The dramatic implication of the near degeneracy of the Z and V states, the polarization catastrophe as suggested by Wulfman and Kumei[4], has initiated a large number of studies concerning the electronic behaviour of the photo-excited states in a wide variety of olefinic compounds in the vicinity of their perpendicular geometry[8, 10, 23-28].

In the first place, since photo-induced alkene isomerization by excitation of one or more double bonds plays an important part in both naturally occurring[29, 30] as well as synthesized compounds[31], several model systems have been investigated to determine the *generality* of the sudden polarization effect in alkenes.

Another motivation has been the determination of the *driving force* behind the occurrence of the polarized, zwitterionic states in these systems. As already mentioned in the opening paragraph, a symmetry lowering perturbation of the wave function is necessary to break the (near-) degeneracy of the two states involved in order to shift their representation towards a zwitterionic form[6, 10, 23].

An important complication of the theoretical description, or at least the interpretation of the theoretical studies dealing with the sudden polarization behaviour is the fact that the Born-Oppenheimer approximation is no longer valid in the vicinity of the crossing between the two potential energy surfaces as the electronic behaviour of these states will be governed by the nuclear motions[32-34]. This leads to an avoided crossing between the two states where the strength of the perturbation will determine the transition probability between the two surfaces[35].

When investigating the literature on the topic of sudden polarization in symmetrical ethylenes, it turns out that only a few studies deal with the theoretical description of this phenomenon[10, 23, 24, 27, 36-38], and most of these studies have been performed on the parent alkene ethylene, in which case the symmetry breaking by means of an internal pyramidalization of one of the CH_2 centers is believed to be the driving force behind the occurrence of large excited state dipole moments. The influence of

substituents on the pyramidalization process has hardly been studied, and in the few reported cases, like the work of Bonacic-Koutecky et al. on propylene[24] the methyl group containing carbon has been excluded from the pyramidalization process.

There are two main reasons for this fact. First of all, the use of computationally challenging correlated wave functions is necessary to properly describe the (near-) degeneracy of the Z and V states of ethylenes. In addition, a sometimes ignored bottleneck in such calculations is the (lack of) molecular symmetry in the excited states of interest. Although the ethylenic nuclear framework in the near perpendicular region of interest still exhibits C_{2h} or even D_{2d} symmetry at the perpendicular geometry, the excited states of interest do not fit into this point group for the following reason.

In D_2 symmetry, the plane of symmetry perpendicular to the C-C bond conflicts with the symmetry broken zwitterionic determinants a^2 and b^2 which form the Z and V states (figure 2.4). This can be understood in the following manner. In C_1 symmetry, the charge symmetrical representations of the excited states of interest can be formed by a linear combination of the two zwitterionic determinants a^2 and b^2. For a^2, the inner shell electrons will polarize towards the opposite carbon atom as a result of the localization of the two outer shell electrons on the first carbon center, thus causing additional relaxation in the charge distribution of this particular determinant. Obviously, the same holds for the b^2 determinant. In higher symmetry like D_2 symmetry, the $a^2 \pm b^2$ states each have to be formed within a symmetrical subset of orbitals. As a result, the aforementioned (low-symmetrical) inner shell relaxation effects cannot be reproduced (unless extensive orbital expansions are included in the active space), which leads to a severe overestimation of the energy of these states.

A description and a prime example of this effect are given in the pioneering work by Broer[39], who showed that the correct description of the core excitations in N_2 is extremely difficult when using truncated active spaces in combination with the full $D_{\infty h}$ symmetry of the molecule. In fact, a non-orthogonal configuration interaction (NOCI) calculation[39] on the two symmetry broken localized excitations from N_a and N_b had to be performed to approximate the experimental excitation energy.

In practice, this means that, in the case of ethylene, only a C_2 symmetry, using the C-C bond as rotation axis, or a C_s symmetrical representation, using the mirror plane coinciding with the C-C bond, is acceptable since this is the highest symmetry representation including the inner shell relaxation effects without having to extend the active space. For now, it should be reminded that the restrictions on the imposable symmetry imply a rapid increase in the dimensions of the wave function with increasing molecular size, thus limiting the application of 'sophisticated' computational methods to modestly sized molecules.

The second fundamental problem arising from the desire to describe such heavily interacting potential energy surfaces (apart from the breakdown of the Born-Oppenheimer approximation) is that the choice of the configurational active spaces (i.e. the number of electrons and orbitals to be included in the computation) should be highly balanced to prevent unphysical polarization in the ethylenic excited states of interest. If one of the two halves of the molecule contributes more virtuals (i.e unoccupied orbitals) to the active space in the calculation, the zwitterionic determinant at this half can become 'more correlated' than on the other half, where a smaller number of active space orbitals are present. Even a small inbalance can already lead to heavily polarized excited states in

regions where the Z and V potential energy surfaces are near degenerate. Especially MCSCF wave functions suffer from this problem[10, 14] due to the fact that the orbital optimization step in MCSCF calculations tends to disturb the delicate balance between the two molecule halves involved (*vide infra*).

In addition, variations in the size of perfectly balanced active spaces as well as basis set quality can have a distinct effect on the excited state behaviour on symmetry breaking. The latter effect is of course not unexpected, since this excited state electronic behaviour can be explained in terms of polarizability, and basis set quality as well as the size of the expansion (or better: active space) of a correlated wave function have a marked effect on this property.

However, the aforementioned difficulties in describing the sudden polarization effect in physically correct way can best be tackled by the use of CI wave functions. Paradoxically, the main reason for the strength of the CI method is caused by one of its restrictions: the quality and applicability of a CI wave function mainly depends on the quality of its reference wave functions.

This is caused by the fact that the CI method is solely based on the 'input orbitals' of the reference wave function. As a result, a complete symmetrical wave function will guarantee symmetrical Z and V states for the obvious reason that 'polar' configuration state functions on either side of the double bond will contribute with equal weights to the optimized CI wave function ensuring the physically correct unpolarized excited states in vacuo. This straightforward advantage is the main reason why the bulk of the computational work on the topic of ethylenic excited states sofar has been on the basis of CI wave functions.

Several theoretical studies using CI techniques to study the sudden polarization effect in ethylene in the vicinity of the crossing of the Z and V potential energy surfaces (PES) have been presented[9, 10, 12, 23]. For a couple of them, their outcomes and conclusions have been accepted as an accurate or even a general description of the driving forces behind the sudden polarization phenomenon in symmetrical alkenes[10, 23]. Both these studies have focussed on a combination of twisting along the central bond and selective pyramidalization of one of the two CH_2 centers.The first report described a CISD study by Brooks and Schaeffer[III] in 1979[10], who used the orbitals of the ^1ab N state in the standard Dunning Huzinaga (DZV) basis as reference. These orbitals were generated in a constrained SCF procedure in which the weights of the a^2 and b^2 configurations were forced to be equal even for C_s geometries. It was shown that upon selective (i.e. one-sided) pyramidalization, the $a^2 + b^2$ state (i.e. the Z state) became more stable in comparison with its unpyramidalized nuclear configuration. Also, upon progressive pyramidalization, it exhibited an increasing dipole moment, with the two unpaired electrons effectively located on the pyramidalized carbon center. This dipole moment (along the C-C bond; μ_z) reached a maximum value of 3.3 D. On the other hand, the V state was increasingly destabilized on progressive pyramidalization with a maximum μ_z of similar magnitude but of opposite sign, indicating that the two elecrons reside on the unpyramidalized carbon center in this state. Furthermore, when using truncated CI spaces (i.e. a CI expansion allowing only the two biradical electrons to excite into the virtual space of the twisted ethylene) the calculated dipole moments are much larger than in the case of the all valence CISD, showing the need for a balanced CISD expansion, in which other configurations than the a^2, b^2 states apparently play an unusually important role. It

was suggested that internal symmetry breaking is indeed the driving force in the sudden polarization of ethylenes. The amount of polarization was suggested to be correlated with the coupling matrix in equation 2.14 in a qualitative fashion, with E_a and E_b the energies of the two ionic forms of ϕ_a and ϕ_b and H_{ab} representing the exchange and overlap terms betweem them.

$$H = \begin{pmatrix} E_a - E & H_{ab} \\ H_{ab} & E_b - E \end{pmatrix} \qquad \textbf{(2.14)}$$

Especially in the vicinity of the 90˚ (perpendicular) twist angles, H_{ab} merely consists of the small exchange term K_{ab}, and excessive mixing can take place as a result of only small perturbations of the symmetrical wave function.

This qualitative description has been refined in a more elaborate study by Buenker, Bonacic-Koutecky and Pogliani[23], in which the simultaneous torsion and pyramidalization of ethylene was studied by means of multi reference CI techniques using configuration selection. Even though the findings were roughly the same as those of Brooks et al. some additions were made to the mechanistical picture. First of all, it was observed that the amount of polarization of the Z and V states depended critically on the choice of reference orbitals. Even though no experimental values were present, which prohibited verification of the computational findings, it was suggested that the use of the MO's of the ^{3}ab state as reference gave the most reliable results.

It was suggested that the minimum energy configuration for the S_1 state was found at the very large pyramidalization angle of 60˚. Furthermore, the maximum polarization was found around 82˚ rather than around the perpendicular geometry. This was quantitatively explained as follows: the amount of polarization depends on the coupling matrix as described in equation 2.14. With respect to the two coefficients in equation 2.1, which ratio describes the amount of mixing of the localized determinants, this can be combined in the following way according to first-order perturbation theory:

$$\left| \frac{c_1}{c_2} \right| \approx \left| \frac{H_{12}}{\Delta E} \right| \qquad \textbf{(2.15)}$$

Therefore, at the 82˚ geometry, where the Z and V state become degenerate, large fluctuations in polarization can occur as a result of minor changes in the off-diagonal matrix element H_{12} only. At the perpendicular geometry, ΔE is large with respect to H_{12}, and polarization effects become less pronounced as a result of that. Even though the results and conclusions in the above described papers are both significant and highly valuable, some puzzling questions remain. Let's for instance take a look at figure 2.2.

It demonstrates the effect of pyramidalization on the internuclear distance of the functional groups attached to the carbon. Obviously, increasing pyramidalization leads to a decreasing internuclear distance between the groups attached to the pyramidalized carbon centre, and figure 2.2 clearly shows that this distance becomes increasingly smaller for larger (or bulkier) groups. This is of course a simplified picture, because the C-R bond lengths will be somewhat longer than that of a C-H bond, thus (partially) counteracting this effect on internuclear distance. However, it does raise the question whether

pyramidalization will always lead to more stable, zwitterionic forms of the ethylenic excited states at near-perpendicular geometries in systems, regardless of the size of the functional groups are attached to the pyramidalized carbon centre.

In practice, some larger alkenes have been studied experimentally and some intriguing results have been obtained. For instance, spectroscopical investigations on tetraphenylethylene (TPE) in the condensed phase[40-43] have indicated that especially in non-polar solvents a considerable fraction of the excited state population is non-polarized, indicating possible limitations of the validity of the generalized picture of sudden polarization by selective pyramidalization. This observation justifies a more detailed study on the effects of pyramidalization on larger ethylenes.

To accomodate this need, in this chapter the outcome of an exploratory study on a couple of small ethylenes (ethylene, tetramethylethylene) at the CASPT2 level of theory will be presented, despite the aforementioned drawbacks of MCSCF methods when studying the sudden polarization effect.

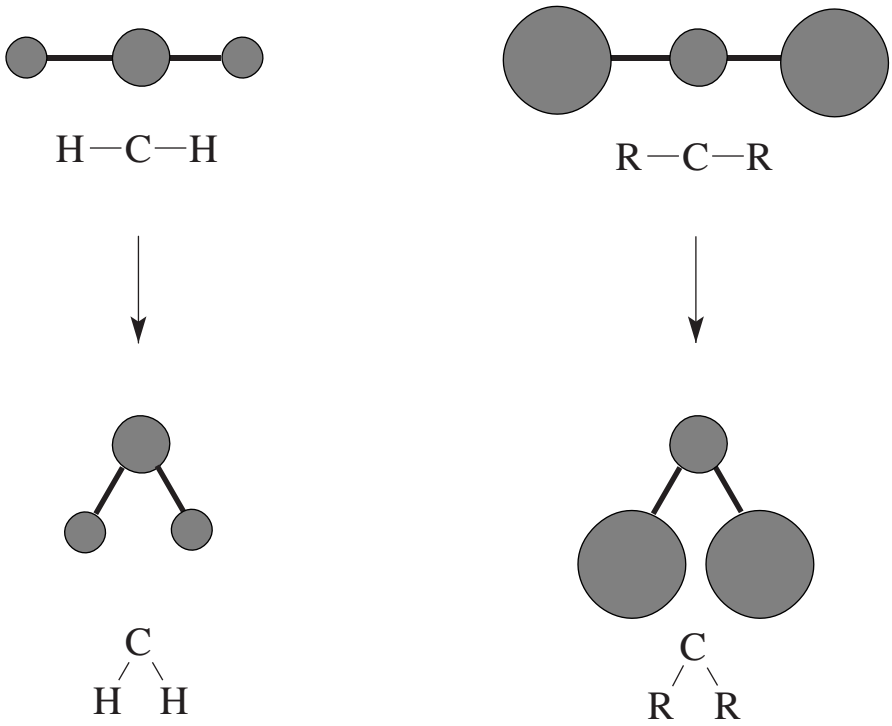

Figure 2.2 Schematic representation of pyramidalization of a CH_2 and a more bulky CR_2 group (viewed alongside the olefenic bond)

The main reason for choosing a MCSCF based approach is that no other appropriate computational tools were available to perform the calculations involving tetramethylethylene (TME). As already mentioned, the use of MCSCF wave functions on studying the sudden polarization effect has some serious limitations with regard to the correct representation of the charge distributions of the electronic states involved. For instance, at the D_{2d} (i.e. unpyramidalized perpendicular) geometry, the electronic representations of the (ionic) Z and V states of ethylene are of a physically incorrect symmetry broken form. This obviously asks for a critical look at the outcome, since the accompanying energies can be unrealistic as well, even though the near-degeneracy of the

two states of interest allows for large polarizations without significantly altering the state energy.

A comparison with the earlier mentioned pioneering work of Brooks and Schaeffer[III] on ethylene[10] will be made to check the validity of the obtained results. It will be shown that even though the obtained dipole moments belonging to the symmetry broken solutions of the Z and V state are clearly unrealistic in the sense that perfectly symmetrical nuclear configurations yield large dipole moments (opposed to results obtained when using CI methods, in which case these configurations have perfectly zero dipole moments), the obtained CASPT2 potential energy surfaces are actually in good agreement with the Brooks' CI results, even at larger pyramidalization angles. Therefore, the results of a pyramidalization study on tetramethylethylene (TME) at its perpendicular geometry will be presented, in order to determine whether the pyramidalized perpendicular geometry of the Z state is still the most stable excited state geometry in cases where the ethylenic double bond carries more sizeable substituents. As explained before, this is a critically important question, since the internal symmetry breaking by one-sided pyramidalization is believed to be the general driving force behind the occurrence of charge separation in symmetrical ethylenes.

2.4 Results and Discussion

The results of the simultaneous torsion and pyramidalization of ethylene and pyramidalization of perpendicular TME will be discussed here. This study has been performed at the CASPT2 level using MOLCAS3.5[44]. In these calculations, the standard Pierloot ANO-s basis[45] of size 4s3p2d on C and 3s2p on hydrogen for ethene and 3s2p1d on carbon and 2s1p on hydrogen for TME has been used. The smaller basis for TME was chosen to reduce computational efforts. All calculations have been performed without imposing symmetry constraints. For ethylene, a CAS of 8 electrons in 12 orbitals has been used. The included occupied orbitals consist of the C-C σ and π bond as well as two H-C-H delocalized orbitals on both sides of the molecule. This selection has been made on the basis of an exploratory RASSCF calculation in which the RAS2 was kept empty and all valence orbitals as well as 20 virtuals were included in the RAS1 and RAS3 respectively, allowing two holes in the RAS1 and 2 electrons in the RAS3. The ethylene geometry used has been identical to the one used by Schaeffer[III] et al.[10] and is depicted in figure 2.3.

Figure 2.3 Adopted ethylene geometry (left) and definition of pyramidalization (or out-of-plane bending) angle ϕ

The TME geometry has been generated in a RHF geometry optimization in the standard 6-31G* basis using Gaussian94. For the CASPT2 calculations, the central C-C bond length was set to 1.416 A after a manual optimization of this bond length at the CASSCF level of theory (see below for details on the CAS) at the TME perpendicular geometry. In this calculation a state averaged wave function with equal weights for the Z and V state was used. The TME active space has been determined by a similar RASSCF procedure as in the ethylene case. Here, an active space of 10 electrons in 10 orbitals has been chosen.

It should be emphasized that these selections have been made by choosing all near-degenerate orbitals from both the occupied and virtual space with the attempt to create a reasonably balanced CAS space. Obviously, better motivated selections could have been made but as already mentioned before, even highly balanced expansions still lead to symmetry broken solutions for the Z and V states so the additional effort was deemed to have a negligible effect. In fact, the current expansions proved to be quite reasonable, since in all unpyramidalized geometries the lowest root (the biradical N state) exhibited near-zero dipole moments at the CASSCF level for both ethylene as well as TME , indicating the balanced nature of the CAS.

Another problem that is frequently encountered when dealing with the electronic spectra of small alkenes is the occurrence of low lying Rydberg states in the spectra, which become 'overcorrelated' in truncated correlation expansions[46-48]. As a result of this, the first excited states incorrectly appear to have Rydberg rather than valence character. For instance, in the case of ethylene it has been demonstrated that large MRCI expansions have to be used to obtain the correct state ordering in the electronic spectrum of the parent alkene[47]. Fortunately, upon twisting away from the planar geometry these Rydberg states destabilize quickly and even very moderate active spaces correctly reproduce the valence nature of the excited states at the geometries of interest in this work.

The CASPT2 calculations were performed in the following manner: first a state averaged CASSCF (with weights 1:1:1) over the three roots of interest (N, Z and V state) has been performed (using a RHF reference as starting orbitals). The thus generated orbitals were used as starting orbitals for the separate CASSCF optimizations of the three roots of interest. In the CASSCF calculations of the Z and V states in the 80-90˚ range some moderate state averaging had to be applied in order to achieve convergence of the calculation. In the case of the Z state ($a^2 + b^2$), a small weight (10%) of the N state needed to be included to ensure convergence of the calculation. For the V state ($a^2 + b^2$), the Z state had to be mixed in (with a weight of maximum 20%) to prevent alternating charge hopping between the two carbon centres in two subsequent SCF cycles.

Subsequently, a CASPT2 calculation was performed to determine the contribution of the inactive and secondary spaces to the electron correlation energy. As already mentioned in section 2.2, this usually is a necessary step in order to get a good estimate of the electron correlation effects when choosing a CASSCF based approach. At this point, it should be mentioned that in all cases the CASPT2 calculations completed without the occurrence of intruder states in the CASPT2 wave functions. This was established by checking the magnitude of the weight of the original CASSCF wave function in the final CASPT2 result. In all cases it was large enough to justify this conclusion.

Two angles were varied in the ethylene calculations; the rotation angle α, which has been varied over a 60-90˚ range with 5 degree increments (with the exclusion of the 65˚

geometry), and the pyramidalization angle ϕ, which has been varied from 0 to 30˚, with 10˚ increments also including ϕ = 5˚ (see also figure 2.4). For TME, ϕ was varied with 10˚ increments at the perpendicular geometry only. More elaborate studies on TME including other values of α had to be abandoned due to lack of time. The resulting CASSCF and CASPT2 energies are given in table 2.1 and 2.2. These results have been visualized in figure 2.4.

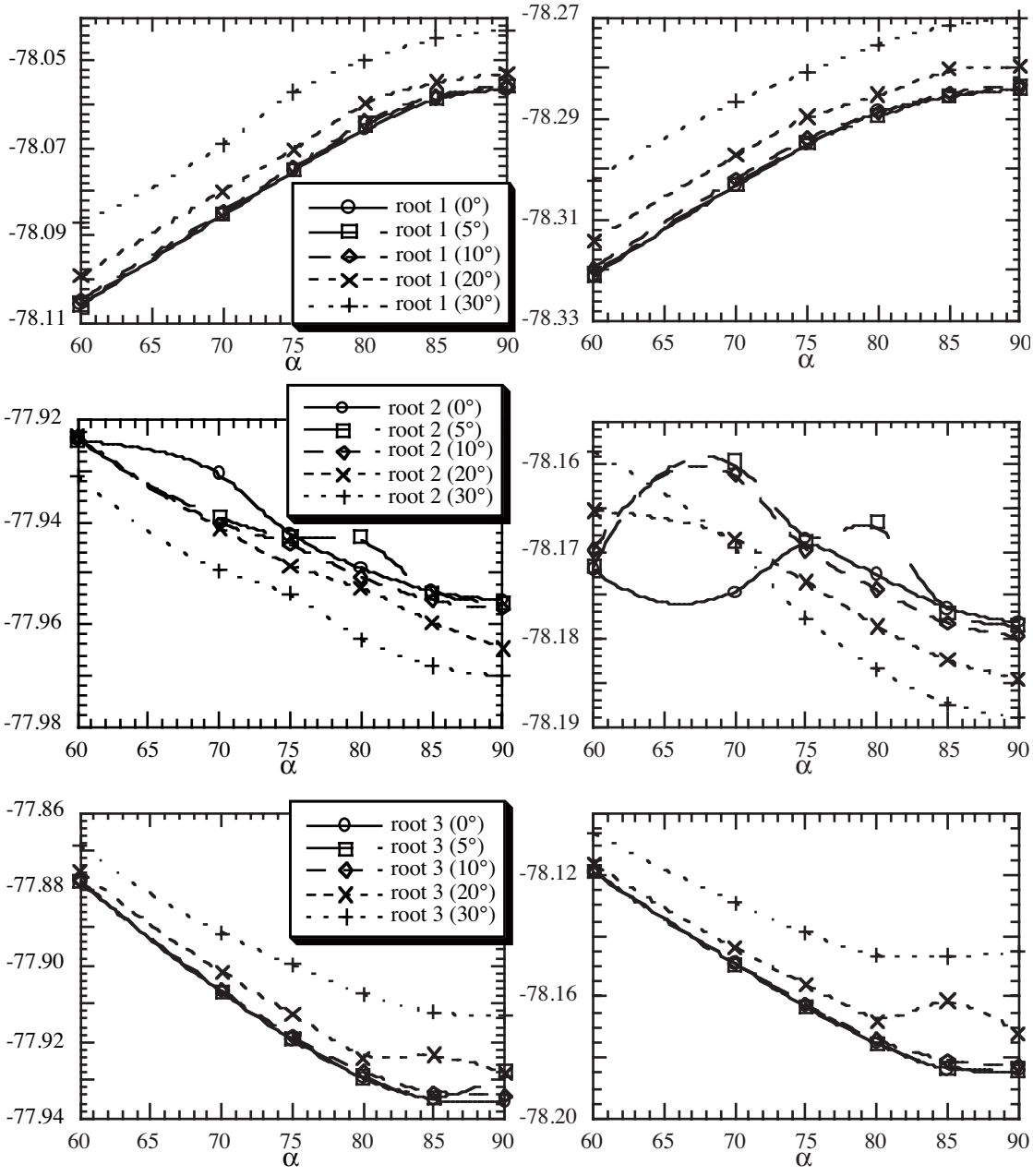

Figure 2.4 CASSCF (left plots) and CASPT2 (right plots) potential energy surfaces (a.u.) of root 1 (top), root2 (middle) and root 3 (bottom) of ethylene at various values of ϕ (in brackets)

α/ϕ	root 1	root 2	root 3
60/0	-78.105921	-77.923929	-77.878015
70/0	-78.085399	-77.930377	-77.906869
75/0	-78.075151	-77.942382	-77.919433
80/0	-78.065764	-77.948938	-77.929560
85/0	-78.058651	-77.953564	-77.935391
90/0	-78.056516	-77.955253	-77.935752
60/5	-78.105749	-77.923614	-77.878027
70/5	-78.085178	-77.939002	-77.907099
75/5	-78.074966	-77.942948	-77.919347
80/5	-78.064414	-77.942830	-77.929182
85/5	-78.058491	-77.954028	-77.934811
90/5	-78.055847	-77.955639	-77.927478
60/10	-78.104734	-77.923151	-77.877883
70/10	-78.084417	-77.940214	-77.906475
75/10	-78.074332	-77.944280	-77.918510
80/10	-78.063782	-77.950778	-77.928029
85/10	-78.057952	-77.955297	-77.933148
90/10	-78.055788	-77.956830	-77.934111
60/20	-78.099233	-77.923085	-77.875197
70/20	-78.079832	-77.941039	-77.901789
75/20	-78.070222	-77.948569	-77.912759
80/20	-78.059546	-77.952806	-77.924171
85/20	-78.054953	-77.959569	-77.923546
90/20	-78.052853	-77.964717	-77.928217
60/30	-78.087165	-77.930968	-77.868481
70/30	-78.069108	-77.949421	-77.891603
75/30	-78.057128	-77.953992	-77.899811
80/30	-78.049867	-77.963011	-77.907431
85/30	-78.044781	-77.968219	-77.912354
90/30	-78.043069	-77.97013	-77.913087

Table 2.1 CASSCF energies (a.u.) of the investigated ethylene geometries in the 60-90˚ torsion (α) and 0-30˚ pyramidalization (ϕ) range.

A number of remarkable observations can be made. First of all, for root 1 (the N state), similar behaviour can be observed at both levels of theory. Typical dipole moments along the z-axis range from 0.1 to 0.3 D at the strongly pyramidalized geometries.
These results compare qualitatively well with the results of both Brooks and Buenker et al.[10, 23]

α/ϕ	root 1	root 2	root 3
60/0	-78.321076	-78.172086	-78.118806
70/0	-78.303250	-78.174723	-78.148982
75/0	-78.295122	-78.168474	-78.163172
80/0	-78.288638	-78.172688	-78.175467
85/0	-78.285696	-78.176530	-78.183978
90/0	-78.284213	-78.178070	-78.184538
60/5	-78.320720	-78.171688	-78.118893
70/5	-78.302890	-78.159660	-78.149292
75/5	-78.294788	-78.168801	-78.163199
80/5	-78.289494	-78.166518	-78.175280
85/5	-78.285489	-78.176977	-78.183636
90/5	-78.283832	-78.178478	-78.183782
60/10	-78.319572	-78.169852	-78.118863
70/10	-78.301944	-78.161017	-78.148815
75/10	-78.293944	-78.169806	-78.162481
80/10	-78.288834	-78.174387	-78.173967
85/10	-78.284821	-78.178227	-78.180973
90/10	-78.283388	-78.179675	-78.182586
60/20	-78.314080	-78.165298	-78.116246
70/20	-78.297236	-78.168465	-78.143810
75/20	-78.289628	-78.173457	-78.155985
80/20	-78.285351	-78.178539	-78.168132
85/20	-78.280240	-78.182419	-78.161246
90/20	-78.279739	-78.184555	-78.172288
60/30	-78.302312	-78.158620	-78.106148
70/30	-78.286627	-78.169510	-78.128945
75/30	-78.280863	-78.177597	-78.138800
80/30	-78.275266	-78.183419	-78.146539
85/30	-78.271408	-78.187456	-78.146793
90/30	-78.270028	-78.188931	-78.145265

Table 2.2 CASPT2 energies (a.u.) of the investigated ethylene geometries in the 60-90˚ torsion (α) and 0-30˚ pyramidalization (ϕ) range.

For the Z and V state the behaviour is less straightforward (see also figure 2.5) As can be seen from figure 2.5, at the CASSCF level root 2 is increasingly stabilized by progressive pyramidalization after a small barrier (ϕ = 5˚) has been taken, whereas root 3 becomes increasingly destabilized, especially at larger pyramidalization angles.

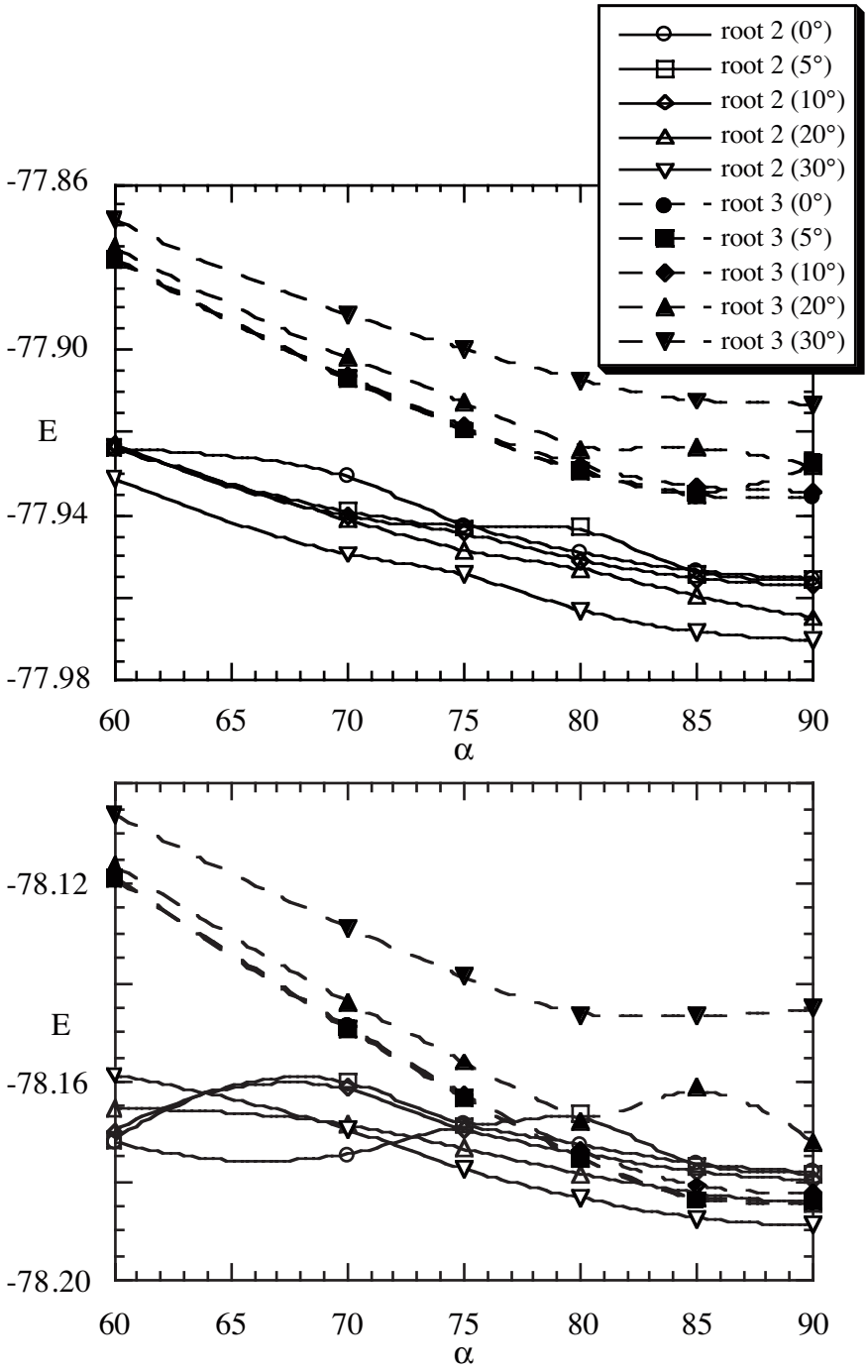

Figure 2.5 CASSCF (top plot) and CASPT2 (bottom plot) potential energy surfaces (a.u.) of root 2 (solid lines) and 3 (dashed lines) for various values of ϕ.

Although the behaviour of root 2 is in agreement with previous findings, which show that a certain amount of activation energy is required (i.e. a pyramidalization barrier has to be taken) before the pyramidalized conformations of root 2 become more stable than the planar one, the overall picture is inaccurate since a significant energy difference exists between root 2 and 3 for all conformations, even at the avoided crossing near 80˚.

This is not unexpected due to the aforementioned limitations of the CASSCF approach. In addition, truncated MCSCF wave functions tend to overcorrelate localized (polar) solutions. The occurrence of such non-degenerate polar solutions at unpyramidalized geometries not only shows that undesired, excessive mixing of the Z and V states take place, but that the expectation values of the accompanying energies are also incorrect. It will be demonstrated in the remainder of this chapter that the latter inaccuracy is largely repaired by the subsequent CASPT2 calculations.

A remarkable difference in dipole moment (μ_z) can be observed as well. Root 2 (as predicted) shows large dipole moments from 70-90˚ (around 3 Debye), whereas root 3 shows much smaller dipole moments (around 1 Debye). This is unexpected, because the antisymmetric nature of the two states involved should direct these calculations towards states having equally large dipole moments that only differ in sign. Apparently, two clearly non-orthogonal states have been obtained. An obvious solution would be to perform a so called Restricted Active Space State Interaction (RASSI) calculation[49] in which the states will be orthogonalized again. Application of this method has lead to a dramatic destabilization of the third root caused by the 'polar' nature of the orbitals. For root 2, the electron pair will effectively be localized at one of the carbons, leaving an electron hole at the other. In the RASSI, root 3 will have both electrons projected in the orbitals of the electron hole which are likely to be very contracted. This will lead to a large electron-electron repulsion term in the energy expression for this state.

In addition, it is questionable whether such a procedure is really necessary in this case. Consider the following hypothetical situation. On assuming a small transition probability between the two PES of interest, an excited state population can pass the crossing area several times without actually crossing to the lower surface. In this situation, the population will remain at the higher of the two potential energy surfaces on progressive twisting. As demonstrated, this surface becomes destabilized by pyramidalization. This is reflected by the lower expectation value of the dipole moments for this state. In fact, if state averaging (i.e. the moderate mixing of root 2 into the CASSCF optimization of root 3) is applied, the magnitude of these dipole moments as well as the difference between the dipole moments of root 2 and 3 is significantly reduced. Therefore, this non-orthogonality can be interpreted as a reflection of the aforementioned difference in PES behaviour. A more elaborate discussion on this difference in behaviour can be found in chapter 5.

At the CASPT2 level the picture is more in accordance with previous work. The overcorrelation of root 2 with respect to root 3 gets repaired and their near-degeneracy at planar or moderately pyramidalized near-perpendicular geometries is restored again, even though the expectation values of the dipole moments do not change significantly from the CASSCF ones. However, some suspicious looking energy barriers can be observed in the various potential energy surfaces in figure 2.5. Especially the PES of root 3 at $\phi = 20^\circ$ appears to be erratic in the vicinity of the perpendicular geometry. This is probably caused by the fact that severe state averaging (ratio 1:4 for root 2 : root 3) was required to reach convergence for the CASSCF calculation. The large amount of root 2 behaviour may have caused the overstabilization of this strongly pyramidalized geometry.

Focussing on the larger picture at the perpendicular geometry, the observation can be made that only at large pyramidalization angles ($\phi = 30^\circ$) root 2 becomes more

α/ϕ	root 1	root 2	root 3
CASSCF			
90/0	-234.2236870	-234.1229404	-234.0995915
90/10	-234.2264883	-234.1230315	-234.0954081
90/20	-234.2124947	-234.117909	-234.0796808
90/30	-234.1655431	-234.0862198	-234.022427
CASPT2			
90/0	-234.9978758	-234.8962502	-234.9065978
90/10	-234.9946143	-234.8964841	-234.9007436
90/20	-234.9818408	-234.8924526	-234.8763497
90/30	-234.9392147	-234.8650318	-234.8126322

Table 2.3 CASSCF and CASPT2 energies (a.u.) of various pyramidalization angles ϕ of perpendicular TME

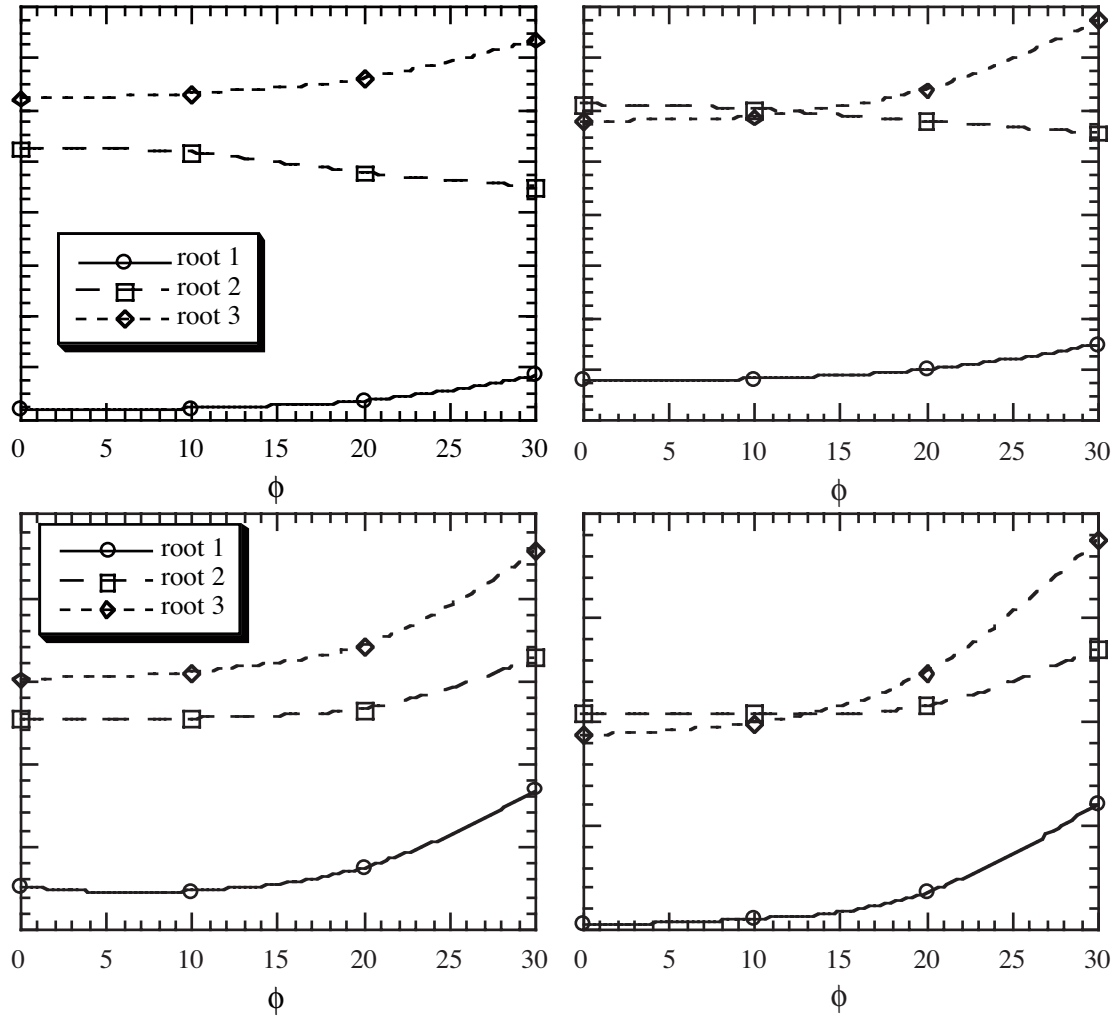

Figure 2.6 CASSCF (left plot) and CASPT2 (right plot) energies (a.u.) of perpendicular ethylene (top plots) and TME (bottom plots) at the investigated values of ϕ.

stabilized than the planar root 3, which is in good agreement with the findings of Brooks et al. at the CISD level of theory[10].

In general, the CASPT2 wave functions appear to reproduce the expectation values of the energies of the excited states of such systems reasonably well even though the expectation values of the dipole moments are still unrealistic. This is not surprising, since it cannot be expected that second-order perturbation theory can repair the strongly polarized input wave functions based on an extensive CAS. However, the fact that potential energy surfaces similar to previous work are reproduced justifies an attempt to investigate the pyramidalization behaviour of TME at the perpendicular geometry. These results are presented in table 2.3 and visualized in figure 2.6.

When comparing the TME and ethylene results, it becomes apparent that the qualitative behaviour of the CASSCF and CASPT2 wave functions is quite similar. For both ethylene and TME the near-degeneracy of root 2 and 3 (the Z and V state) is best reproduced at the CASPT2 level of theory. In fact, for both systems a crossing of the Z and V surface is predicted near $\phi = 13^{\circ}$. This is a clear indication of the generic nature of the sudden polarization effect in D_2-symmetrical alkenes.

However, there is a striking difference in the PES behaviour of the two systems. Where root 2 gets stabilized on progressive pyramidalization in the ethylene case, the corresponding root in the TME case lacks this stabilization. Even though both the CASSCF and CASPT2 PES of root 2 of TME are rather flat for the more moderate values of ϕ, at which in fact a shallow minimum can be observed (see table 2.3), at progressive pyramidalization all three roots become significantly destabilized. This can be explained by the nature of the substituents on the carbon double bond; the small hydrogens can be pushed towards each other without significantly increasing repulsion between them. The more bulky methyl groups are much more prone to 'feeling' the repulsion, as schematically depicted in figure 2.2. Therefore, this contribution to the state energy will dominate the PES behaviour when ϕ becomes large enough. This effect is even more dramatic for root 3, since both pyramidalization as well as repulsion destabilize the state, leading to a steep PES for this state in the TME case.

These observations raise the suspicion that internal symmetry breaking may not be the main driving force in the occurrence of polarized, zwitterionic excited states of D_2-symmetrical alkenes, since for large substituents (like for instance the phenyl groups at TPE) the steric hindrance is likely to prevent significant stabilization by pyramidalization due to the expected large amount of introduced steric hindrance.

Nevertheless, large excited state dipole moments have been reported for systems like TPE[31, 50]. Interestingly, these experimentally observed polar states have always been reported for alkenes in the condensed phase. In addition, solvent dependent behaviour has been observed in many cases[31, 40, 42, 43]. This justifies the question whether external symmetry breaking, like an intrisically low-symmetry solvent shell, is capable of providing a large enough perturbation of the ethylenic wave function in order to produce effective symmetry breaking. In other words, is a solvent solely capable of polarizing ethylenic excited states at near-perpendicular geometries ?

The answer to this question will be given in the remainder of this thesis.

2.5 Conclusion

In this chapter, the simultaneous torsion and pyramidalization of ethylene at in the vicinity of the perpendicular geometry as well as the pyramidalization of TME at the perpendicular geometry has been investigated at the CASPT2 level of theory in an attempt to study the sudden polarization effect. It has been explained that the description of this phenomenon by these types of wave functions is not necessarely the best choice, since truncated MCSCF expansions lead to (over)polarized solutions of the excited states of interest in the vicinity of the avoided crossing between the $a^2 + b^2$ (Z) and $a^2 - b^2$ (V) state.

It has been shown by comparing the ethylene results with earlier reported work that the relative CASSCF energy differences between the excited states of interest were inaccurate. This has been attributed to the fact that the polarized first excited state benefits more from the (unwanted) wave function polarization than its antisymmetric counterpart. The correct behaviour was reproduced at the CASPT2 level of theory, however. At this level of theory, the near degeneracy of the two states was reproduced, indicating that as far as relative energies are concerned, the CASPT2 method provided results bearing some physical significance. Furthermore, the stabilization by selective pyramidalization of the lowest of the two surfaces involved in the avoided crossing was established as well, also in good agreement with previously reportes studies.Therefore, it was concluded that as far as the shape of the ethylenic potential energy surfaces of interest is concerned, the CASPT2 level of theory is capable of reproducing them with acceptable accuracy.

On the basis of this positive conclusion, the selective pyramidalization of TME at the perpendicular geometry has also been investigated at the CASPT2 level of theory. The aforementioned differences in the CASSCF and CASPT2 energies of the ethylene PES were also observed in the TME case, as can be seen in figure 2.6. This indicates the similar excited state behaviour of the two alkenes at the perpendicular geometry. However, a significant difference in the PES shape of the lowest of the two surfaces involved in the avoided crossing (i.e. root 2) has been observed. In contrast with the ethylene case, where this PES became stabilized as a result of this symmetry lowering perturbation, the TME PES of root 2 was significantly destabilized at larger pyramidalization angles. This has been explained by the much larger increase in steric hindrance between the two methyl groups with respect to the hydrogens when these groups are forced together by the pyramidalization as schematically depicted in figure 2.2. This remarkable observation has led to the conclusion that the widely accepted theory, in which the intramolecular lowering of the molecular symmetry (i.e selective pyramidalization) is held mainly responsible for the formation of ethylenic excited states with large dipole moments, might not hold for larger D_2-symmetrical alkenes.

2.6 References

1. R.S. Mulliken, Phys. Rev., **41**, 751-758 (1932).
2. L. Salem and C. Rowland, Angew. Chem., Int. Ed. Engl., **11**, 92-111 (1972).
3. J.A. Marshall, Science, **170**, 137-141 (1970).
4. C.E. Wulfman and S. Kumei, Science, **172**, 1061 (1971).
5. C.E. Wulfman and G.C. Hyatt, Proc. Indian Acad. Sci. (Chem. Sci.), **107**, 813-823 (1985).
6. V. Bonacic-Koutecky, P. Bruckmann, P. Hiberty, J. Koutecky, C. Leforestier and L. Salem, Angew. Chem., Int. Ed. Engl., **14**, 575-576 (1975).
7. V. Bonacic-Koutecky, J. Cizek, D. Döhnert and J. Koutecky, J. Chem. Phys., **69**, 1169-1176 (1978).
8. V. Bonacic-Koutecky, J. Am. Chem. Soc., **100**, 396-404 (1978).
9. V. Bonacic-Koutecky, R.J. Buenker and S.D. Peyerimhoff, J. Am. Chem. Soc., **101**, 5917-5922 (1979).
10. B.R. Brooks and H.F Schaefer III, J. Am. Chem. Soc., **101**, 307-311 (1979).
11. S. Ramasesha and I.D.L. Albert, Chem. Phys., **142**, 395-402 (1990).
12. R.W.J. Zijlstra, A.H. de Vries and P.Th. van Duijnen, Chem. Phys., **204**, 439-446 (1996).
13. A. Szabo and N.S. Ostlund, *Modern Quantum Chemistry*, Macmillan Publishing Co. Inc., New York, 1982.
14. B.O. Roos Ed., *Lecture Notes in Quantum Chemistry*, Springer-Verlag, Heidelberg, 1992.
15. B.O. Roos, P.R. Taylor and P.E.M. Siegbahn, Chem. Phys., **48**, 157-173 (1980).
16. B.O. Roos, in: Ab Initio Methods in Quantum Chemistry II, Ed: K. P. Lawley, John Wiley & Sons Ltd., New York, 1987.
17. P-Å Malmqvist, A. Rendell and B.O. Roos, J. Phys. Chem., **94**, 5477-5482 (1990).
18. C. Möller and M.S. Plessett, Phys. Rev., **34**, 618 (1934).
19. K. Andersson, P-Å Malmqvist, B.O. Roos, A.J. Sadlej and K. Wolinski, J. Phys. Chem., **94**, 5483-5488 (1990).
20. K. Andersson, P-Å. Malmqvist and B.O. Roos, J. Chem. Phys., **96**, 1218-1226 (1992).
21. H.-J. Werner and P.J. Knowles, J. Chem. Phys., **89**, 5803-5814 (1988).
22. B.O. Roos and K. Andersson, Chem. Phys. Lett., **245**, 215-223 (1995).
23. R.J. Buenker, V. Bonacic-Koutecky and L. Pogliani, J. Chem. Phys., **73**, 1836-1849 (1980).
24. V. Bonacic-Koutecky, L. Pogliani, M. Persico and J. Koutecky, Tetrahedron, **38**, 741-751 (1982).
25. P. Bruckmann and L. Salem, J. Am. Chem. Soc., **98**, 5037-5038 (1976).
26. C.M. Meerman-van Benthem, H.J.C. Jacobs and J.J.C. Mulder, Nouv. J. Chim., **2**, 123-127 (1977).
27. G. Orlandi, P. Palmieri and G. Poggi, J. Am. Chem. Soc., **101**, 3492-3497 (1979).
28. I.D.L. Albert and S. Ramasesha, J. Phys. Chem., **94**, 6540-6543 (1990).

29. M. Merchán and R. González-Luque, J. Chem. Phys., **106**, 1112-1122 (1997).
30. L. Salem, Acc. of Chem. Res., **12**, 87-92 (1979).
31. W. Schuddeboom, S.A. Jonker, J.M. Warman, M.P. de Haas, M.J.W. Vermeulen, W.F. Jager, B. de Lange, B.L. Feringa and R.W. Fessenden, J. Am. Chem. Soc., **115**, 3286-3290 (1993).
32. G. Orlandi and W. Siebrand, Chem. Phys. Lett., **14**, 19-22 (1972).
33. G. Orlandi and W. Siebrand, Chem. Phys. Lett., **80**, 399-403 (1981).
34. A. Farazdel, M. Dupuis, E. Clementi and A. Aviram, J. Am. Chem. Soc., **112**, 4206-4214 (1990).
35. C. Zener, Proc. Roy. Soc. London, A, **137**, 696-702 (1932).
36. M. Persico, J. Am. Chem. Soc., **102**, 7839-7845 (1980).
37. I.D. Petsalakis, G. Theodorakopoulos, C.A. Nicolaidis, R.J. Buenker and S.D. Peyerimhoff, J. Chem. Phys., **81**, 3161-3167 (1984).
38. I.D. Petsalakis, G. Theodorakopoulos and C.A. Nicolaidis, J. Chem. Phys., **81**, 5952-5956 (1984).
39. R. Broer-Braam, *Localized orbitals and broken symmetry in molecules*, Ph.D. thesis, University of Groningen, 1981.
40. P.F. Barbara, S.D. Rand and P.M. Rentzepis, J. Am. Chem. Soc., **103**, 2156-2162 (1981).
41. C.L. Schilling and E.F. Hilinski, J. Am. Chem. Soc., **110**, 2296-2298 (1988).
42. Y-P. Sun and C.E. Bunker, J. Am. Chem. Soc., **116**, 2430-2433 (1994).
43. R.W.J. Zijlstra, P. Th. van Duijnen, B.L. Feringa, T. Steffen, K. Duppen and D.A. Wiersma, J. Phys. Chem. A, **101**, 9828-9836 (1997).
44. K. Andersson, M.R.A. Blomberg, M.P. Fülscher, V. Kellö, R. Lindh, P.-Å. Malmqvist, J. Noga, J. Olsen, B.O. Roos, A.J. Sadlej, P.E.M. Siegbahn, M. Urban and P.-O. Widmark, *Molcas version 3*, University of Lund, Sweden, 1994.
45. K. Pierloot, B. Dumez, P-O. Widmark and B.O. Roos, Theor. Chim. Acta, **90**, 87-114 (1995).
46. R.J. Buenker and S.D. Peyerimhoff, Chem. Phys., **9**, 75-89 (1976).
47. C.C. Ballard, M. Hada and H. Nakatsuji, Bull. Chem. Soc. Japan, **69**, 1901-1906 (1996).
48. J.D. Watts, S.R. Gwaltney and R.J. Barrett, J. Chem. Phys., **105**, 6979-6988 (1996).
49. P.-Å. Malmqvist and B.O. Roos, Chem. Phys. Lett., **155**, 189-194 (1989).
50. J. Morais, J. Ma and M.B. Zimmt, J. Phys. Chem., **95**, 3885-3889 (1991).

Polarization of the Excited States of Twisted Ethylene in a Non-Symmetrical Environment

3.1 Introduction

For various reasons, the dynamic behavior of the photo-induced excited states of ethylenic systems has been the subject of numerous theoretical and experimental studies. For instance, interest in understanding cis-trans isomerization processes of ethylenic compounds in which the cis-trans isomerization of retinal, the key molecule in the mechanism of vision, is probably the most exciting example[1] and has contributed to the large number of studies performed on this class of compounds.

One of the most intriguing aspects of the behavior of the excited states of (symmetrical) alkenes is the existence of a polarized (charge separated) state, in which two electrons—unpaired and distributed in the initial biradical excited state—are localized at one side of the molecule, thus leading to the formation of a considerable dipole moment.

Both direct and indirect experimental evidence of the existence of such a suddenly polarized[2] 'phantom' state has been obtained from time resolved photo induced excitation experiments on tetraphenylethylene (TPE)[3-9] and several other alkenes[10-12], in which a polarized state could be detected in various solvents.

A remarkable observation in the experiments concerning TPE is the dependence of the lifetime of the polarized state on solvent polarity[5, 6], in which a decreasing lifetime with increasing solvent polarity was observed. In these studies, increased coupling due to an decreased energy gap between the twisted (D_{2d}) ground state and the more stabilized polarized excited state was suggested as a possible explanation for this observation. The occurrence of the polarization of TPE, in twisted geometries only, was deduced from the observation of a strong reduction of the quantum yield for formation of polarized excited TPE with increasing solvent viscosity[8] and by Resonance Raman spectroscopy[13]. The twisting around the central bond will be increasingly hindered and fluorescence from the—nearly planar—relaxed vertically excited state, will become the dominant relaxation pathway.

On the origin of the localized states it should be noted that after the vertical excitation of an electron from the D_{2h} ground state of ethylene, and other symmetrical alkenes, the C-C bond length will increase and a twist around the central C-C bond will be initiated[14]. On progressive twisting, three low lying singlet states arise, which at the perpendicular D_{2d} geometry ($\theta=90^0$) are denoted as N ($^1B_1$; ab), V($^1B_2$; a^2-b^2) and Z ($^1A_1$; a^2+b^2) and are sensitive to rotation around the C-C bond. The N state is destabilized going from the D_{2h} to the D_{2d} geometry, while the V and Z states are stabilized, coming close together at near perpendicular geometries and—in the Born-Oppenheimer approximation—cross for $\theta\approx80^0$. At and around the crossing V and Z are (nearly) degenerate and therefore wave functions of type V ± Z are equally acceptable, resulting in localized a^2 or b^2 states which will have considerable dipole moments. A theoretical description of the vacuum situation should be based on the appropriate (open shell, many determinant) wave functions and symmetry, i.e.V ± Z should have equal weights as long as the D_{2d} symmetry remains, and no dipole should exist.

Previous theoretical studies provided valuable insight into the possible polarization of the (near) perpendicularly twisted (D_{2d}) excited states of ethylene. CISD studies by Brooks and Schaefer III[15] showed that lowering the nuclear symmetry to C_s by pyramidalization of one of the two carbon centers leads to the build up of large dipole

moments due to considerable mixing between the —originally (D_{2d}) V and Z —states. MRCI studies of Buenker et al.[16, 17] have shown that combined pyramidalization and twisting of the central double bond leads to the formation of highly polarized states in the vicinity of the crossing of the Z and V state energy surfaces.

Since experimental results always are related to the condensed phase, it can be worthwhile to investigate whether solvent polarization on its own could be responsible for the lowering of the symmetry required for localization of these states. If the system is embedded in some polarizable medium, the transient a^2 or b^2 states can generate reaction potentials which may live sufficiently long to lift the degeneracy and stabilize one with respect to the other, without lowering the symmetry of the nuclear arrangement.

To that end the Direct Reaction Field approach[18-20] has been applied, which allows various ways of modeling solvent effects, e.g. representing the "solvent" by (sets of) discrete semi-classical solvent molecules (distributed multipoles + polarizabilities) or by a dielectric continuum, or both. The model can treat ab initio RHF, ROHF, GVB, MCSCF and CI wave functions for ground and excited states in equilibrium and non-equilibrium situations, while the solute/solvent interactions may be accounted for fully self consistent or as first-order perturbations. For solvent effects from the discrete model at finite temperatures Monte Carlo sampling of the solvent's degrees of freedom is provided. All this was implemented in the ab initio package HONDO 8.1[21]. A general description of the DRF model will be given in the next paragraph.

In this chapter it was decided to use the dielectric model only[22], although it has been pointed out that this is not without problems[23]. Moreover, since ab initio calculations on TPE are not feasible on the level of theory required, ethylene has been used as model compound.

3.2 The DRF Model

3.2.1 Introduction

Solvent effects play a very important role in chemistry since most chemical reactions and biological processes take place in solutions. The properties of molecules and the interactions between them in solution can differ greatly from the properties and interactions in vacuum, the state to which most quantum chemical calculations refer. Including solvent effects in quantum chemical calculations by adding quantum mechanically treated solvent molecules would lead to an enormous increase in computational cost. A more fruitful approach is the development of a mixed quantum mechanical/classical model in which the system of interest (the solute) is treated quantum mechanically and the surrounding solvent is treated classically.

The first attempts to combine a quantum mechanical system with classical surroundings were based on a dielectric continuum description[24] of the solvent. In these models the (quantum mechanical) solute is placed in a cavity in a dielectric continuum. These models have been used with reasonable success, however there are important limitations. They employ a macroscopic property of the solvent, the dielectric constant, to model the interactions on a microscopic scale, which means that they can never accurately

describe specific solvent-solute interactions e.g. hydrogen bonding[25, 26]. Another drawback is the need to reparameterize the model for each different solvent.

These difficulties can be resolved by using explicit solvent models. A number of these have been developed over the last years[27, 28]. Most of them are based on a Lennard-Jones type force field for the dispersion and short range repulsion terms, and point charges for modeling electrostatic effects. Recently, polarization effects were added to these models to include induction interactions[28-30], however the explicit polarizabilities are not used for modeling the dispersion. The Lennard-Jones parameters are fitted to ground state interaction energies and so no distinction can be made between dispersion interaction in the ground state and the excited states without reparameterizing for the excited states.

These problems are all omitted in the Direct Reaction Field (DRF)[18-20] model. The model is summarized in Figure 3.1. The quantum system is surrounded by discrete classical systems (A, B,.....) modeling the first few solvent shells. These solvent shells can optionally be surrounded by a dielectric continuum for modeling bulk effects. The total energy of the system consisting of a quantum mechanically described solute and a discrete classical solvent is given by :

$$\Delta U^{discr} = \Delta U^{QM} + \Delta U^{MM} + \Delta U^{QM/MM} \qquad \textbf{(3.1)}$$

in which ΔU^{QM} is the expectation value of the vacuum Hamiltonian over the nonvacuum wave function, ΔU^{MM} represents the interactions between the classical subsystems and $\Delta U^{QM/MM}$ is the interaction between the quantum system and the classical surroundings.

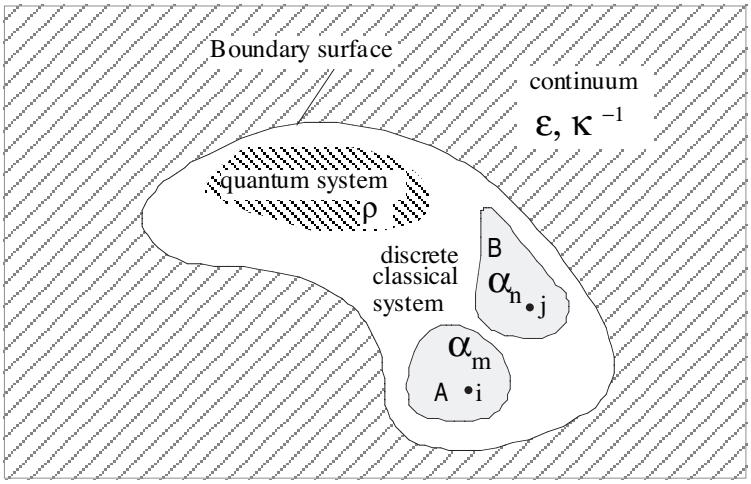

Figure 3.1 DRF model for the condensed phase.

3.2.2 Classical Interactions in the DRF Model

The interactions between classical solvent molecules are modeled by point charges, radii and polarizabilities. These parameters can all be derived from the monomer properties, either from experiments or from calculations. Point charges can be derived from ab initio wave functions on the monomers (A,B,....) using a dipole preserving population analysis[31] or by fitting charges to the electrostatic potential[32]. For the radii experimental values like Van der Waals radii can be used, but calculated values can also be obtained (e.g. from the quadrupole moment or from polarizabilities). Atomic

polarizabilities can be obtained by fitting them to experimental or calculated molecular polarizabilities in a procedure developed by Thole[33, 34].

The classical interactions in the DRF model can be written as :

$$\Delta U^{MM} = \sum_{\substack{i\in A, j\in B \\ A>B}} q_i^A \, \upsilon_{ij} \, q_j^B + \frac{1}{2} \sum_{\substack{i\in A, j\in B \\ A,B \\ rs\notin AB}} q_i^A \, f_{ir} \, A_{rs} \, f_{sj} \, q_j^B + \Delta U_{disp}^{MM} + \Delta U_{rep}^{MM} \qquad \textbf{(3.2)}$$

with $\upsilon_{ij} = \frac{1}{|r_i - r_j|}$, the Coulomb potential in **j**, brought about by a source in **i** and $f_{ij} = -\nabla_j V_{ij}$ is the corresponding electric field. The first two terms are the Coulomb interaction and the induction interaction (also called 'screening of the electrostatic interaction'). q_i^A is the i-th point charge of classical group A. The A_{rs} are elements of the matrix $\mathbb{A}$, which can be considered as the total polarizability of a system of molecules (see below). It should be noted that in Equation 3.2 all interactions within monomers are set to zero.

For the classical dispersion interaction, the Slater-Kirkwood expression[35] is used:

$$\Delta U_{disp}^{MM} = \sum_{i<j} \frac{1}{4R^6} \frac{Tr\left(\alpha_i \, \mathbb{t}(\mathbf{i};\mathbf{j})^2 \, \alpha_j\right)}{\left(\sqrt{\alpha_i/n_i} + \sqrt{\alpha_j/n_j}\right)} \qquad \textbf{(3.3)}$$

in which $\mathbb{t}(\mathbf{i};\mathbf{j})$ is the interaction tensor for the induced dipoles at **i** and **j**. For the short range repulsion the CHARMM[36] expression is used :

$$\Delta U_{rep}^{MM} = \sum_{i<j} \frac{3}{4} \frac{\bar{\alpha}_i \, \bar{\alpha}_j \, (r_i + r_j)^6}{\left(\sqrt{\bar{\alpha}_i/n_i} + \sqrt{\bar{\alpha}_j/n_j}\right)} r_{ij}^{-12} \qquad \textbf{(3.4)}$$

in which $\bar{\alpha}_i$, n_i, and r_i are the isotropic polarizability, number of valence electrons, and radius of atomic center i, respectively, and r_{ij} is the distance between centers i and j. The integral number of valence electrons of an atom and the same atomic polarizabilities that go into the electrostatic, response, and dispersion terms are used, leaving only the atomic radii as independent parameters.

3.2.3 Coupling of the Classical and Quantum Mechanical Systems

The static electric field, brought about by the point charges of the classical groups, can easily be introduced in the solute Hamiltonian. Adding reaction field effects due to interaction with classical polarizabilities however, is more difficult. The coupling of the quantum mechanical solute and the polarizable solvent system can be done by performing a so called coupled-SCF procedure described by Thompson[29] in which the wave function has to be solved from a nonlinear equation:

$$\left[\hat{H}^{Q} + \hat{H}^{RF}\left(\Phi_Q\right)\right]\Phi_Q = E\left(\Phi_Q\right)\Phi_Q \qquad \textbf{(3.5)}$$

$\hat{H}^{Q}$ is the normal vacuum Hamiltonian, $\hat{H}^{RF}$ is the reaction field Hamiltonian which is dependent on the wave function itself because it includes the dipole moments induced by the quantum system (in the classical polarizable system). This nonlinear equation has to be solved in an iterative scheme in which first the induced moments are calculated:

$$\mu_p = \alpha_p \left[f_p + \sum_{p \neq q} f(m_q,p) + f_p^Q (\Phi_Q) \right] \qquad \textbf{(3.6)}$$

f_p is the static field felt in p, $f(m_q, p)$ is the field in p due to a (classically induced) moment in q and f_p^Q is the field in p due to the quantum system. These induced moments are put into the reaction field hamiltonian $\hat{H}^{RF}$, which is then used to calculate a new wave function which is in turn used to generate new induced moments, etc., until convergence is reached. In this way the solute feels the average response of the classical polarizabilities to the field due to the solute (i.e., the Average Reaction Field) and the induction interaction between the quantum system and the classical system can be calculated.

A more elegant approach is presented by the *direct* reaction field model (DRF)[18-20, 31] in which the effect of the solvent polarizability is introduced directly into the vacuum solute hamiltonian (H^0) :

$$H = H^0 + H^{es} + H^{rf} \qquad \textbf{(3.7)}$$

with H^{es} and H^{rf} the electrostatic and reaction potential *operators*. The interaction energy between a quantum mechanically described solute and a system of (classical) point charges and polarizabilities $\mathbb{A}$ (i.e. the solvent, see below)—for a single determinant, closed shell wave function —is given by :

$$\begin{aligned}
\Delta U_{int}^{QM/MM} = & \sum_{A,i,j} q_i^A \vartheta_{ij} Z_j + e \sum_{A,i} q_i^A \langle \vartheta \rangle_i + \\
& \sum_{A,i,j,r,s} q_i^A f_{ir} A_{rs} f_{sj} Z_j + e \sum_{A,k,j,r,s} q_j^A f_{jr} A_{rs} \langle f(s;k) \rangle + \\
& \frac{1}{2} \sum_{i,j,r,s} Z_i f_{ir} A_{rs} f_{sj} Z_j + e \sum_{i,k,r,s} Z_i f_{ir} A_{rs} \langle f(s;k) \rangle + \\
& \frac{\gamma}{2} e^2 \sum_{k,r,s} \langle f(k;r) A_{rs} f(s;k) \rangle + \frac{1}{2} e^2 \sum_{k,l,r,s} \langle f(k;r) \rangle A_{rs} \left(1 - \frac{\gamma}{2} P_{12} \right) \langle f(s;l) \rangle \\
& + \Delta U_{rep}^{QM/MM}
\end{aligned} \qquad \textbf{(3.8)}$$

In the first two terms of equation 3.8 we see the electrostatic interactions of nuclei and electrons with the point charges. The third term contains the interactions of the point charges with the dipoles induced by the nuclei and vice versa. The fourth represents the

interaction between the point charges and the dipoles induced by the electrons and vice versa. The fifth and sixth terms are the screening of the nuclear repulsion and attraction respectively (part of the induction). The seventh term contains the interaction of each electron with its own induced dipoles, the eighth is the interaction of each electron with the dipoles induced by the other electrons, hence it is a two electron term. This term contains the induction interaction and part of the dispersion. The scaling factor, γ, is for the dispersion which is discussed below, and P_{12} is the permutation operator. If one takes $\gamma = 0$ term seven disappears and in term eight only the induction part remains. In order to distinguish between source and recipient in the expectation values of the field—e.g. $\langle f(k;s) \rangle$, i.e. the electric field at **s** due to electron k—the electron labels (k,l) and the electronic charge (e) have been made explicit so as to avoid ambiguity in the signs of the various terms. In equation 3.8 the cost of inducing all the dipoles in the classical system has already been included.

The repulsion term in equation 3.8 is the same as in equation 3.4, although the radii of the QM atoms may optionally be obtained "on the fly" (i.e. when needed) instead of fixing them on their vacuum values.

The difference of the expectation values

$$\langle \Psi | H | \Psi \rangle - \langle \Psi^0 | H^0 | \Psi^0 \rangle + \Delta U_{rep}^{QM/MM} = \Delta U_{int}^{QM/MM} \qquad \textbf{(3.9)}$$

contains all first and second order contributions usually obtained when Ψ refers to a super molecule SCF calculation, and more. The expectation value of H^{rf} can be rewritten as:

$$\begin{aligned} \langle H^{rf} \rangle &= -\frac{1}{2} \langle f^{\dagger} \mathbb{A} f \rangle = -\frac{1}{2} \langle f \rangle^{\dagger} \mathbb{A} \langle f \rangle - \frac{1}{2} \left\{ \langle f^{\dagger} \mathbb{A} f \rangle - \langle f \rangle^{\dagger} \mathbb{A} \langle f \rangle \right\} \\ &= \Delta U_{DRF}^{ind} + \Delta U_{DRF}^{disp} \end{aligned} \qquad \textbf{(3.10)}$$

The first term in equation 3.10 is the DRF induction interaction. The term between { }, the difference between the expectation value of the DRF hamiltonian and the average reaction field term, is the *unscaled* DRF dispersion interaction. It has been shown to be just the difference between the screened self energy and the screened exchange contribution (see equation 3.8). Moreover it has been shown that this expression approximately equals the second order perturbation theory (SOP) expression for dispersion, apart from a scaling factor[26, 37]

$$\Delta U_{disp}^{SOP} \approx \left(\frac{E_{solvent}^{i}}{E_{solute}^{i} + E_{solvent}^{i}} \right) \Delta U_{disp}^{DRF} = \gamma \, \Delta U_{disp}^{DRF} \qquad \textbf{(3.11)}$$

where E_{solute}^{i} and $E_{solvent}^{i}$ are the ionization energies of the quantum mechanical solute and the classical solvent respectively.

The reaction field operator was redefined accordingly[26, 37] i.e. by scaling with γ the integrals for screening of the one-electron self energy and of the two-electron

exchange contributions (see also equation 1.8). This is only possible if the exchange interaction is explicitly under control, i.e. only for single determinant wave functions. When using $\gamma = 0$ the wave function does not feel the effect of dispersion with the classical system and the method renders in fact the Average Reaction Field (ARF) method rather than the DRF approach. This will thus lead to the same induction as is obtained when using the coupled-SCF method described above. With $\gamma \neq 0$ the quantum system does feel the effect of dispersion which will modify the wave function, this in turn will lead to a somewhat different induction interaction.

The matrix $\mathbb{A}$—used in equation 3.2, 3.8 and 3.10—is a (super)matrix representing the total linear response of the complete discrete classical part, in which all parts interact self consistently. Taking a set of points $\{\mathbf{p}\}$ with polarizabilities $\{\alpha_p\}$ in a uniform electric field $\mathbf{F}^0$ we have for the induced dipole moment in point $\mathbf{p}$:

$$\mathbf{m}_p = \alpha_p \left(\mathbf{F}^0(\mathbf{p}) - \sum_{q \neq p}^{N^{pol}} t(\mathbf{p};\mathbf{q})\, \mathbf{m}_q \right) \qquad \textbf{(3.12)}$$

A formal solution for $\{\mathbf{m}_p\}$ can be found by collecting the N^{pol} equations into a single super matrix equation of dimension N^{pol} x N^{pol}:

$$\mathbf{M} = \alpha \left(\mathbf{F}^0 - \mathbb{T}\, \mathbf{M} \right) \qquad \textbf{(3.13)}$$

where $\mathbf{F}^0$ and $\mathbf{M}$ are $3N^{pol}$-dimensional vectors, and α and $\mathbb{T}$ are square $3N^{pol}$ x $3N^{pol}$ matrices. The super vectors and matrices are blocked into $3N^{pol}$ and $3N^{pol}$ x $3N^{pol}$ elements, respectively: $\mathbf{M}_p = \mathbf{m}_p$, $\alpha = \alpha_p \delta_{pq}$, $\mathbb{T}_{pq} = t(\mathbf{p};\mathbf{q})(1-\delta_{pq})$, and δ_{pq} is the Kronecker delta. Then

$$\mathbb{A} = \left(\alpha^{-1} + \mathbb{T} \right)^{-1} \qquad \textbf{(3.14)}$$

may be considered as an ordinary polarizability matrix (but of an N^{pol} membered system):

$$\mathbf{M} = \mathbf{F}\,\mathbb{A} = \mathbf{F} \left(\alpha^{-1} + \mathbb{T} \right)^{-1} \qquad \textbf{(3.15)}$$

$\mathbb{A}$ is obtained either by an exact matrix inversion or by solving the associated linear equations by iteration. It should be noted that equation (3.15) is a self consistent solution for any field, e.g. the electric field of QM during any stage of e.g. the Hartree-Fock procedure, and can expressed in terms of integrals over any basis set, which can be added to the vacuum Hamiltonian.

The $\{t(\mathbf{p};\mathbf{q})\}$ are, when appropriate, screened according to the method described by Thole[31] in which (atomic) polarizabilities are taken as related to (model) charge distributions, the widths of which are related to the $\{\alpha_p\}$. This leads also to a consistent screening of the potentials and fields of interaction for overlapping charge distributions.

In general the polarizabilities are constructed following Thole's original recipe and parametrization for obtaining (molecular) polarizabilities with experimental accuracy. This model has been reparametrized, also for computed polarizabilities from specific basis sets[34]. The advantage of this way of treating the relay matrix is that only atomic polarizabilities are needed as input, while changes in geometry will be automatically reflected in $\mathbb{A}$. Optionally one may reduce parts of $\mathbb{A}$ first to group polarizabilities so as to reduce the dimensionality of the problem. For a detailed description of the DRF model and its implementation the reader is referred to the paper published recently by de Vries *et al.*[20], this paper also descibes the extension of the DRF model with a third level of detail, a dielectric continuum surrounding the first few discrete solvent layers.

Thus in the DRF model the energy can be obtained as the expectation value of the DRF hamiltonian without the need for an iterative solution scheme. Furthermore the electrons in the quantum system are directly correlated with the classical charge distributions modeled by polarizabilities, thus the dispersion interaction between classical and quantum system is included. When a wave function for an excited state is used instead of that for the ground state, the dispersion interaction will be different, so the DRF model allows to model the effect of dispersion on spectral transitions.

3.3 Computational Details

In this study, only the dielectric model has been used to simulate the effect of a non-symmetrical solvent shell around the ethylene molecule. The adopted geometry of ethylene is shown in figure 3.2.

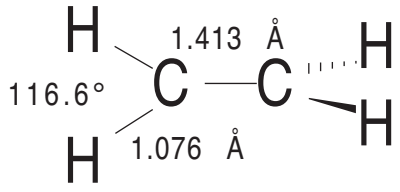

Figure 3.2 Adopted ethylene geometry.

Calculations in vacuum should yield symmetric wave functions with zero dipole moments for both ground and excited states at any point of the twisting energy surface. In the calculations presented here the Dunning-Huzinaga double valence (DZV) basis was used. The singlet ROHF vectors for the N state were used to define the reference configuration in an all valence CISD (~ 60.000 determinants involved). For all rotation angles, the CI wave functions yielded perfectly zero dipole moments for both the ground and the investigated excited states.

A non-symmetrical reaction potential was obtained from the dielectric continuum with various dielectric constants, generated by a localized charge density for the near 90° twist angles, which was obtained from a closed shell RHF procedure, in which an a^2 solution was obtained with a considerable dipole moment (μ_z ~ 4.0 Debye). Although physically incorrect in vacuo, this localized wave function yields a reasonable electron density distribution for a polarized excited state.

For the necessary boundary between discrete and continuum parts a Connolly surface[38] defined at twice the Van der Waals radii of the ethylene atoms around the geometry of the solute at hand, was taken. This distance was considered large enough to avoid unphysical polarizations[23]. The point density was chosen such that about 600 surface elements resulted. Reaction potentials are obtained by solving numerically appropriate Poisson equations. At the selected geometries, self consistent reaction potentials from the "closed shell" RHF (a^2) wave functions were obtained and added to the one-electron Hamiltonian in the CISD calculations.
This procedure was performed for ε=2.0, 4.0, 6.0 and 10.0, which are typical values for a range of non-hydrogen bonding organic solvents with increasing polar behavior.

3.4 Results and Discussion

The vacuum energies of the states of interest of ethylene were obtained from the first series of calculations. Since Buenker et. al. showed the crossing surface between the Z and V states of ethylene, at a twist angle of approximately 80° for the central bond[17], to be the twist region highly sensitive to polarization, the investigation was restricted to the 70-90° twist area.

In the CISD calculations, all 12 valence electrons were included from the reference singlet ROHF wave function and were allowed to excite into the complete virtual space (17 virtuals) thus leading to a CI space of 60.480 determinants. Results are given in table 3.1.

twist angle (°)	70	75	80	85	90
N	-78.12256	-78.11431	-78.10736	-78.10260	-78.10088
Z*	-77.96553	-77.96810	-77.96996	-77.97108	-77.97145
V*	-77.94613	-77.95858	-77.96858	-77.97519	-77.97753

Table 3.1 CISD vacuum energies (a.u.) of the N, Z and V state of ethylene in the 70-90° twist range (* See figure 3.4 for graphical representation of the potential energy surface of the Z and V states)

ε	Ψ_{RHF} (a.u.)	μ_z (Debije)	Ψ_{ROHF} (a.u.)	μ_z (Debije)
vacuo	-77.80991	+ 3.760	-77.93843	0.000
2.0	-77.81122	+ 3.887	-77.93715	+0.095
4.0	-77.81212	+ 3.972	-77.93625	+0.161
6.0	-77.81247	+ 4.006	-77.93590	+0.186
10.0	-77.81278	+ 4.034	-77.93563	+0.208

Table 3.2 SCF energies (a.u.) and dipole moments (Debije) of the Ψ_{RHF} and Ψ_{ROHF} singlet wave functions at different values of ε

These CI expansions lead to perfectly zero dipole moments for all states at all investigated geometries, which shows that these CI expansions can reproduce the desired symmetrical wave functions in vacuo. At this point, these findings differ from those by

Schaefer III and Brooks[15], who found non zero dipole moments for the D_{2d} Z and V states in similar expansions. Results of the reaction field calculations with the closed and open shell RHF wave functions in the (non-)equilibrium reaction potentials of the former are shown in table 3.2.

It should be noted that only geometries near 90˚ are able to yield such a polarized RHF wave function, since increasing overlap between the "p_z" orbitals on the carbon centers on decreasing twist angles will lead to a delocalized RHF solution.

	"μ^+"				"μ^-"			
twist angle	E_{tot} (a.u.)	μ_z (D)	"a^2"	"b^2"	E_{tot} (a.u.)	μ_z (D)	"a^2"	"b^2"
70˚								
ε=2.0	-77.96463	+0.657	.669	-.566	-77.94481	-0.349	.507	.618
ε=4.0	-77.96435	+1.073	.700	-.526	-77.94377	-0.592	.467	.649
ε=6.0	-77.96431	+1.226	.710	-.512	-77.94355	-0.669	.452	.660
ε=10.0	-77.96431	+1.353	.718	-.499	-77.94297	-0.731	.439	.669
75˚								
ε=2.0	-77.96751	+1.183	.720	-.502	-77.95716	-0.894	.459	.687
ε=4.0	-77.96744	+1.802	.764	-.428	-77.95601	-1.317	.383	.734
ε=6.0	-77.96795	+1.997	.777	-.403	-77.95553	-1.437	.357	.747
ε=10.0	-77.96818	+2.148	.787	-.382	-77.95510	-1.522	.337	.757
80˚								
ε=2.0	-77.97099	+2.885	.856	-.165	-77.96672	-2.592	.137	.848
ε=4.0	-77.97211	+3.090	.865	-.108	-77.96513	-2.599	0	.855
ε=6.0	-77.97270	+3.143	.866	-.097	-77.96448	-2.575	0	.856
ε=10.0	-77.97314	+3.185	.867	-.088	-77.96392	-2.551	0	.857
85˚								
ε=2.0	-77.97534	+2.191	.805	.340	-77.96954	-1.896	.352	-.805
ε=4.0	-77.97638	+2.762	.843	.235	-77.96823	-2.266	.248	-.840
ε=6.0	-77.97686	+2.895	.851	.208	-77.96766	-2.322	.846	-.221
ε=10.0	-77.97731	+2.991	.857	.188	-77.96714	-2.349	.201	-.851
90˚								
ε=2.0	-77.97719	+1.781	.774	.417	-77.96811	-1.474	.772	-.423
ε=4.0	-77.97799	+2.465	.824	.313	-77.96858	-1.941	.319	-.817
ε=6.0	-77.97823	+2.647	.835	.285	-77.96802	-2.047	.291	-.828
ε=10.0	-77.97858	+2.778	.843	.263	-77.96751	-2.107	.269	-.835

Table 3.3 CISD total energies (a.u.), dipole moments (Debije) and CI coefficients of both examined (polarized) excited states of twisted ethylene

A remarkable observation is that the energy gap between the closed shell and the open shell wave functions at the HF level yields a reasonable estimate of the energy gap between the ground state and the 'polarized excited state' (0.128 a.u at the HF level in vacuo against 0.129 a.u. at the CISD level with singlet open shell orbitals as reference, see table I and II for actual values). Furthermore, when using the polarized closed shell orbitals in an all valence CISD expansion at the D_{2d} geometry in vacuo, an energy similar

to those of the symmetrical first excited state is obtained (E_{CI} = -77.97897 a.u., μ_z = 3.232 Debye for this polarized state).

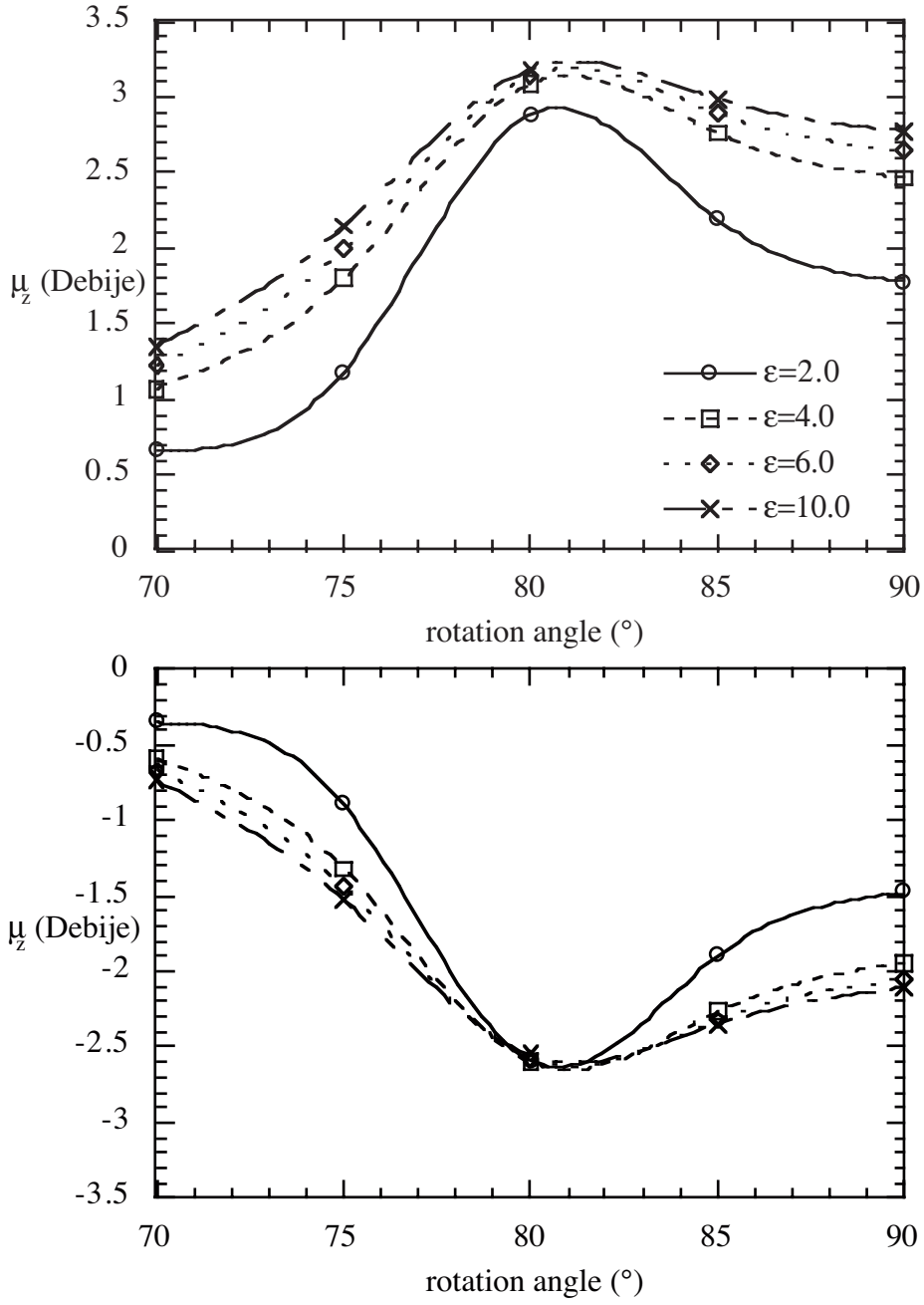

Figure 3.3 Polarized continuum induced dipole moments (Debije) of the two ethylenic excited states of interest on progressive twisting at various values of ε.

The total energies (E_{CI} + E_{DRF}) of the CISD expansion in the singlet ROHF orbitals of the three lowest lying states in the non-equilibrium reaction potentials, as well as the CI coefficients for the a^2 and b^2 contributions of the first two excited states are reported in table 3.3.

As can be seen from the CI coefficients, strong polarization occurs in the vicinity of the crossing of the 'pure' Z and V states in vacuo. This is emphasized in figure 3.3, which shows the dipole moments of the first two excited states in the 70-90° twist angle region.

A most remarkable feature from the observed dipole moments is the inability of the weak dielectric to maintain the large dipole moment on progressive twisting beyond the 80° point. From these findings, the conclusion can be made that for nonpolar solvents the weak electrostatic interactions with the solute are too small to sufficiently stabilize the polar state after formation. This can also be related to the total energies ($E_{CI}+E_{DRF}$) of the investigated excited states. In comparison with the vacuum CI energies of the non-localized Z and V states, all lowest lying polarized states except for ε=2.0 are stabilized relative to the vacuum lowest lying state (figure 3.4).

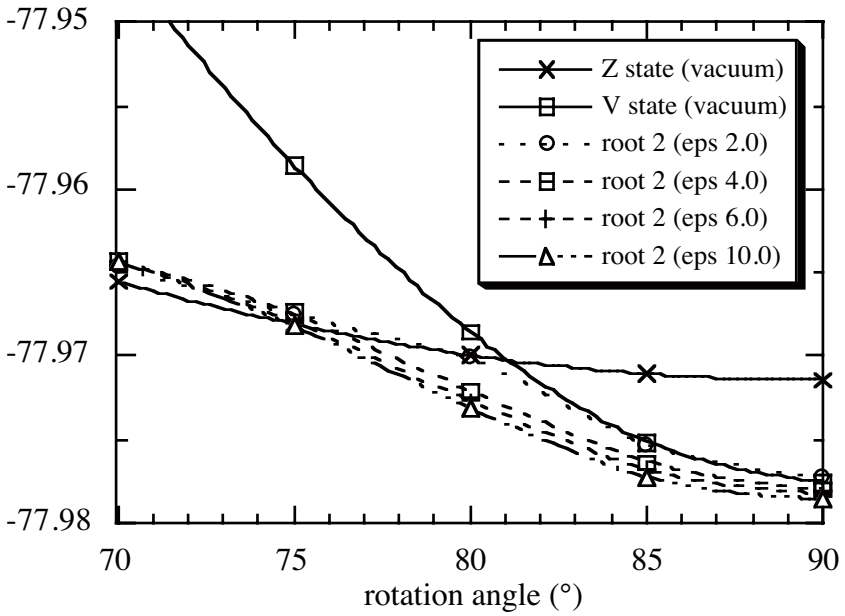

Figure 3.4 Total energies (a.u.) of embedded lowest excited states (dashed lines) and vacuum energies of the two excited states of interest (solid lines)

Another interesting observation when examining the CI coefficients of the excited states along the twisting coordinate is the switch of the dipole moment with positive sign from a "V state symmetry" ($c_1.a^2-c_2.b^2$) for twist angles α≤80° to a "Z state symmetry" ($c_1'.a^2+c_2'.b^2$), the state with the positive dipole moment always being the lowest in energy since they couple favorably with the external potential.

Figure 3.5 shows that this can be seen in terms of an avoided crossing between these states, in which the solvent asymmetry provides the required coupling for the occurrence of the avoided crossing of the Z and V state. This coupling of the dipole moment with the state lowest in energy has, to the best of our knowledge, not been reported in earlier studies.

Finally, investigation of the energy gap between the polarized excited states and the twisted ground state in the D_{2d} symmetry shows a significant lowering in energy of these

states in comparison with the vacuum energies, which is in agreement with earlier made assumptions.

It should be noted that the solvent model applied here is a simulation of an equilibrium situation, which especially for short-living polarized states (lifetime within the limit of the relaxation time of the solvent) in fact leads probably to an overestimation of the stabilizing effect from the solvent. On the other hand, the distance between the ethylene charge distribution and the boundary is so large, that the reaction field will be too small to account for the total electrostatic part of the solvation energy[23].

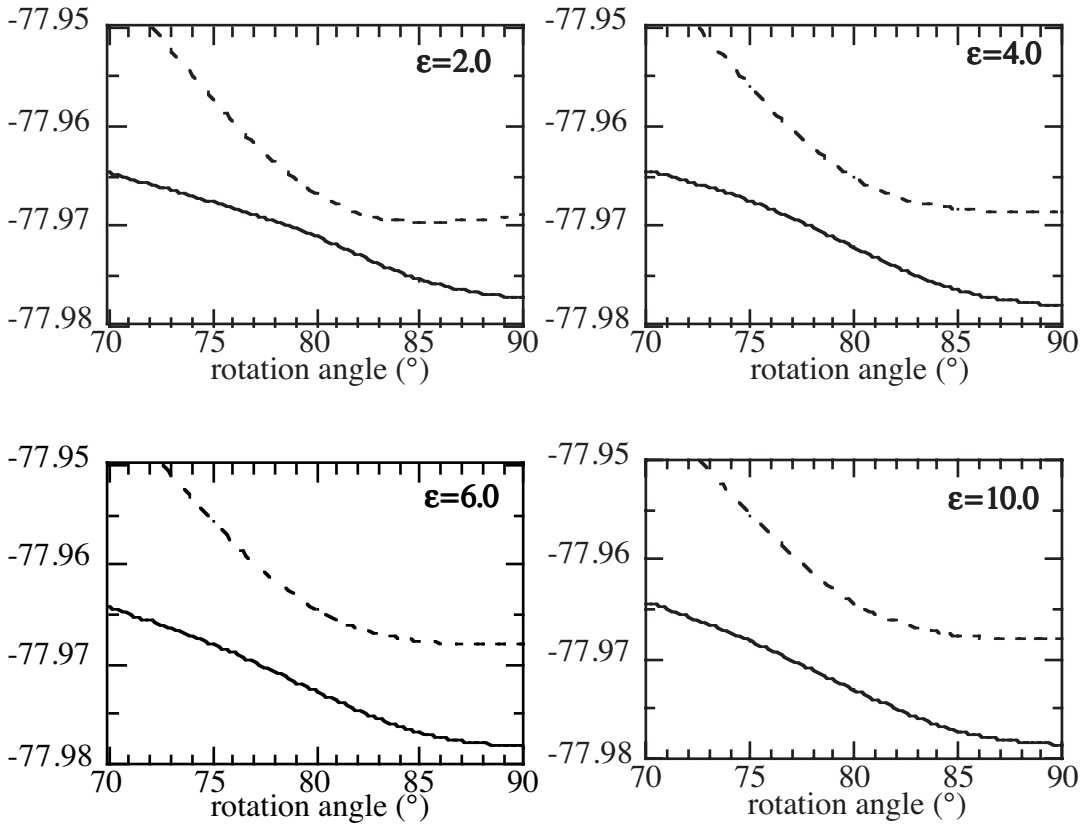

Figure 3.5 Total energies (a.u.) of second (solid line) and third root (dashed line) of ethylene as a function of rotation angle in various dielectrics.

DRF calculations in which discrete, classically described solvent layers with explicit molecular polarizabilities are used as a model for the first solvent shells have shown to give a quantitatively correct description of the various contributions in the solvent-solute interactions[26]. The results of this study are presented in the next chapter.

It can also be expected that symmetrical alkenes with stronger polarizable functional groups (like tetrachloro- or tetraphenylethylene) will show a more explicit behavior on the changes in solvent polarity. Unfortunately, the bulk of the theoretical investigations described in this thesis had to be limited to ethylene due to the unfeasability of the calculations on larger systems at similar levels of theory.

3.5 Conclusion

The presence of solvent layers with low symmetry around the twisted excited states of ethylene, here modeled by a dielectric in equilibrium with a prepared polarized state, effectively leads to large charge separations in the vicinity of the crossing intersection between these low lying excited (Z and V) states of ethylene. For dielectrics modeling (weakly) polar solvents, the energy of the lowest polarized excited state is stabilized relative to the pure Z and V states in vacuo. This is emphasized by the remaining dipole moments for those states on progressive twisting beyond the 80˚ point. The strong decrease in dipole moment on progressive twisting, together with the lack of stabilization of the polar state for a dielectric with ε=2.0 suggests that a relatively strongly polar compound in the various contributions of the solvation stabilization is needed to trap the polarized states in the near perpendicular geometries of the ethylene.

The lowest lying polarized state switches from V to Z symmetry around the 80˚ twisting point of the central bond (the crossing region of the Z and V *in vacuo* potentials), which is in nice agreement with earlier findings. The dipole moment of both states changes from sign when the avoided crossing has taken place.

The intriguing features of the abovementioned observations justify a more detailed description of the solvent, i.e. modelling the solvent by means of classically described discrete polarizable solvent molecules, to investigate whether these remarkable findings still hold in a more sophisticated treatment of the simulation. Especially the fact that a *polarized* dielectric had to be used to induce the symmetry breaking in the ethylene excited states may have biased the outcome and findings of this study, demands a more refined investigation. Therefore, the next chapter will be dedicated to the behaviour of the near-perpendicular excited states of ethylene in various solvents modelled by discretely described solvent shells in equilibrium with non-polarized ethylene.

3.6 References

1. Q. Wang, R.W. Schoenlein, L.A. Peteanu, R.A. Mathies and C.V. Shank, Science, **266**, 422-424 (1994).
2. V. Bonacic-Koutecky, P. Bruckmann, P. Hiberty, J. Koutecky, C. Leforestier and L. Salem, Angew. Chem., Int. Ed. Engl., **14**, 575-576 (1975).
3. W. Schuddeboom, S.A. Jonker, J.M. Warman, M.P. de Haas, M.J.W. Vermeulen, W.F. Jager, B. de Lange, B.L. Feringa and R.W. Fessenden, J. Am. Chem. Soc., **115**, 3286-3290 (1993).
4. B.I. Greene, Chem. Phys. Lett., **79**, 51-53 (1981).
5. C.L. Schilling and E.F. Hilinski, J. Am. Chem. Soc., **110**, 2296-2298 (1988).
6. J. Morais, J. Ma and M.B. Zimmt, J. Phys. Chem., **95**, 3885-3889 (1991).
7. Y-P. Sun and C.E. Bunker, J. Am. Chem. Soc., **116**, 2430-2433 (1994).
8. J. Ma and M.B. Zimmt, J. Am. Chem. Soc., **114**, 9723-9724 (1992).
9. E. Lenderink, K. Duppen and D.A. Wiersma, J. Phys. Chem., **99**, 8972-8977 (1995).
10. J. Saltiel, J. Am. Chem. Soc., **89**, 1036-1037 (1967).
11. J. Saltiel, D-H. Ko and S.A. Fleming, J. Am. Chem. Soc., **116**, 4099-4100 (1994).
12. D.B. Toublanc, R.W. Fessenden and A. Hitachi, J. Phys. Chem., **93**, 2893-2896 (1989).
13. T. Tahara and H. Hamaguchi, Chem. Phys. Lett., **217**, 369-374 (1994).
14. R.S. Mulliken, Phys. Rev., **41**, 751-758 (1932).
15. B.R. Brooks and H.F Schaefer III, J. Am. Chem. Soc., **101**, 307-311 (1979).
16. R.J. Buenker and S.D. Peyerimhoff, Chem. Phys., **9**, 75-89 (1976).
17. R.J. Buenker, V. Bonacic-Koutecky and L. Pogliani, J. Chem. Phys., **73**, 1836-1849 (1980).
18. P. Th. van Duijnen, A.H. Juffer and H.P. Dijkman, J. Mol. Struct. (THEOCHEM), **260**, 195-205 (1992).
19. B.T. Thole and P. Th. van Duijnen, Theor. Chim. Acta, **55**, 307-318 (1980).
20. A.H. de Vries, P.Th. van Duijnen, J.A.C. Ruhlmann, J.P. Dijkman, H. Merenga and B.T. Thole, J. Comp. Chem., **16**, 37-55 (1995).
21. M. Dupuis, A. Farazdel, S.P. Karma and S.A. Maluendes, *HONDO: A General Atomic and Molecular Electronic Structure System*, in: MOTECC, Ed: E. Clementi, ESCOM, Leiden, The Netherlands, 1990.
22. A.H. Juffer, E.F.F. Botta, B.A.M. van der Keulen, A. van der Ploeg and H.J.C. Berendsen, J. Comput. Phys., **97**, 144-171 (1991).
23. A.H. de Vries, P. Th. van Duijnen and A.H. Juffer, Int. J. Quant. Chem., Quant. Chem. Symp., **27**, 451-466 (1993).
24. J. Tomasi and M. Persico, Chem. Rev., **94**, 2027-2094 (1994).
25. M. Karelson and M.C. Zerner, J. Am. Chem. Soc., **112**, 9405-9406 (1990).
26. A.H. de Vries and P. Th. van Duijnen, Int. J. Quant. Chem., **57**, 1067-1076 (1996).
27. J. Gao and X. Xia, Science, **258**, 631-635 (1992).
28. J. Gao, Theor. Chim. Acta, **96**, 151-156 (1997).
29. M.A. Thompson and G.K. Schenter, J. Phys. Chem., **99**, 6374-6386 (1995).

30. M.A. Thompson, J. Phys. Chem., **100**, 14492-14507 (1996).
31. B.T. Thole and P. Th. van Duijnen, Theor. Chim. Acta, **63**, 209-221 (1983).
32. C.M. Breneman and K.B. Wiberg, J. Comp. Chem., **11**, 361-373 (1990).
33. B.T. Thole, Chem. Phys., **59**, 341-350 (1981).
34. P. Th. van Duijnen and M. Swart, J. Phys. Chem. A, **102**, 2399-2407 (1998).
35. J.C. Slater and J.G. Kirkwood, Phys. Rev., **37**, 682-697 (1931).
36. B.R. Brooks, R.E. Bruccoleri, B.D. Olafsson, D.J. States, S.J. Swaminathan and M. Karplus, J. Comp. Chem., **4**, 187-217 (1983).
37. P. Th. van Duijnen and A.H. de Vries, Int. J. Quant. Chem., **60**, 1111-1132 (1996).
38. M.L. Connolly, Science, **221**, 709-713 (1983).

Solvent-Induced Charge Separation in the Excited States of Symmetrical Ethylene:

A Direct Reaction Field Study

4.1 Introduction

One of the most fundamental processes in chemistry is the photo-induced cis-trans isomerization involving an olefinic double bond[1]. The importance of this process is illustrated by its presence in a large number of biological systems, for instance the ultra-fast cis-trans isomerization in the retinal chromophore of rhodopsin which triggers a series of events ultimately leading to vision in mammals[2, 3]. An overwhelming number of both theoretical[4-26] and experimental[3, 27-56] studies focussing on the dynamics, lifetimes and electronic features of these isomerizations in a wide variety of olefins has been performed in order to gain deeper insight in this process.

The first study of the electronic features of cis-trans isomerizations dates back to 1932 when Mulliken[1] predicted that the (π,π->π,π^*) excited state should undergo a large intramolecular rearrangement due to rotation around the ground state double bond from a planar ground state geometry to a (near) perpendicular excited state geometry, the so called phantom state[57]. By now it is well accepted that the driving force behind this conformational relaxation is the reduction of the bond order in this bond accompanied by the repulsion of the two 'non-bonding' π-electrons and the opposite substituents on either side of the double bond.

An interesting feature of this rearrangement is the possible occurrence of an avoided crossing between the S_1 (π,π^*) and S_2 (π^*,π^*) surfaces in the vicinity of the phantom state geometry. On the basis of a simple two electrons in two orbitals description it was suggested that the determinants that give rise to these singlet excited states should be of ionic character (a^2, b^2)[1, 57]. As a consequence, the avoided crossing can lead to the occurrence of large dipole moments in situations where, due to symmetry breaking by for instance asymmetric substitution, the equivalence in the weight of both determinants is no longer present. Therefore even D_2 symmetrical alkenes, which lack a permanent dipole moment in their ground state configuration, can exhibit large dipole moments in their relaxed excited states geometries.

A large number of both experimental[28, 29, 35, 39, 43, 44, 47, 50, 53, 56] and theoretical[4, 10, 13, 16, 24, 58-60] studies have been performed in attempts to gain both experimental evidence as well as additional information about the driving forces governing this symmetry breaking, which is often referred to as sudden polarization[5], especially in the condensed phase.

The most direct evidence for the charge transfer (CT) character of the tetraphenylethylene (TPE) relaxed excited state has been reported by Schuddeboom et. al., who performed Flash-Photolysis Time-Resolved-Micro-Conductivity (FP-TRMC) experiments[44]. A considerable increase in microwave absorption was observed upon excitation of the TPE with a laser pulse, which is indicative of a highly dipolar excited state.

Other studies on TPE have revealed a strong correlation between the lifetime of this polarized excited state and solvent polarity. A spectacular drop in lifetime is observed when the solvent becomes more polar. Schilling and Hilinsky observed a dramatic drop in TPE excited state lifetime from several nanoseconds in non-polar solvents to only a few hundreds of picoseconds in (di)polar solvents[35]. Picosecond optical calorimetry studies by Ma et al. showed a decrease of the energy gap between ground and excited state of several (*para*-substituted)-TPEs with increasing solvent polarity, which has led to the

suggestion that the energy difference between ground and excited state is a measure for the coupling between the two states, thus explaining the decrease in lifetime of CT states in polar solvents[43, 47].

The avoided crossing has also been suggested to play an important role in the isomerization of retinal which indicates the generality of its occurrence in cis-trans isomerizations[3].

From a theoretical point of view, various attempts have been made to describe the process of sudden polarization in symmetrical alkenes. Several configuration interaction (CI) studies on ethylene[10, 13] have shown that at (near) perpendicular geometries three important singlet states arise; the N state, which is the biradicaloid ground state at this geometry, and the ionic Z and V states, these states become degenerate at a central bond twist angle of about 80°. In the vicinity of this degeneracy, lowering of the nuclear symmetry by pyramidalizing one of the carbon centers leads to the formation of considerable dipole moments in the Z and V state of ethylene.

These calculations in vacuum clearly point out the necessity of symmetry breaking to allow polarization to occur, in this case achieved by lowering the nuclear symmetry of ethylene. It was concluded from these studies that at (near) perpendicular geometries, the lowest energy conformation of the ethylene excited state must be of a zwitterionic nature and only exhibit C_s symmetry . The outcome of these studies has led to the general belief that intramolecular symmetry breaking (e.g. the pyramidalization of one of the two carbon centers forming the central olefinic bond) is an exothermic process and, for that reason, the twisted excited state of these olefins is of an *intrinsically* zwitterionic nature[44], where the solvent dependent lifetimes are caused by the more effective stabilization of the zwitterion by more polar solvents[39]. This would lead to shorter lifetimes due to the narrowing of the gap between the photo-excited and ground state potential energy surfaces and hence to an enhanced radiationless transition rate. However, these assumptions are not supported by the work presented in chapter 2, where it was suggested that an increasing size of the functional groups attached to the carbons forming the olefinic bond reduces or even prohibits the stabilization of the zwitterionic excited state by intramolecular symmetry breaking (i.e. pyramidalization).

In addition, numerous spectroscopic studies on for instance *cis*-stilbene[40] and TPE[28, 29, 43, 56] indicate that the observed solvatochromic dependence of the excited state behavior cannot be explained by pure charge transfer (CT) character in all cases. In fact, the CT state in such systems is only effectively populated in polar solvents, as was recently demonstrated by means of femto-second pump-probe experiments on TPE[56](see also chapter 5). These studies revealed that for nonpolar solvents an equilibrium exists between a nonpolarized, charge-resonant (CR) state and the CT state of TPE, which is in good agreement with earlier suggestions of a similar nature[29, 50]. It should be noted that in the work presented here this nonpolarized excited state is addressed to as a charge resonant (CR) rather than a biradical state. It is emphasized that, due to the ionic nature of the determinants involved in the description of these excited states, the names 'biradical' or 'biradicaloid structure' are at best misleading. The term 'biradical' is only an appropriate nomenclature for the near-degenerate states described by the ^{1}ab and ^{3}ab determinants at the phantom state geometry, for which the singlet-triplet splitting is small. A more extensive discussion on the nomenclature of the involved states can be found in chapter 5.

Based on the observed solvatochromic excited state CT behavior of (for instance) TPE in the experiments mentioned above, it should be interesting to investigate the solvent induced charge separation in the (in vacuo) charge symmetrical excited states of the parent alkene ethylene. In the condensed phase, the necessary lowering of symmetry is automatically provided by the finite number of solvent molecules surrounding the solute, leading to a low symmetry environment of the ethylene. It is therefore worthwhile to investigate the ability of various solvents to provide enough symmetry breaking to generate the charge separated states.

It has been shown in the previous chapter, by enveloping ethylene with a Connolly surface[61] carrying a nonsymmetrical distribution of dipole densities (i.e. a model for a solvent in equilibrium with a polarized solute), that an increase of the dielectric constant of the continuum leads to more pronounced polarization as well as stabilization for the ethylene excited states[24].

In this chapter the results of a study of the ability of several organic solvents with varying polarity as well as polarizability to "suddenly" polarize the ethylene excited states at near perpendicular geometries will be presented.

In order to achieve this the Direct Reaction Field (DRF) method has been employed. The DRF method is a hybrid quantum mechanical/classical (QM/MM) method for including the effect of surroundings, e.g. a solvent shell in quantum chemical calculations[62-64]. In this method the system of interest (in this case the ethylene) is described quantum mechanically using an ab initio or semi-empirical wave function whereas the surroundings are described classically by means of point charges and explicit polarizabilities. The DRF method is briefly discussed below.

It will be shown that increasing solvent polarity not only increases the expectation value of the ethylene dipole moment but that even for non-equilibrium solvent surroundings (i.e. a solvent in equilibrium with a non-polarized charge distribution of the ethylenic excited state) a distinct stabilization of the charge separated excited state can occur.

4.2 Description Of The Calculations

4.2.1 Direct Reaction Field Calculations

The DRF method combines a quantum mechanical description of a solute with a classical description of its surroundings and is schematically shown in Figure 3.1. This method has been extensively described in several publications[62-66] as well as in chapter 3. Therefore, only some specific issues that are relevant to the work presented here, will be discussed.

The computational level that is used to describe the quantum system in the DRF method can be of arbitrary complexity. The DRF method has been implemented for a number single determinant ab initio methods, e.g. Restricted Hartee-Fock (RHF) and Restricted Open Shell Hartree-Fock (ROHF) as well as for multi-determinant methods like Configuration Interaction (CI). The latter type of wavefunction is of obvious importance for the description of excited states and will be used in the present study.

The solvent molecules surrounding the 'quantum system' are described classically by a set of point charges and explicit polarizabilities centered on all atomic centra. The whole system (quantum mechanical and classical) can optionally be surrounded by a dielectric continuum for modeling bulk effects. The point charges used in this study were obtained by fitting to electrostatic potentials obtained from Hartee-Fock calculations in points selected according to the CHelpG scheme using Dunnings cc-pVDZ basis set[67]. The atomic polarizabilities used here were taken from an extensive study by Van Duijnen and Swart[68] who optimized the values used in the DRF method by fitting to a set of experimental polarizabilities according to a method developed by Thole[69]. The actual values of all parameters used are listed in the Appendix.

For the present study the ethylene (quantum system) was surrounded by 50 classical solvent molecules modeling approximately the first three solvent shells. A set of more or less random solvent shells was generated by performing fully classical Monte Carlo (MC) calculations[70] using the DRF force field. After equilibration, a simulation of 200,000 MC steps was performed from which 20 randomly chosen solvent conformations were saved for the actual QM/MM analysis. The whole system was constrained to a spherical cavity with a radius chosen to obtain the experimental density.

In these simulations the ethylene solute was also treated classically by fitting it with charges and polarizabilities in its vacuum (i.e. nonpolarized) N-state. This way it was assured that any polarization arising in the ethylene excited states can be regarded as "sudden" since the solvent shells represent the equilibrium surrounding of the nonpolarized ethylene.

The above described procedure was performed using ethane, tetrachloromethane, chloroform, acetone and carbon dioxide (CO_2) as solvents. All of these solvents have little internal degrees of freedom which make them attractive solvents for the MC sampling since the internal degrees of freedom can be omitted in these simulations. The choice of ethane and carbon dioxide as solvents deserves some further explanation since both of them are gases at ambient conditions. Ethane can be considered as a model system for nonpolar hydrocarbons like *n*-hexane but has the advantage of little internal degrees of freedom. Additionally, supercritical ethane has been used in experimental studies by Sun et al.[50] on the charge separation behavior of TPE and it was found that its effect on the CT character and excited state lifetime was comparable to that of *n*-hexane. Supercritical carbon dioxide was also used in the same study and despite its lack of a permanent dipole moment it was shown to exhibit behavior that is typical for polar solvents.

The influence of the different solvent configurations on the polarization and stabilization of the excited states of ethylene was investigated by performing mixed QM/MM calculations on the 20 solvent conformation obtained from the classical MC simulations The ethylene was described using a CI wavefunction including all single and double excitations from the valence orbitals using the vacuum orbitals of the N-state as the reference determinant (CISD). These reference orbitals were obtained from a singlet ROHF calculation using Dunning's DZV basis set[67]. Such a procedure is known to produce perfectly zero dipole moments[24] in vacuum which is an obvious requirement for the present study.

The use of a multi-determinant wavefunction in the DRF method introduces a complication for the evaluation of the dispersion contribution to the interaction energy between the quantum system and the classical solvent. This becomes evident when

considering the DRF-definition of the interaction energy between the classical system and single determinant wave function:

$$\Delta U_{int}^{QM/MM} = \sum_{A,i,j} q_i^A \vartheta_{ij} Z_j + e \sum_{A,i} q_i^A \langle \vartheta \rangle_i +$$
$$\sum_{A,i,j,r,s} q_i^A f_{ir} A_{rs} f_{sj} Z_j + e \sum_{A,k,j,r,s} q_j^A f_{jr} A_{rs} \langle f(s;k) \rangle +$$
$$\frac{1}{2} \sum_{i,j,r,s} Z_i f_{ir} A_{rs} f_{sj} Z_j + e \sum_{i,k,r,s} Z_i f_{ir} A_{rs} \langle f(s;k) \rangle + \quad \textbf{(4.1)}$$
$$\frac{\gamma}{2} e^2 \sum_{k,r,s} \langle f(k;r) A_{rs} f(s;k) \rangle + \frac{1}{2} e^2 \sum_{k,l,r,s} \langle f(k;r) \rangle A_{rs} \left(1 - \frac{\gamma}{2} P_{12} \right) \langle f(s;l) \rangle$$
$$+ \Delta U_{rep}^{QM/MM}$$

In this expression the first two terms describe the electrostatic interaction of the nuclei and electrons with the point charges of the solvent. The next two terms describe the interactions between the point charges and the dipoles induced by the nuclei and electrons and vice versa. The fifth and sixth term represent the screening of the nuclear repulsion and attraction, respectively. The seventh and eighth term describe the interaction of an electron with its own and the other electrons' induced dipole moments, the latter term is therefore a two-electron term which contains the induction and part of the dispersion interaction. The scaling factor γ is used for the dispersion and was shown to be roughly equal to the following expression including the second order perturbation theory expression (SOP) for the dispersion[66]:

$$\Delta U_{disp}^{SOP} \approx \left(\frac{E_{solvent}^i}{E_{solute}^i + E_{solvent}^i} \right) \Delta U_{disp}^{DRF} = \gamma \Delta U_{disp}^{DRF} \quad \textbf{(4.2)}$$

The scaling factor γ can be used to redefine the reaction field operator by scaling the integrals for the screening of the one-electron self-energy as well as the two-electron exchange contributions. The latter rescaling is only then possible when the exchange interaction is explicitly defined, i.e. when dealing with a single determinant wavefunction. The present calculations were therefore performed using $\gamma = 0$.

An estimate of the dispersion interaction was added afterwards by performing a series of separate DRF calculations on the R(O)HF wavefunctions corresponding to the three dominating determinants (a^2, b^2 and ab; the two zwitterionic and the biradical determinants) of the CI wavefunction.
These wave functions were constructed from the vectors used in the CI calculations in the corresponding solvent configurations without allowing orbital relaxations, ensuring the use of the same MO space in the estimation of the dispersion contributions. The thus obtained dispersion contributions were weighted by the normalized CI coefficients of the corresponding determinant.

Solvent	Ionization Potential (eV)	γ (with ethylenic N / Z,V state)
ethane	11.5	0.540 / 0.647
tetrachloromethane	11.47	0.539 / 0.646
chloroform	11.42	0.538 / 0.645
carbondioxide	13.77	0.584 / 0.687
acetone	9.69	0.497 / 0.609
ethylene (N state / Z,V state)	9.80 / 6.28	--

Table 4.1 Ionization potentials and resulting γ of applied solvents and perpendicular ethylene.

For the ionization potentials of the solvent molecules used in equation 4.2 experimental values were taken[71]. The ionization potentials of the various states of ethylene in its twisted geometry had to be determined theoretically, since for obvious reasons experimental data is lacking. The ionization potential of the biradical was extracted from two successive ROHF calculations, the first one describing the full electron configuration at this geometry and the second one in which one electron was removed from the system without allowing orbital relaxations. The difference between these two energies can be used as an estimate of the vertical ionization potential of the N-state of ethylene. The ionization potential of both the Z and V state, which were taken to be degenerate, was obtained by taking the excitation energy (energy difference between the N-state and the Z and V states) from the vacuum CISD calculations described above and subtracting it from the ionization potential of the N-state. The ionization potentials obtained in this way can be considered reasonable estimates of the ionization potentials of twisted ethylene in the N, V and Z states and are listed in Table 4.1 together with the values for the scaling factor γcalculated according to Eq. 2.

4.2.2 The Ethylene Geometry

The geometry of ethylene used in this study is shown in figure 4.1. Bond lengths and angles were taken from a RHF geometry optimization using a basis set of double zeta quality including polarization functions. In the present work all calculations were performed using a single twist angle (i.e. the H-C-C-H dihedral angle) of 81˚ which was found to be the angle where the maximum excited state polarizability occurs (*vide infra*) and therefore the maximum polarization effect can be expected at this angle.

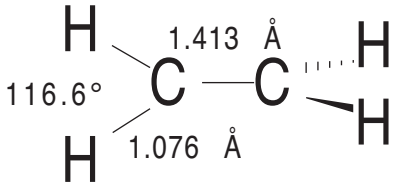

Figure 4.1 Adopted ethylene geometry.

It is questionable whether the explicit investigation of several ethylene geometries (i.e. at various twist angles) would provide valuable additional information, as the results from the study presented in chapter 3, where a polarized dielectricum only as a surrounding was used, already pointed out that this angle had a distinct optimum value for the polarizability of the excited state(s) regardless of the ε applied. Deviations from this value are likely to provide less explicit polarizations of the ethylene excited state charge density which for instance is shown by FFPT calculations in which the polarizability as a function of the twist angle near the perpendicular geometry is investigated for the electronic states of interest (*vide infra*).

The most suitable value for this twist angle has to be determined carefully to ensure the optimal response of the ethylene polarizability towards symmetry breaking by the solvent shells. In other words, the region for the highest probability of the avoided crossing has to be determined.

Although the most appropriate value for this property already has been the subject of previous studies[10, 13], the drawback there was that these calculations were performed without an external perturbation (for instance an electric field) applied to the wave function of the ethylene. Since this study is focussed on the likelyhood of sudden polarization occurring on the excited state potential energy surface of the twisting ethylene it was decided to include such effects in the determination of the ideal candidate geometry for this study.

To this purpose, a finite field (FFPT) calculation[72, 73] at the CISD level in the DZV basis[67] using HONDO 8.1[74] was employed by which the polarizability of the ethylene ground and excited state potential were calculated as a function of the abovementioned twist angle from the Taylor expansion of the total dipole moment:

$$\mu_j = \mu_{j,0} + \alpha_{ji} \cdot F_i + \frac{1}{2} \cdot \beta_{jii} \cdot F_i^2 + \frac{1}{6} \cdot \gamma_{jiii} \cdot F_i^3 \ldots \qquad \textbf{(4.3)}$$

Twist angles from 70 to 90˚ have been examined and polarizabilities of both ground and first excited state have been determined by taking steps of 1˚ in this region. From this work as well as from the earlier mentioned study using a polarized dielectricum only as environment, the $H_aC_a—C_bH_b$ dihedral angle was set to 81˚ (*vide infra*).

4.3 Results and Discussion

4.3.1 Polarizability of Ethylene Excited States at Different Twist Angles

The finite field method was used to calculate the polarizability of the first excited state of ethylene in the 70-90° twist area. Initial calculations using field strengths of ~ 10^{-4} a.u. revealed a strongly non-linear behavior of the polarizability component along the C-C bond at a twist angle of 81˚ as evident from Figure 4.2. An induced dipole moment of 2.8 Debye is obtained at a field strength of $5*10^{-5}$ a.u., further increase of the electric field increases the dipole moment only slightly. Thus the electric field of $5*10^{-5}$ a.u. is already sufficient to cause an energy difference between the two carbon atoms that is large enough for a full charge separation to occur.

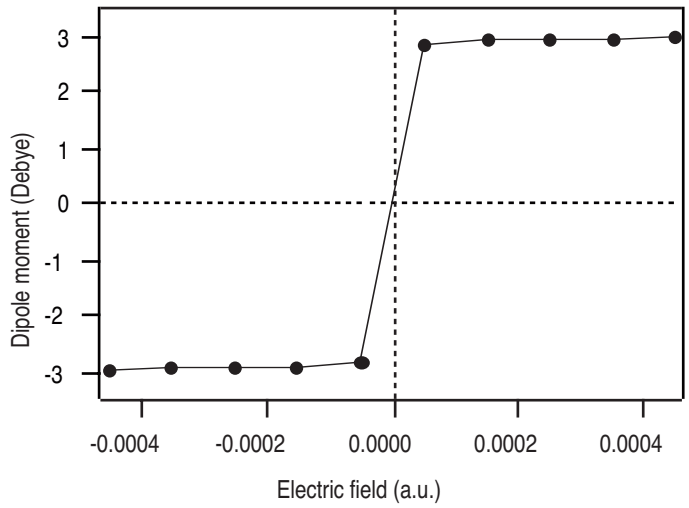

Figure 4.2 Induced dipole moment of the first excited state of 81˚ twisted ethylene.

Further calculations were performed using electric fields strengths of the order of 10^{-6} a.u., at these values the induced dipole moment was found to depend linearly on the electric field. The results obtained from these calculations for the component of the polarizability along the C-C axis at various twist angles are shown in figure 4.3.

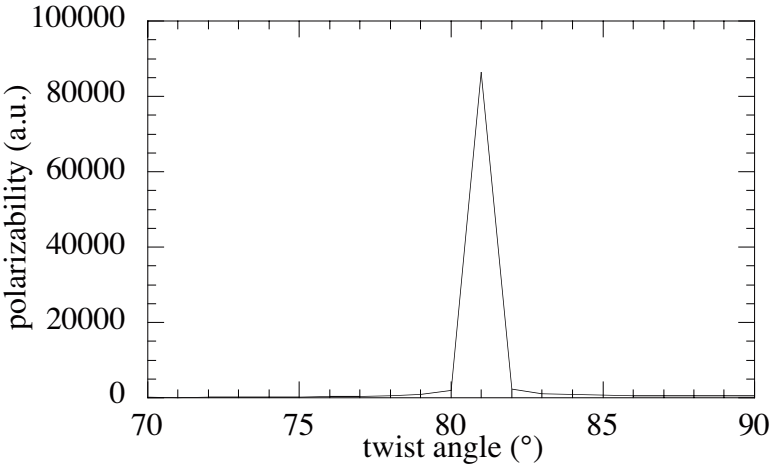

Figure 4.3 Polarizability component (a.u.) along the C-C axis of the first excited state of twisted ethylene as a function of the twist angle in the 70-90˚ range.

The largest polarizability was found for near-perpendicular ethylene with a twist angle of 81°. However, the dramatic increase shown in figure 4.3 should be interpreted with some caution, since the (near-)degeneracy of the Z and V surfaces in the vicinity of this geometry leads to a heavy mixing of both states resulting in an avoided crossing area for which the Born-Oppenheimer approximation no longer holds. Inclusion of the coupling between electronic and nuclear motion in the wavefunction (as for instance in a quantum dynamical treatment) would lead to a better description of the phenomenon but is beyond the scope of this work.

These finite field calculations clearly point out that, within the theoretical framework of choice in this study, the degeneracy of the Z and V surfaces leading to the enhanced excited state polarizability occurs around the 81˚ twist angle. Therefore, the twist angle was set equal to this value in the remainder of the work presented here.

4.3.2 Solvent-Induced Charge Separation in Twisted Ethylene

The solvent induced dipole moments along the central C-C bond obtained from the DRF calculations described above are listed in Table 4.2 for the three states of interest. These values represent the absolute value for the dipole moment averaged over the 20 CI calculations with different solvent conformation. In reality, the calculated values exhibit both positive and negative values, dependent of the direction of the effective (static) field of the surrounding solvent. Averaging over the actual values would result in near-zero dipole moments, which is undesirable here since this provides no insight into the magnitude of the polarization of especially the excited states (states 2 and 3) of the twisted ethylene.
In all the CI calculations, the dipole moments along the z-axis of the two excited states within a single calculation were of opposing signs, a direct result of the orthogonality (a^2 vs. b^2) of the two (heavily mixed) states.

	$\|\mu_z\|$ (Debye) state 1	$\|\mu_z\|$ (Debye) state 2	$\|\mu_z\|$ (Debye) state 3
ethane	0.00 (*±0.00*)	0.09 (*±0.06*)	0.08 (*±0.06*)
tetrachloromethane	0.01 (*±0.01*)	0.72 (*±0.46*)	0.70 (*±0.44*)
chloroform	0.05 (*±0.05*)	2.07 (*±0.92*)	1.93 (*±0.82*)
carbon dioxide	0.09 (*±0.06*)	2.62 (*±0.75*)	2.37 (*±0.59*)
acetone	0.10 (*±0.05*)	2.61 (*±0.66*)	2.38 (*±0.53*)

Table 4.2 Average solvent induced dipole moments (μ_z, absolute values) of the three roots of interest in the 81˚ twisted ethylene. Standard deviations shown in parenthesis.

The most interesting feature that can be observed from the results in Table 4.2 is the distinct difference in expectation values of the dipole moments of the, in vacuum, near-degenerate Z and V states (states 2 and 3) in non-polar and polar solvents. In the non-polar solvents ethane and tetrachloromethane the induced dipole moments of these states are relatively small, especially in ethane (~±0.1 D). In tetrachloromethane, slightly larger dipole moments (~0.7 D) are induced, although the spread (standard deviation) in the values is rather large (~0.45 D). In fact, dipoles ranging from approximately 0.2 to 1.6 Debye were obtained from the various calculations using tetra as a solvent. This indicates that an asymmetric distribution of polarizabilities around the ethylene can sometimes introduce enough symmetry breaking to induce charge separation, even if no permanent electric field is present.

The excited states of the twisted ethylene exhibit larger dipole moments in the more polar solvents. In chloroform, which exhibits medium polarity, the average dipole moments are already 2.0 D, although the spread is still large (~ ±0.9 D). Calculated dipoles ranged from 0.1 to 3.2 D, indicating that large polarization can take place in certain but not all solvent geometries.

When looking at CO_2 and acetone, induced dipole moments in the excited states are very large (~ 2.6 D) with a small spread compared to that of the less polar solvents (~ ±0.6 D; under 25% of the average induced dipole moment), indicating that in (nearly) every solvent configuration large excited state polarization is achieved. For instance, in acetone the excited state dipole moments are mainly ranging between 1.8 and 3.3 D.

Observations for the 'ground' state (state 1) are less dramatic; moderately small polarizations up to 0.1 D in acetone are found and show the expected correlation with increasing solvent polarity (or polarizability) and will not be discussed any further.

The results presented above clearly demonstrate that there is a relation between the nature of the solvent and the magnitude of symmetry breaking in the ethylenic excited states. In order to gain deeper insight in the origin of this relation a more detailed look into the interactions between the various electronic states of the twisted alkene and its solvent-surroundings is necessary.

Tables 5.3 to 5.8 specify the total interaction energy as well as the various components of that energy of the three states of interest of the 81˚ twisted ethylene with ethane, tetrachloromethane, chloroform, carbon dioxide and acetone respectively.

Four components contributing to that energy are specified:

- The electrostatic interaction (ΔE_{elec}), which is the interaction between the permanent charge distribution of the quantum system with the static charge distribution of the solvent.
- The dispersion interaction (ΔE_{disp}) between the quantum system and the solvent.
- The induction interaction (ΔE_{ind}), which is the interaction between the permanent charge distribution of the quantum system with the dipole moments it induces in the classical system.
- The polarization energy (ΔE_{pol}) consist of three contributions; the interaction between the quantum system and the moments induced by the classical charge distribution in the classical system (1), the interaction between the classical charge distribution and the moments that the quantum system induces in the classical system (2), and the cost of inducing all the dipoles in the classical system.

Note that this kind of decomposition is rather arbitrary since the 'permanent' charge distribution of the quantum system depends very much on the solvent surrounding it as shown above, however, this polarized charge distribution is taken as the permanent charge distribution for the evaluation of ΔE_{elec}. The tables also include an estimate of the short range repulsion interaction (ΔE_{rep}), this interaction between the quantum system and the classical surroundings is evaluated fully classically in the present implementation. Therefore this contribution is the same for all states. Furthermore, it should be realized that this contribution is not 'felt' by the electrons in the quantum system and is only included to get an estimate of the total interaction energy. For the evaluation of the interaction difference between different states it is irrelevant.

The main advantage of being able to breakdown the total interaction energy into its separate physically relevant components is that the origin of possible state particulate interactions can be detected.

	State 1	State 2	State 3
ΔE_{tot}	**-3.25**	**-4.77**	**-4.71**
ΔE_{rep}	4.23	4.23	4.23
ΔE_{pol}	0.02	0.03	0.03
ΔE_{ind}	-0.04	-0.06	-0.07
ΔE_{elec}	0.00	0.00	0.00
ΔE_{disp}	-7.46	-8.97	-8.90

Table 4.3 Various averaged contributions to the average total interaction energy of the three roots of interest in the 81° twisted ethylene with ethane (kcal·mol^{-1}).

Table 4.3 shows the interaction energies of the three electronic states of interest of ethylene in ethane solution. It clearly shows that for all states the only significant stabilizing contribution to the interaction energy is the dispersion interaction, which is therefore solely responsible for the larger interaction of the excited states with the solvent. No significant charge separation takes place in this solvent and therefore the electrostatic contribution to the interaction energy is zero. The same applies of course to ΔE_{pol} and ΔE_{ind}.

In the case of tetrachloromethane, similar observations can be made (Table 4.4). Again, the dispersion term is the only significant contribution to the interaction energy of each state. Only a very small increase is observed in the electrostatic interaction between the first excited state (root 2) and tetrachloromethane when compared with ethane, this is the interaction of the charge separated ethylene with the point charges that model the tetrachloromethane. This small charge separation is caused by the asymmetric distribution of polarizabilities around the ethylene as argued above.

In the weakly polar chloroform, some significant differences with the earlier discussed solvents occur (table 4.5). The dispersion interaction still is the main contributor to the total interaction energy. No significant difference in dispersion interaction occurs between the two excited states which was the same for the previous solvents.

However, here for the first time a significant difference in electrostatic interaction with the solvent occurs for these states. The first, lower lying excited state has an attractive interaction with the solvent, whereas the state with the roughly equal but opposing dipole moment has a repulsive electrostatic interaction with the field.

	State 1	State 2	State 3
E_{tot}	**-0.99**	**-1.69**	**-1.69**
ΔE_{rep}	2.44	2.44	2.44
ΔE_{pol}	0.01	0.03	0.03
ΔE_{ind}	-0.01	-0.05	-0.06
ΔE_{elec}	-0.03	-0.06	0.00
ΔE_{disp}	-3.40	-4.05	-4.10

Table 4.4 Various averaged contributions to the average total interaction energy of the three roots of interest in the 81° twisted ethylene with tetrachloromethane (kcal·mol^{-1}).

This can be rationalized by realizing that the solvent shell, especially in the case of a polar solvent, introduces an electric field with a more or less random direction at the position of the twisted ethylene solute. This field will in general have some component along the C-C bond of the ethylene which causes charge separation to occur if the field is large enough.

This leads to two charge separated stated with opposing dipole moments. The lowest of these states will have an attractive electrostatic interaction with the solvent which lowers its energy whereas the higher one has a repulsive interaction with the static field of the solvent and hence its energy increases.

	State 1	State 2	State 3
$\mathbf{E_{tot}}$	**-1.93**	**-3.31**	**-2.33**
ΔE_{rep}	2.62	2.62	2.62
ΔE_{pol}	0.02	0.25	0.11
ΔE_{ind}	-0.02	-0.37	-0.32
ΔE_{elec}	-0.13	-0.75	0.38
ΔE_{disp}	-4.42	-5.06	-5.12

Table 4.5 Various averaged contributions to the average total interaction energy of the three roots of interest in the 81˚ twisted ethylene with chloroform ($kcal \cdot mol^{-1}$).

As a result, the interaction with the solvent removes the degeneracy between the two excited states. The equilibrium electronic state of ethylene will therefore shift towards the polarized shape, unlike the case of ethane and tetra, where both excited states stay more or less degenerate. It can be seen in table 4.5 that there is also a contribution from the induction interaction to the total interaction energy, the magnitude of this component is similar for both the excited states which indicates that the magnitude of the dipole moments is about the same (see also Table 4.2) but they have opposing directions.

	State 1	State 2	State 3
$\mathbf{E_{tot}}$	**-4.09**	**-7.22**	**-4.77**
ΔE_{rep}	3.57	3.57	3.57
ΔE_{pol}	0.07	0.59	0.26
ΔE_{ind}	-0.05	-0.82	-0.67
ΔE_{elec}	-0.64	-2.26	0.33
ΔE_{disp}	-7.04	-8.30	-8.26

Table 4.6 Various averaged contributions to the average total interaction energy of the three roots of interest in the 81˚ twisted ethylene with carbon dioxide ($kcal \cdot mol^{-1}$).

For the polar solvents CO_2 and acetone (tables 4.6 and 4.7) the results are quite similar and resemble those found for chloroform. The dispersion interaction dominates the interaction energy of all states. The main difference with chloroform is the magnitude of the electrostatic interaction. This contribution is much larger in CO_2 and acetone for the second state (the first excited state). For CO_2 this may seem surprising because CO_2, unlike chloroform, does not exhibit a permanent dipole moment. However, CO_2 does have

a large quadrupole moment which apparently is enough to provide substantial electrostatic interactions with the induced ethylenic dipole moments. For acetone the contribution of the induction interaction is somewhat larger (for both excited states), probably because of the larger polarizability of acetone.

The marked difference in the polarization and stabilization of the ethylene excited state in ethane and CO_2 provides an explanation for the experimentally observed shortening of the TPE excited state lifetime in supercritical CO_2 compared to supercritical ethane by Sun et al.[50]

	State 1	State 2	State 3
$\mathbf{E_{tot}}$	**-3.81**	**-9.13**	**-6.38**
ΔE_{rep}	8.06	8.06	8.06
ΔE_{pol}	0.09	0.85	0.46
ΔE_{ind}	-0.07	-1.44	-1.15
ΔE_{elec}	-0.41	-2.49	0.27
ΔE_{disp}	-11.48	-14.11	-14.02

Table 4.7 Various averaged contributions to the average total interaction energy of the three roots of interest in the 81° twisted ethylene with acetone (kcal·mol^{-1}).

In CO_2, an additional stabilization of 1.5 kcal·mol^{-1} is observed for the second state (the first excited state) compared to the ground state which lowers the energy gap and therefore leading to an enhanced radiationless crossing rate between the two states, resulting in a shortening of the excited state lifetime. It should be emphasized that the solvent shells used here are in equilibrium with the non-polarized ethylene charge distribution (i.e. the ground state), which means that a considerable additional stabilization of the polarized excited state can be expected upon relaxation of the solvent on the polarized charge distribution of the ethylene. This will further decrease the excited state life time. This additional stabilization is absent in ethane.

Table 4.8 summarizes the solvent effect on the energy difference between the three states studied in this work. Negative values indicate a decrease in the energy gap between the two states whereas positive values represent an increase. The energy gap between the ground state and the first excited state decreases in all solvents. This is mainly caused by dispersion interactions as argued above. This dispersion contribution is always larger in the excited states, and hence lowers the energy gap.

	$\Delta\Delta E_{int}$ (kcal.mol^{-1}) (root 1-root 2)	$\Delta\Delta E_{int}$ (kcal.mol^{-1}) (root 2-root 3)
ethane	-1.52	0.00
tetrachloromethane	-0.70	0.00
chloroform	-1.78	+0.98
carbon dioxide	-3.13	+2.45
acetone	-5.32	+2.75

Table 4.8 Average solvent induced gap closure ($\Delta\Delta E_{int}$, kcal·mol^{-1}) between (root 1-root 2) and (root 2-root3) respectively in the 81° twisted ethylene.

The decrease in the energy gap is more pronounced in polar solvents. This is a direct consequence of the charge separation in the excited state which leads to enhanced electrostatic interactions between solvent and solute in this state. The energy gap between the two excited (nearly degenerate) states is not influenced by apolar solvents. In polar solvents however, the charge separation that occurs causes a distinct energy splitting between these two states. This is of course mainly caused by the electrostatic interactions between the polarized ethylene and the solvent. This interaction is attractive for the lower state while it is repulsive for the second excited state.

4.4 Summary and Conclusion

All valence CISD calculations at the 81˚ twist angle of ethylene using the Dunning-Huzinaga DZV basis were performed, embedding the quantum system in a discrete classical surrounding using the Direct Reaction Field Model. The classical surrounding consisted of 50 discretely described solvent molecules, each fitted with a molecular polarizability. 20 different solvent configurations were selected from a fully classical Monte Carlo simulation. This procedure was performed using ethane, tetrachloromethane, carbon dioxide, chloroform and acetone as solvents.

The 81˚ twist angle was chosen from a finite field study using the same wave function in vacuo. At this angle the excited state polarizability of the twisted ethylene proved to be the largest in this basis set, making this geometry the most likely candidate to be used for solvent induced sudden polarization studies.

The DRF studies revealed that the expectation value of the ethylenic excited state dipole moments remain small in the investigated non-polar solvents, ~±0.1 D in ethane and ~ ±0.7 D in tetra. Furthermore, the degeneracy of the two excited states was not lifted in these solvents which indicates that these solvents are not capable of breaking the symmetry of the excited state wave functions to a large extent. It can therefore be concluded that nonpolar solvents are unlikely to induce the sudden polarization in the twisted excited states of ethylene and that some sort of intramolecular symmetry breaking is required to generate the zwitterionic states.

The solvent-induced stabilization of the degenerate excited states with respect to the biradicaloid ground state is solely governed by the enhanced dispersion interaction with the solvent for these states. Even though this has to be treated with some caution, due to the approximate way this interaction is calculated, it is in agreement with intuitive concepts based on the assumed larger polarizabilities of excited states in general in comparison to their electronic ground state configuration.

A marked difference with the behavior mentioned above was observed in the more polar solvents chloroform, carbon dioxide and acetone. In these solvents, significant dipole moments (> 2 D) were generated in the ethylenic excited states. For the weakly polar chloroform there were still significant fluctuations between the values in various solvent configurations.

The more polar carbon dioxide and acetone showed a more pronounced polarization of the ethylene excited states, in (nearly) all investigated solvent configurations. In addition, a significant lift of the degeneracy of the two excited states was observed in these solvents (Table 4.8). This splitting between the two excited states is

most pronounced in acetone (~2 kcal·mol^{-1}). Analysis of the various contributions to the interaction energy show that the difference in electrostatic interaction with the solvent is mainly responsible for this splitting. Interestingly, the induction interaction had no significant influence on this process, suggesting that the polarity rather than the polarizability of the solvent is responsible for the symmetry breaking.

It can therefore be concluded that polar solvents are capable of breaking the symmetry of the ethylene excited states even when the alkene exhibits a symmetrical (i.e. unpyramidalized) nuclear configuration. It is emphasized that in all cases the surrounding solvent shells were in equilibrium with an unpolarized charge distribution. The inclusion of solvent relaxation will lead to more pronounced differences in excited state energies in cases where large dipoles are being generated and stabilized. Although beyond the scope of this work, this is an interesting topic to address in the future since the solvent-dependent narrowing of the gap between ground and excited state has been used as an explanation for the shortened lifetimes of the excited states in for instance tetraphenylethylene (TPE) as a function of increasing solvent polarity.

In experimental studies performed on the excited state behavior of TPE and other symmetrical olefins, it is usually assumed that the electronic structure of the twisted excited states of these alkenes was zwitterionic of nature due to an intramolecular symmetry breaking. The results of this work show that the solvent plays a very important role in the symmetry breaking. This is especially relevant for substituted symmetrical ethylenes since in these cases the steric repulsion between the substituents will make intramolecular symmetry breaking by pyramidalization rather unlikely, as has been reported in chapter 2.

4.5 Appendix

Atomic polarizabilities (A.U.) and VanderWaals Radii (Bohr)

C	8.6959	3.4015
H	2.7927	1.5118
O	5.7494	3.0236
Cl	16.1979	4.3240

CHELPG Derived Partial Charges (A.U.)

Acetone

C	-0.3276	-0.3289	0.7153
H	0.0828	0.0831	0.0928
O	-0.5751		

Chloroform

C	-0.1250
H	0.2300
Cl	-0.0350

Tetrachloromethane

C	-0.2440
Cl	0.0610

Carbondioxide

C	0.9092
O	-0.4546

Ethane

C	0.0150
H	-0.0050

Ethene (used in Monte Carlo solvent configuration generation)

C	-0.0962
H	0.0481

4.6 References

1. R.S. Mulliken, Phys. Rev., **41**, 751-758 (1932).
2. G. Wald, Science, **162**, 230-239 (1968).
3. Q. Wang, R.W. Schoenlein, L.A. Peteanu, R.A. Mathies and C.V. Shank, Science, **266**, 422-424 (1994).
4. C.E. Wulfman and S. Kumei, Science, **172**, 1061 (1971).
5. V. Bonacic-Koutecky, P. Bruckmann, P. Hiberty, J. Koutecky, C. Leforestier and L. Salem, Angew. Chem., Int. Ed. Engl., **14**, 575-576 (1975).
6. L. Salem and W-D. Stohrer, J. Chem. Soc. Chem. Commun., 140-143 (1975).
7. L. Salem and P. Bruckmann, Nature, **258**, 526-528 (1975).
8. L. Salem, Acc. of Chem. Res., **12**, 87-92 (1979).
9. R.J. Buenker and S.D. Peyerimhoff, Chem. Phys., **9**, 75-89 (1976).
10. R.J. Buenker, V. Bonacic-Koutecky and L. Pogliani, J. Chem. Phys., **73**, 1836-1849 (1980).
11. P. Bruckmann and L. Salem, J. Am. Chem. Soc., **98**, 5037-5038 (1976).
12. V. Bonacic-Koutecky, J. Am. Chem. Soc., **100**, 396-404 (1978).
13. B.R. Brooks and H.F Schaefer III, J. Am. Chem. Soc., **101**, 307-311 (1979).
14. G. Orlandi, P. Palmieri and G. Poggi, J. Am. Chem. Soc., **101**, 3492-3497 (1979).
15. M. Persico, J. Am. Chem. Soc., **102**, 7839-7845 (1980).
16. R.P. Johnson and M.W. Schmidt, J. Am. Chem. Soc., **103**, 3244-3249 (1981).
17. I. Nebot-Gil and J-P. Malrieu, Chem. Phys. Lett., **84**, 571-574 (1981).
18. I. Nebot-Gil and J-P. Malrieu, J. Am. Chem. Soc., **104**, 3320-3325 (1982).
19. V. Bonacic-Koutecky, M. Persico, D. Döhnert and A. Sevin, J. Am. Chem. Soc., **104**, 6900-6907 (1982).
20. I.D. Petsalakis, G. Theodorakopoulos and C.A. Nicolaidis, J. Chem. Phys., **81**, 5952-5956 (1984).
21. I.D. Petsalakis, G. Theodorakopoulos, C.A. Nicolaidis, R.J. Buenker and S.D. Peyerimhoff, J. Chem. Phys., **81**, 3161-3167 (1984).
22. I.D.L. Albert and S. Ramasesha, J. Phys. Chem., **94**, 6540-6543 (1990).
23. P. Piotrowiak, Chem. Phys. Lett., **241**, 387-392 (1995).
24. R.W.J. Zijlstra, A.H. de Vries and P.Th. van Duijnen, Chem. Phys., **204**, 439-446 (1996).
25. M. Merchán and R. González-Luque, J. Chem. Phys., **106**, 1112-1122 (1997).
26. V. Molina, M. Merchán and B.O. Roos, J. Phys. Chem. A, **101**, 3478-3487 (1997).
27. J.A. Marshall, Science, **170**, 137-141 (1970).
28. B.I. Greene, Chem. Phys. Lett., **79**, 51-53 (1981).
29. P.F. Barbara, S.D. Rand and P.M. Rentzepis, J. Am. Chem. Soc., **103**, 2156-2162 (1981).
30. B.H. Baretz, A.K. Singh and R.S.H. Liu, Nouv. J. Chim., **5**, 297-303 (1981).
31. F.E. Doany, E.J. Heilweil, R. Moore and R.M. Hochstrasser, J. Chem. Phys., **80**, 201-206 (1984).
32. A.G. Doukas, M.R. Junnarkar, R.R. Alfano, R.H. Callender, T. Kakitani and B. Honig, Proc. Natl. Acad. Sci. USA, **81**, 4790-4794 (1984).
33. W. Rettig, Angew. Chem., Int. Ed. Engl., **25**, 971-988 (1986).

34. E. Gilabert, R. Lapouyade and C. Rullière, Chem. Phys. Lett., **145**, 262-268 (1988).
35. C.L. Schilling and E.F. Hilinski, J. Am. Chem. Soc., **110**, 2296-2298 (1988).
36. H. Ephardt and P. Fromherz, J. Phys. Chem., **93**, 7717-7725 (1989).
37. C.T. Lin, H.W. Guan, R.K. McCoy and C.W. Spangler, J. Phys. Chem., **93**, 39-43 (1989).
38. D.B. Toublanc, R.W. Fessenden and A. Hitachi, J. Phys. Chem., **93**, 2893-2896 (1989).
39. J. Morais, J. Ma and M.B. Zimmt, J. Phys. Chem., **95**, 3885-3889 (1991).
40. D.H. Waldeck, Chem. Rev., **91**, 415-436 (1991).
41. R. Lapouyade, K. Cheschka, W. Majenz, W. Rettig, E. Gilabert and C. Rullière, J. Phys. Chem., **96**, 9643-9650 (1992).
42. S. Marguet, J.C. Mialocq and P. Millie, Chem. Phys., **160**, 265-279 (1992).
43. J. Ma and M.B. Zimmt, J. Am. Chem. Soc., **114**, 9723-9724 (1992).
44. W. Schuddeboom, S.A. Jonker, J.M. Warman, M.P. de Haas, M.J.W. Vermeulen, W.F. Jager, B. de Lange, B.L. Feringa and R.W. Fessenden, J. Am. Chem. Soc., **115**, 3286-3290 (1993).
45. L. Sun and H. Görner, Chem. Phys. Lett., **208**, 43-47 (1993).
46. J-M. Rodier and A.B. Myers, J. Am. Chem. Soc., **115**, 10791-10795 (1993).
47. J. Ma, G. Bhaskar Dutt, D.H. Waldeck and M.B. Zimmt, J. Am. Chem. Soc, **116**, 10619-10629 (1994).
48. J. Saltiel, D-H. Ko and S.A. Fleming, J. Am. Chem. Soc., **116**, 4099-4100 (1994).
49. K. Sandros and M. Sundahl, J. Phys. Chem., **98**, 5705-5708 (1994).
50. Y-P. Sun and C.E. Bunker, J. Am. Chem. Soc., **116**, 2430-2433 (1994).
51. T. Tahara and H. Hamaguchi, Chem. Phys. Lett., **217**, 369-374 (1994).
52. J-M. Viallet, F. Dupuy, R. Lapouyade and C. Rullière, Chem. Phys. Lett., **222**, 571-578 (1994).
53. E. Lenderink, K. Duppen and D.A. Wiersma, J. Phys. Chem., **99**, 8972-8977 (1995).
54. P. Piotrowiak, G. Strati, J. Warman and W. Schuddeboom, J. Am. Chem. Soc., **118**, 8981-8982 (1996).
55. J. Saltiel, Y. Zhang and D.F. Sears Jr., J. Am. Chem. Soc., **119**, 11202-11210 (1997).
56. R.W.J. Zijlstra, P. Th. van Duijnen, B.L. Feringa, T. Steffen, K. Duppen and D.A. Wiersma, J. Phys. Chem. A, **101**, 9828-9836 (1997).
57. L. Salem, Science, **191**, 822-830 (1976).
58. V. Bonacic-Koutecky, J. Cizek, D. Döhnert and J. Koutecky, J. Chem. Phys., **69**, 1169-1176 (1978).
59. V. Bonacic-Koutecky, R.J. Buenker and S.D. Peyerimhoff, J. Am. Chem. Soc., **101**, 5917-5922 (1979).
60. C.E. Wulfman and G.C. Hyatt, Proc. Indian Acad. Sci. (Chem. Sci.), **107**, 813-823 (1985).
61. M.L. Connolly, Science, **221**, 709-713 (1983).
62. B.T. Thole and P. Th. van Duijnen, Theor. Chim. Acta, **55**, 307-318 (1980).
63. P. Th. van Duijnen, A.H. Juffer and H.P. Dijkman, J. Mol. Struct. (THEOCHEM), **260**, 195-205 (1992).

64. A.H. de Vries, P.Th. van Duijnen, J.A.C. Ruhlmann, J.P. Dijkman, H. Merenga and B.T. Thole, J. Comp. Chem., **16**, 37-55 (1995).
65. P. Th. van Duijnen and A.H. de Vries, Int. J. Quant. Chem., **60**, 1111-1132 (1996).
66. A.H. de Vries and P. Th. van Duijnen, Int. J. Quant. Chem., **57**, 1067-1076 (1996).
67. T.H. DunningJr. and P.J. Hay, *Gaussian basis sets*, in: Methods of Electronic Structure Theory, Ed: H. F. Schaeffer. III, 1977.
68. P. Th. van Duijnen and M. Swart, J. Phys. Chem. A, **102**, 2399-2407 (1998).
69. B.T. Thole and P. Th. van Duijnen, Theor. Chim. Acta, **63**, 209-221 (1983).
70. M.P. Allen and D.J. Tildesley, *Computer Simulation of Liquids*, Clarendon Press, Oxford, 1987.
71. R.C. Weast, M.J. Astle and W.H. Beyer, *Handbook of Chemistry and Physics*, CRC Press Inc., Boca Raton, Fl., USA, 1985-1986.
72. H.D. Cohen and C.C.J. Roothaan, J. Chem. Phys., **43**, S34-S39 (1965).
73. H.A. Kurtz, J.J.P. Stewart and K.M. Dieter, J. Comp. Chem., **11**, 82-87 (1990).
74. M. Dupuis, A. Farazdel, S.P. Karma and S.A. Maluendes, *HONDO: A General Atomic and Molecular Electronic Structure System*, in: MOTECC, Ed: E. Clementi, ESCOM, Leiden, The Netherlands, 1990.

Excited State Dynamics of Tetraphenylethylene:

Ultrafast Stokes Shift, Isomerization and Charge Separation

5.1 Introduction

One of the most fundamental, yet simplest chemical processes involves rotation around a chemical bond. While many molecules exhibit this effect in the ground state, there are several important systems where isomerization is solely a photon driven process. The most famous example is rhodopsin[1], where a cis-trans isomerization in the retinal pigment triggers a series of events that ultimately lead to vision. The primary step in this reaction is thought to proceed via a nonadiabatic crossing to the ground state surface[2]. Other typical examples are molecules like stilbene and azobenzene. Stilbene is the prototype alkene and has been studied both in the gas[3] and condensed[4, 5] phases. Using a variety of nonlinear optical techniques, much has been learned about the initial dynamics along the reaction coordinate. Since cis-trans isomerization reactions occur on a picosecond time scale, this effect has potential for optical switching applications. When an alkene or azobenzene is embedded in a liquid crystal or polymer, photon induced isomerization leads to large structural changes in these materials[6, 7]. This effect could possibly be exploited for optical information storage. In the discussion of the photochemistry of stilbene the so-called "phantom state" plays a major role[8]. This is the lowest energy state along the twisting coordinate where the phenyl rings are (nearly) perpendicular to one another and which is presumed to be the activated complex for cis-trans isomerization. While in stilbene the energetic minimum occurs at a twist angle of ~105^0, in ethylene the perpendicular conformation has the lowest energy. Calculations show[9-11] that for ethylene an *avoided crossing* exists near the phantom state between the electronic states $^1B_2$ and $^1A_1$, which are the singly excited π-π^* and the doubly excited π^*-π^* states, respectively. Figure 5.1 shows a schematic picture of the energies of these states as a function of twist angle.

In the vicinity of the avoided crossing, where these states are degenerate within the Born-Oppenheimer approximation, the molecule becomes extremely polarizable. This effect is known as "sudden polarization"[12]. Small perturbations, as, for instance, induced by solvent collisions, heavily mix these levels, leading to states that exhibit large induced dipoles due to charge separation across the C-C bond. Such ionic states can be further stabilized by pyramidalization of one of the carbon centers, thus shifting the excited state charge distribution from a so-called biradical to a zwitterionic nature[9, 10].

Although solvent polarity has a marked effect on the lifetime of cis-stilbene[13], the importance of ionic states in the isomerization process has not been assessed yet. The same holds for rhodopsin and bacteriorhodopsin, although in the latter case an avoided crossing has been held responsible for the presence of a small barrier along the twisting coordinate[14].

In the case of ethylene it has been suggested[15] that the ion-pair character of the lowest excited state near the phantom configuration facilitates a 1,2 hydrogen atom shift in the photodecomposition process. For 9,9'-bianthryl (BA) and tetraphenylethylene (TPE), microwave conductivity[16, 17] and optical calorimetry[18, 19] measurements clearly showed twisting induced charge separation across the central C-C bond. This process is only possible when the intrinsic inversion symmetry of BA and TPE is broken by solute-solvent interactions. Since solvation-shell dynamics occur on time scales of 100 fs to

several ns, an intriguing question concerns the time scale on which symmetry breaking occurs.

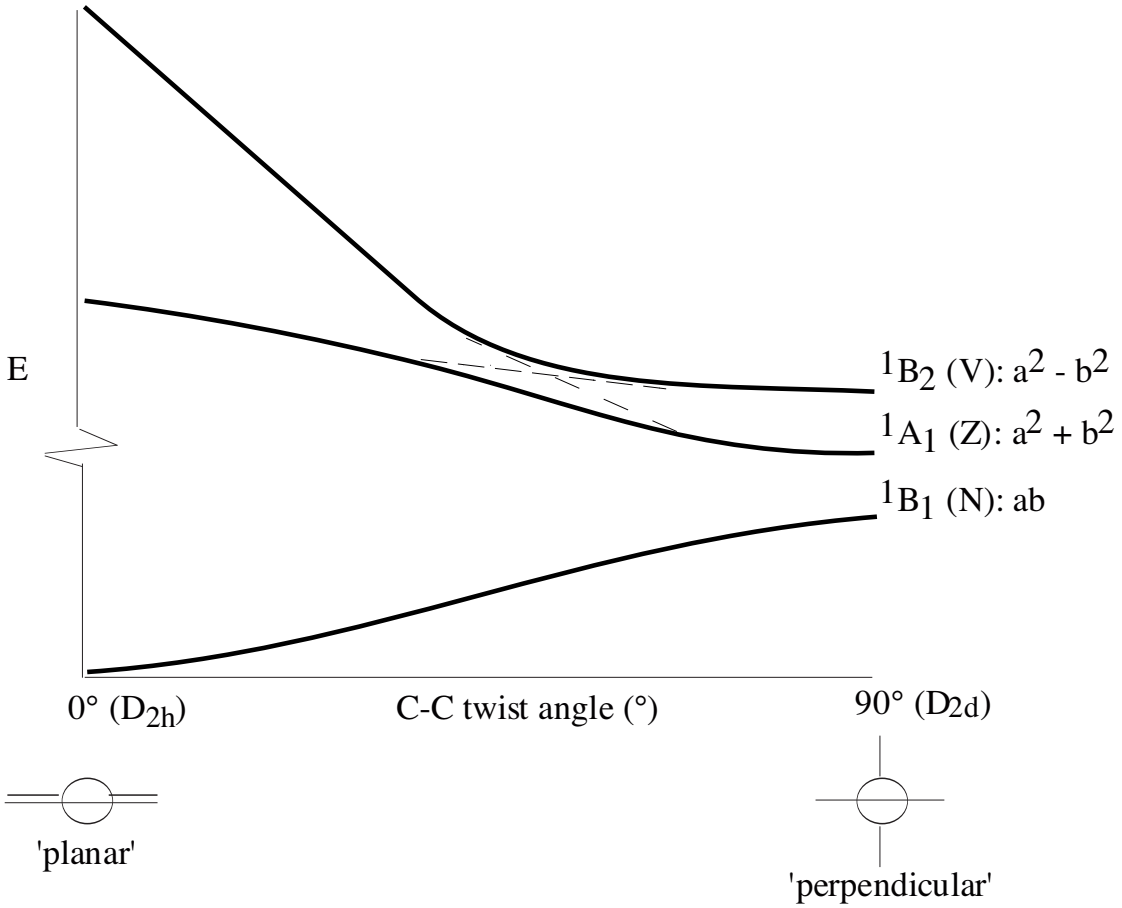

Figure 5.1 Schematic representation of the lowest potential energy surfaces of symmetric alkenes, as a function of the central bond twist angle. Newman projections of the two limiting cases of D_{2h} and D_{2d} symmetry are shown below. The position of the avoided crossing between the two excited states presumably depends on the substituents of the central alkene backbone. The nomenclature of the states (N, Z, V and ab, a^2+b^2, a^2-b^2) is explained in Section 5.4.

This chapter focusses on the twisting and charge-separation dynamics of TPE using femtosecond pump-probe spectroscopy. There is a long history on the spectroscopy and dynamics of TPE. Most noteworthy for TPE is its dual fluorescence and nonexponential fluorescence decay kinetics in nonpolar solvents. A landmark picosecond pump-probe study on TPE in 3-methylpentane was published in 1981 by Barbara *et al.*, who proposed a three-state model to account for the spectroscopy and dynamics around the central bond[20]. Although the nature of the intermediate states was not identified, the model accounted for all spectroscopic observations, including the large Stokes shift in emission, the dual fluorescence, the viscosity dependence of the fluorescence lifetime and the radiationless decay from the last state along the isomerization coordinate back to the ground state.

Soon thereafter Greene reported[21] that TPE in hexane has an excited state absorption at about 620 nm, which decays on a ps time scale. In view of earlier experiments on stilbene this time scale was attributed to twisting around the ethylenic bond. Greene also suggested a transient absorption at 420 nm to be due to a charge-resonance state, formed on twisting around the C-C bond. Schilling and Hilinski[22] examined the effect of solvent polarity on the decay of this band, and concluded from its solvation dynamics that a zwitterionic rather than a charge-resonance state was involved. They proposed that with increasing solvent polarity the zwitteronic state is stabilised, thereby reducing the energy gap with the ground state. This latter effect would also explain the increased rate for radiationless decay to the ground state in a polar solvent.

Morais *et al*. performed picosecond optical calorimetry measurements on TPE, which strongly suggested the existence of a zwitterionic state along the twist coordinate[18]. Ma *et al*. extended this study[19] and determined the energy differences between the two twisted states (the second and third state in the model of Barbara et al.) to be only a few kT. They went further and assigned the three states to the vertically excited state, the conformationally relaxed state and the twisted excited state, which they interpreted as a zwitterionic state.

Schuddeboom *et al*.[17] recently reported results of time-resolved microwave conductivity measurements on TPE in alkanes, which clearly showed the existence of a long-lived polar excited state. They further concluded that the so-called "prompt emission" of TPE, at about 500 nm, derives from a partially relaxed S_1 state, while the fluorescence around 560 nm was assigned to a conformationally relaxed S_1 state. They also suggested this latter state to be in equilibrium with the zwitterionic state.

Recently, Lenderink *et al*.[23, 24] reported the first results of a fs pump-probe study on TPE. On this time scale vibrational wave packet motion on the excited state potential and an ultrafast dynamic Stokes shift is observed. From the fact that the Stokes shift seemed to occur on the same time scale as the buildup of the wave packet motion, it was concluded that ethylenic bond twisting proceeds on a sub-ps time scale, just as in the case of cis-stilbene. The results presented in this chapter, however, are not in agreement with this earlier conclusion. In line with earlier work it is observed that ethylenic bond twisting in TPE takes place on a ps time scale and that the sub-ps Stokes shift dynamics is caused by ultrafast vibrational relaxation of the vertically excited state. The pump-probe data presented here further show that no phase shift occurs in the oscillatory transient probed at 650 run, as suggested earlier by Lenderink[23]. It turns out that these oscillations -which are much more pronounced in the measurements presented here- can be fitted very well assuming instantaneous response.

This chapter reports a detailed account of fs pump-probe measurements on TPE in solvents of different polarity, focusing in particular at the mechanism of the charge separation reaction. A novel finding is that in alcohols there is a direct relation between the decay of the 650 nm absorption and the buildup of the transient at 500 nm. In alkanes the latter signal exhibits a delayed buildup compared to the decay of the 650 nm band. In alcohols these dynamics relate the decay of the Franck-Condon relaxed planar excited state to the formation of a zwitterionic state. In alkanes this zwitterionic state is less stabilised and formed on a slower time scale. All these dynamics can be explained when the avoided crossing between singly and doubly excited states of TPE is taken into account. A unified description of the electron-transfer process is proposed in terms of

adiabatic crossing between solvation-dressed excited state energy surfaces. Large parts of the work described in this chapter have also been published in literature[25].

5.2 Pump-Probe Spectroscopy: A Short Introduction

The field of molecular dynamics has matured significantly by the development of spectroscopic techniques based upon non-linear optical phenomena[26]. Both intramolecular rearrangements as well as interactions with the environment on ground and excited state potentials can be studied in great detail using a wide variety of such techniques, aided by the continuing improvement of the resolution of such measurements. This is mainly due to the ongoing reduction of the temporal width of the laser pulses applied. It is beyond the scope of this thesis to give an extensive overview of the available techniques, nor is it the intention to provide the reader with a detailed theoretical description of pump-probe spectroscopy. Several excellent publications on the subject matter are available, and the interested reader is kindly requested to confer to these books and articles for more details[24, 26-28]. However, to be able to understand the processes under investigation when performing pump-probe spectroscopy, a general explanation of the technique will be given in this section.

Pump-probe spectroscopy is a time-resolved technique in which the evolution of a (non-equilibrium) system like an ensemble of molecules in a condensed phase is investigated. The experiment is initiated by applying an intense pump pulse to the system in order to drive it away from its equilibrium. This generally means that the system is brought into a (superposition of) photo-excited electronic state(s). Subsequently, these photo-excited states are probed by a second pulse, the probe pulse, which monitors the evolution of the system from its non-equilibrium starting point on the excited state potential energy surface(s). With the use of a short pump pulse, a system will generally be brought into a superposition of vibrationally excited states, which is commonly referred to as a vibrational wave packet[26]. This formalism is frequently used to describe the time-dependent evolution of a system under investigation.

$$\phi_j(q,t) = \sum_v c_{jv}(t)\phi_{jv}(q,t) = \sum_v c_{jv}(t)\phi_{jv}(q)\exp(-i\omega_{jv}t) \qquad \textbf{(5.1)}$$

In equation 5.1, ϕ_{jv} are the vibrational eigenstates of the nuclear Hamiltonian H_j of the time-dependent Schrödinger equation, with $\omega_{jv} = 2\pi E_{jv}/h$ as their energy eigenvalues. However, ϕ_j does not need to be an eigenfunction of H_j, in which case it can be written as the given sum of eigenfunctions ϕ_{jv} with coefficients c_{jv} and phase factors $-i\omega_{jv}t$. This is referred to as a vibrational wave packet.

In pump-probe spectroscopy, care has to be taken when probing with pulses with a broad spectral width, since the various parts of the frequency of the pulse can be temporally separated. Such frequency dependent time delay, usually referred to as a chirp[29], can lead to a destruction of the experiment when the first arriving frequencies effectively alter the state of the system, in which case the delayed frequencies probe a different state as intended. Another complication may arise when probing at the pump

wavelength, in which case coherent coupling effects may influence the excited state population. However, the experiments reported in this chapter are so-called dual colour pump-probe experiments, meaning that pump and probe pulses are located in non-overlapping frequency domains, thus avoiding the latter complication. In addition, the possible influence of a chirped pulse has been minimized by a number of measures, which are described in more detail in section 5.3.

A useful way to interpret the wave packet dynamics in pump-probe experiments is by means of the so-called 'doorway-window picture'[30]. In this approach, the dynamics of the system under investigation are assumed to take place at time scales which are significantly larger than the width of the pump-pulse, i.e. pump and probe pulse are well separated in time. This is an important precondition, since temporal overlap of these pulses gives rise to coherent interactions between the two, complicating the interpretation of the signals as a result. However, the pump pulse widths used in the here described experiments (vide infra) are in the 50-80 fs range, whereas the relevant dynamical processes take place in the (sub)picosecond domain, thereby generally obeying this precondition.

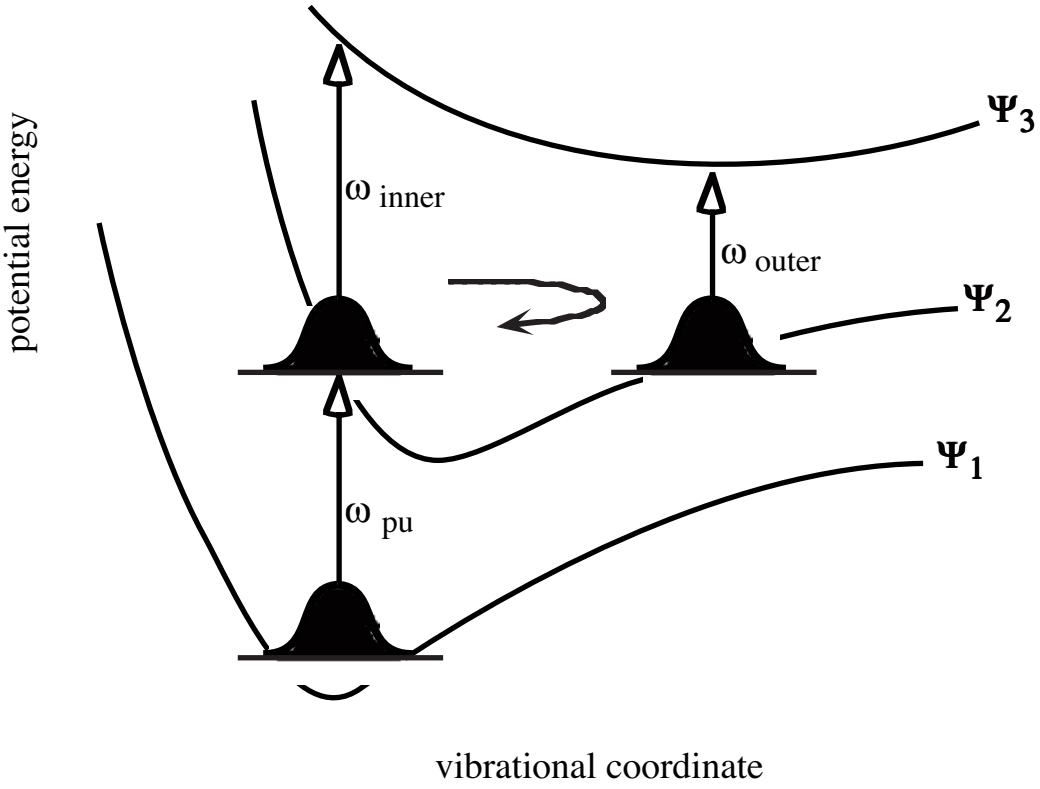

Figure 5.2 Schematic drawing of a pump-probe process in the doorway-window picture for a bound Ψ_2 potential. Upon excitation by a pump pulse with frequency ω_{pu}, the excited state wave packet moves back and forth between inner and outer turning points marked ω_{inner} and ω_{outer}, respectively.

In the doorway-window picture, a system is pushed into a non-equilibrium state through the doorway by the pump pulse, after which the probe pulse monitors the evolution of the wave packet 'from the outside' through a window (figure 5.2). A system is lifted from its ground state Ψ_1 to its excited state potential energy surface (PES) Ψ_2 by a

pump pulse with frequency ω_{pu}. In figure 5.2, Ψ_2 is chosen to be a bound potential, even though this is not necessarily the case. For example, photo-dissociation reactions take place on an unbound Ψ_2 (or another excited state PES). No further attention will be payed to such processes, since they bear no relevance to this work. On Ψ_2, the wave packet will periodically move back and forth between the inner and outer positions, which can be probed at frequencies ω_{inner} and ω_{outer}. If the resolution of pump and probe pulses is high enough, i.e about three times as short as the period of the wave packet oscillation, and $\omega_{inner} \neq \omega_{outer}$, the wave packet motion can be observed in the recorded transients. For instance, when probing at frequency ω_{outer}, the signal will be low at t=0 due to the fact that the wave packet is mainly located at the inner side of Ψ_2. However, when probing with the same frequency half a period later, the intensity of the transient will have reached a maximum because the wave packet will have moved to the outer side of the PES. This way, intramolecular vibrational modes can be observed, which can provide valuable insights in the ultrafast processes of systems under investigation. Although not depicted in figure 5.2, probing can also induce a transition from Ψ_2 back to Ψ_1 (i.e. stimulated emission).

When using linearly polarized pulses, the pump pulse will create a polarization anisotropy in the system. Molecules having the relevant transition dipole oriented in parallel with the polarization direction of the pump pulse have a larger chance of being excited to Ψ_2 than molecules in which this orientation is of a perpendicular nature. This can be quantified in the following manner[31]. Assume a molecular axis system that coincides with the principle axis of the diffusion tensor. Its orientation with respect to the laboratorium fixed axis system can be defined in terms of the three Euler angles $(\alpha, \beta, \gamma) = \mathbf{\Omega}$. A normalized probability distribution can be defined as $f^{(i)}(\mathbf{\Omega}, t)d\mathbf{\Omega}$, describing the probability of finding a molecule in level (i) with an orientation between $\mathbf{\Omega}$ and $d\mathbf{\Omega}$. Now, the number density of molecules in electronic state i is given by:

$$K^{(i)}(t) = \int d\mathbf{\Omega} f^{(i)}(\mathbf{\Omega}, t) \qquad \textbf{(5.2)}$$

with integration limits according to the conventional limits of Euler angles.

In order to allow quantification of f(i), orientation-dependent operators are defined that enable the definition of the effective parallel and perpendicular concentrations of molecules giving rise to electric-dipole emissions or absorptions from a given level:

$$\begin{aligned} N_{\parallel}^{(i)}(t,\gamma) &= d\mathbf{\Omega}\hat{P}_{\parallel}(\mathbf{\Omega}, \gamma) f^{(i)}(\mathbf{\Omega}, t) \\ N_{\perp}^{(i)}(t,\gamma) &= d\mathbf{\Omega}\hat{P}_{\perp}(\mathbf{\Omega}, \gamma) f^{(i)}(\mathbf{\Omega}, t) \end{aligned} \qquad \textbf{(5.3)}$$

In equation 5.3, $\hat{P}_{\parallel}(\mathbf{\Omega}, \gamma)$ and $\hat{P}_{\perp}(\mathbf{\Omega}, \gamma)$ are proportional to the probabilities of a molecule with orientation $\mathbf{\Omega}$ having a transition dipole with a direction cosines in the molecular axis system γ, interacting with a light field polarized in the laboratory z (parallel) or laboratory x or y (perpendicular) directions, respectively. The operators are normalized such, that:

$$K^{(i)}(t) = N_{\parallel}^{(i)}(t, \gamma) + 2N_{\perp}^{(i)}(t, \gamma) \qquad \textbf{(5.4)}$$

regardless of orientation γ. An effective anisotropy associated with transition dipole γ can be defined as follows:

$$r^{(i)}(t, \gamma) = \frac{N_{\parallel}^{(i)}(t, \gamma) - N_{\perp}^{(i)}(t, \gamma)}{N_{\parallel}^{(i)}(t, \gamma) + 2N_{\perp}^{(i)}(t, \gamma)} \qquad \textbf{(5.5)}$$

where the following relations hold:

$$N_{\parallel}^{(i)}(t, \gamma) = \frac{1}{3}K^{(i)}(t)[1 + 2r^{(i)}(t, \gamma)]$$
$$N_{\perp}^{(i)}(t, \gamma) = \frac{1}{3}K^{(i)}(t)[1 - r^{(i)}(t, \gamma)] \qquad \textbf{(5.6)}$$

$r^{(i)}(t, \gamma)$ contains information about the orientational distribution of the transition dipoles γ for molecules in state (i). Description of an experiment is now reduced to defining appropriate expressions for the time-dependent r and K functions. In the experiments described in this chapter, only one initial state is mainly prepared, and r(t) is given by the familiar expression (equation 5.7) involving the second Legendre polynomial (P_2) of the correlation of the transition-moment direction at t = 0 with that at at time t.

$$r(t, \gamma) = \left\langle \frac{2}{5} P_2(\mu(0) \bullet \gamma(t)) \right\rangle \qquad \textbf{(5.7)}$$

For example, at $t = t_0$ combining (5.5) and (5.7) leads to an initial ratio around 3:1 for parallel and perpendicularly oriented populations when the pump and probe transition dipoles are oriented in a (near-)parallel fashion.

When using polarized pulses, an experiment may be performed at the 'magic angle', a fixed angle (54.7˚) between the respective fields of polarization of the linearly polarized pump and probe pulses at which depolarization effects, as for instance caused by molecular reorientation in the solvent, are averaged out. This allows straightforward interpretation of the data, which is especially useful if one is particularly interested in the intramolecular dynamics rather than, for instance, the behaviour of the molecule in its solvent cage. However, as will be demonstrated in this and the following chapter, the nature and driving forces of inter- as well as intramolecular dynamics can become apparent by performing polarization dependent measurements at various angles and comparing their outcome. Therefore, all experiments reported in these chapters were performed at parallel and perpendicular orientation of the pump and probe pulse polarization direction to obtain a qualitative impression of the depolarization processes in TPE.

5.3 Experimental

The femtosecond pump-probe experiments were performed with an amplified CPM-laser system[23, 24], yielding 10 μJ pulses at 620 nm with a repetition rate of 9 kHz. The pump pulse at 310 nm was generated by frequency doubling in a 300 μm thick KDP crystal, while probe pulses were derived from a continuum, obtained by focusing part of the amplified pulse in a 2 mm thick sapphire plate. The chirp in the continuum was removed by use of a pair of quartz prisms in nearly retroreflecting geometry and a double-pass grating pair, resulting in cross-correlation widths between pump and probe of 70-100 fs in the frequency range of 450-700 nm. This corresponds to continuum pulse widths of 50-65 fs for these parts of the spectrum.

The pump-probe signals were measured for parallel and perpendicular polarizations of the pump and probe pulses. Frequency selection was achieved by placing suitable interference filters in front of the photodiode detector. In addition, the spectrum of the continuum was narrowed in front of the sample, by positioning an adjustable slit in the probe beam after the first passage of the two quartz prisms. In this way, only the desired part of the total spectrum, with a width of about 50 nm, reaches the sample. This proved to be essential, since otherwise probe pulse-induced artefacts determine the observed transients.

Previously, Lenderink[23] used the uncompressed continuum as a probe with frequency selection behind the sample. A consequence of this arrangement is that all frequency components of the continuum interact with the sample. Although the probe pulse may be weak for a given spectral component, the pulse energy, integrated over the entire spectrum, is sometimes capable of altering the state of the system. In particular for experiments on the blue side of the spectrum, where light arrives with a time delay for a positively chirped pulse, a totally different state may be probed than originally excited by the pump pulse. To some extent, this proved indeed to be the case, since the transients reported by Lenderink differ occasionally from those shown here. The lesson learnt is that it is much preferred to perform wavelength selection in front instead of behind the sample.

Tetraphenylethylene (TPE) was recrystallized from ethanol/chloroform mixtures until whiteness was obtained. Following crystallization, the purity of TPE was checked by ^{13}C NMR and determination of the melting point (226-227° C, uncorrected). Cyclohexane, ethanol and 1-butanol (Merck, p.a.) and 1-octanol (Aldrich) were used as received. The investigated solutions were >99% pure, based on GC analysis. The sample consisted of a 300 μm free flowing jet with 0.2 mM 300 ml solutions. In cyclohexane solutions, the TPE concentration may have been slightly higher, due to the volatility of cyclohexane. This effect was compensated for by slowly adding cyclohexane to the solution. GC analysis of the solutions after the experiment showed no evidence of buildup of photobyproducts.

5.4 Nomenclature of the States near the Avoided Crossing

Before the results of the experiments are discussed, the character of the states involved in the "sudden polarization" phenomenon will be commented upon. The parent molecule C_2H_4 will serve as an example. Around the 90^0 twisted conformation, one deals

with a two-electron, two-orbital open shell problem[32]. Indicating the p-orbitals on the two carbon atoms that form the double bond in the ground state, as "a " and "b", the states $^1(ab)$, $^1(a^2\pm b^2)$, and $^3(ab)$ arise, of which only the last one can be described - as far as the energy is concerned - with a single determinant wave function. States with a dipole moment, in which the electron density on one of the carbon atoms is higher than that on the other carbon atom, are associated only with the $^1(a^2\pm b^2)$ states. At the twist angle where the $^1(a^2+b^2)$ and $^1(a^2-b^2)$ Born-Oppenheimer surfaces cross (see Fig. 1), these two states are degenerate and any appropriate symmetry lowering interaction, be it intramolecular (Jahn-Teller effect) or external (solvent reorganization), will induce localization of the electronic charge distribution on one side of the molecule. This leads to an avoided crossing and to solvent stabilization of a charge-transfer state $^1(c_1a^2+c_2b^2)$, where $c_1 \gg c_2$ or vice versa. This is also known as a "zwitterionic-", or, referring to the D_{2d} parent state, as the "Z"-state.

Thus, the $^1(a^2+b^2)$ state is "stabilized" by symmetry breaking, which leads to a new state with an appreciable dipole moment. In contrast, the $^1(a^2-b^2)$ state, also known as the "V" state, is destabilized by solvation. Hence, there is a tendency to reduce the dipole moment when the molecule is on this potential surface. The $^1(a^2-b^2)$ state itself carries no dipole moment, which has led -erroneously- to classifying it as a "biradical" state. Note that the V and Z states are no longer orthogonal, when dressed with the solvent-interactions as described here.

In the practice of organic chemistry and ESR spectroscopy, it is common to use the phrase "biradical" for systems where two unpaired electrons are localized on relatively distant parts of the molecule and consequently the singlet/triplet splitting is small. For C_2H_4 and the like, the only states that may give rise to this situation are the $^{1,3}(ab)$ states. The CT states are essentially singlets and cannot be "biradical" at all. We will therefore call a state "charge resonance" (CR) when the electron distribution is symmetric, and "charge transfer" (CT) or "zwitterionic" when an electron has been transferred from one half of the molecule to the other.

In light of the above discussion, the assignment of a transient absorption at 1000 nm in the ethylenic system biphenanthrenylidene to a biradical-zwitterionic transition, by Piotrowiak *et al* [33] is, most likely, incorrect. The lack of a solvatochromic effect on this transition strongly suggests the initial and/or final states to have only a very weak CT character, indicative of a small interaction between the two non-degenerate energy surfaces.

5.5 Results and Discussion

5.5.1 The First Two Picoseconds

The initial pump-probe response of TPE, up to about two picoseconds, is solvent independent. This suggests that on this time scale the dynamics are predominantly intramolecular. Figure 5.3 displays typical transients for TPE in cyclohexane at probe wavelengths from 500 to 650 nm. At all wavelengths, from 450 to 700 nm, the absorption rises instantaneously, which is interpreted as a signature of excited state absorption. While

the green part of the spectrum displays fast changes, the transient absorptions at 450 nm and in the 600-650 nm range persist on a ps time scale, as already noted by Greene[21].

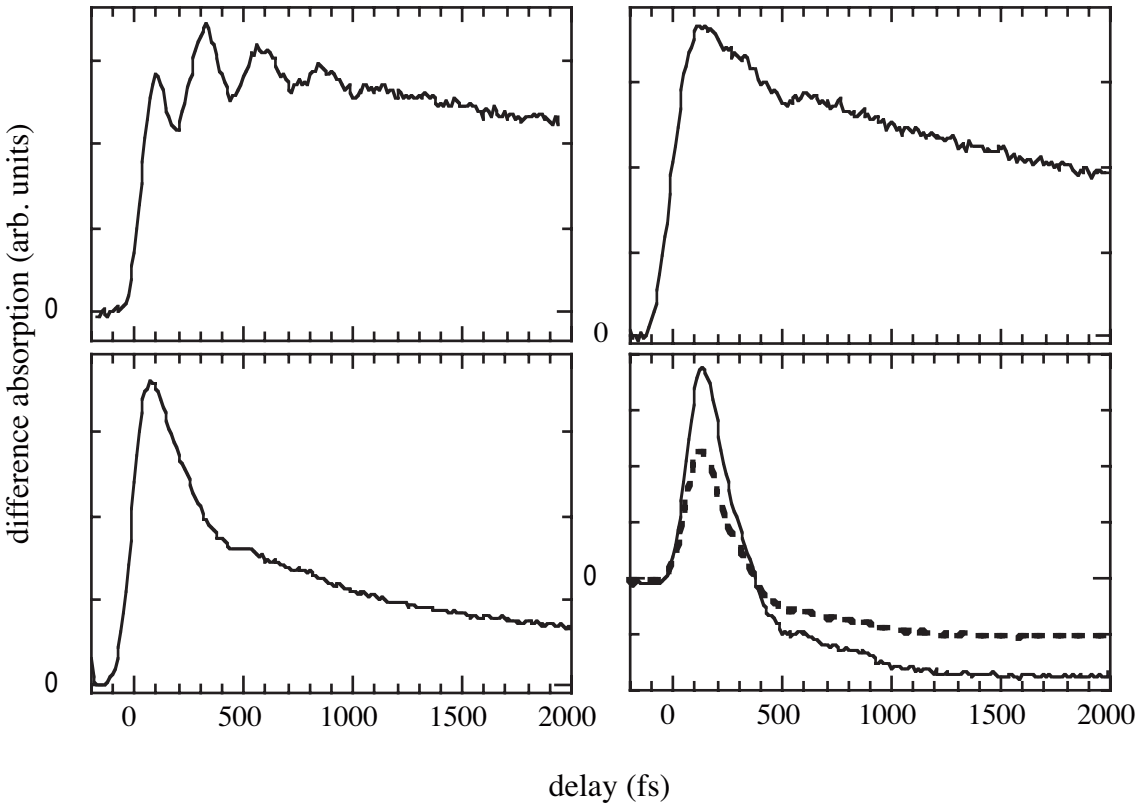

Figure 5.3 Pump-probe spectra of TPE in cyclohexane up to 2 ps. In all cases the excitation wavelength is 310 nm. The probe wavelengths are 650, 600 (top left and right panels), 550 and 500 nm (bottom left and right panels). All transients are largely solvent independent. For λ_{pr}=500 nm, the results for both parallel (solid line) and perpendicular (dashed line) pump and probe polarization are shown.

As shown in the bottom right panel of figure 5.3, the transient at 500 nm changes sign after a few hundred femtoseconds. The excited state absorption turns into a bleach, which is assigned to stimulated emission. This signal is largest for parallel pump and probe polarizations. In TPE, the $S_1 \leftarrow S_0$ transition is polarized along the p_z orbitals, which form the central double bond. The fact that the stimulated emission remains polarized along the excitation direction over the first 2 picoseconds, implies that on this time scale no ethylenic bond twisting occurs. The transient stimulated emission, probed at 500 nm, therefore must reflect vibrational cooling from an initial state that has kept its ground state configuration, except for elongation of the central C-C bond. Indeed, the C-C bond in the π-π^* excited state is formally a single bond, which is stretched compared to the ground state. This picture is corroborated by the resonance Raman spectrum of TPE, which is dominated by the 1585 cm^{-1} stretching vibration of the central bond[24]. The vertically excited state therefore quickly relaxes to the potential minimum along the C-C stretch mode, by coupling to other intramolecular vibrations. Thereby, a sizable Stokes shift is generated.

The Stokes shift of 12,000 cm^{-1}, observed in the stimulated emission, is indeed large. Although this suggests a large structural change in the TPE excited state[23], calculations on the parent molecule ethylene confirm that a lengthening of the C-C bond in the excited state of about 0.3 Å accounts for a shift of 11,000 cm^{-1}. This ab initio calculation was performed at the all-valence CISD level in a standard double zeta valence (DZV) basis for the planar geometry (C-H bond length 1.076 Å; H-C-H bond angle 116.6^0). The fact that the Stokes shift occurs on a subpicosecond time scale and is solvent independent, points to strong intramolecular vibrational coupling, leading to fast energy redistribution among the many modes of TPE.

At 650 nm, the pump-probe signal exhibits strong oscillations due to a low frequency vibration (124 cm^{-1}), which decays on a subpicosecond time scale. Previously, Lenderink[23] assigned this mode to a torsional and/or scissoring motion of the phenyl rings. The oscillations displayed here are much more pronounced than reported earlier, which is probably due to the fact that in the previous experiments the probe pulse carried a substantial chirp. This may enhance or suppress the wave packet dynamics, depending on the sign of the chirp[29, 34]. The first impression from the trace at 650 nm (see the top left panel of fig. 5.3) is that the wave packet builds up in time. Previously, this was interpreted as a phase shift[23], caused by indirect excitation of this mode by, for instance, the C-C strech mode. However, closer inspection of these transients obtained with higher time resolution, reveals that the apparent build-up results from the finite pulse durations used in the pump-probe experiment. Figure 5.4 shows that an excellent fit to the pump-probe data at 650 nm can be obtained by convoluting the experimental time resolution with a response function of the form[5]:

$$M(t) = A_{650} \exp(-t/\tau_{650}) + B_{osc} \exp(-t/\tau_{osc}) \times \cos[2\pi\nu_{osc} + \theta] \qquad \textbf{(5.8)}$$

with phase $\theta=0$. Here, A_{650} and τ_{650} are the amplitude and decay time of the overall response at 650 nm, while B_{osc} and τ_{osc} are the same quantities for the vibrational wavepacket with frequency ν_{osc}. Fits with a quality similar to that of figure 5.4 could be obtained for all solvents, with phase $\theta=0$. This indicates that the wave packets are directly excited from the ground state. The fit parameters are shown in Table I. Damping of the torsional mode increases slightly at higher solvent viscosity, showing the importance of intermolecular vibrational mode coupling for these low frequency, large amplitude motions.

For a probe wavelength of 700 nm, the same 124 cm^{-1} motion of the phenyl rings dominates the response. Surprisingly, again a phase shift $\theta=0$ is found (see also figure 5.2 for a graphical representation of the involved process). The presence of a steep higher-excited state potential in the probing process may be the explanation for this probe wave length independent phase. This interpretation implies that shifts should be observable much further to the red of the current probe wave lengths. At the moment, it has not been possible to probe in that range yet.

solvent	lifetime τ_{650} (ps)	frequency ν_{osc} (cm^{-1})	damping τ_{osc} (fs)
ethanol	4.2	122	305
1-butanol	6.7	124	345
1-octanol	9.9	123	430
cyclohexane	11.8	126	406

Table 5.1 Parameters of the fits of the wave packet motion at 650 nm. The overall damping of the pump-probe transient at this wavelength (τ_{650}), the frequency of the oscillation (ν_{osc}) and the damping time of the oscillation (τ_{osc}) are listed for the various solvents.

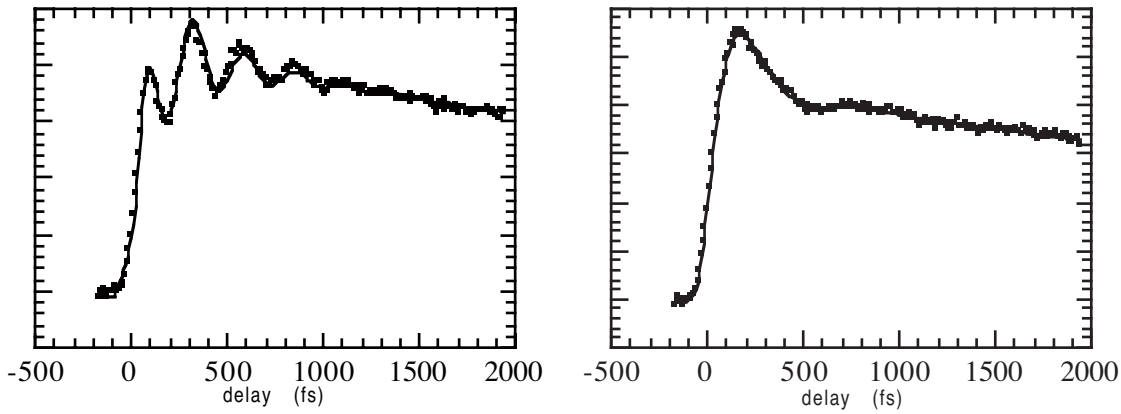

Figure 5.4 Fits (solid lines) to the two type of oscillations, observed in the short-time pump-probe spectra of TPE (dots). In the left panel the result is shown for the 650 nm transient of TPE in cyclohexane; in the right panel that for the 600 nm transient of TPE in octanol. The parameters of the fits at 650 nm can be found in Table I for the different solvents. The parameters for the fits of the much weaker oscillation at 600 nm were, within the experimental error margins, identical for all solvents.

At the high energy side (500-600 nm) the transients do not display this phenyl ring motion, but instead a slight undulation at lower frequency is observed. As shown in figure 5.4 for the 600 nm transient of TPE in octanol, this can be fitted with equation 1 as well, yielding a mode of about 58 cm^{-1}. This frequency is close to one observed in pump-probe spectra of rhodopsin. There, a 60 cm^{-1} mode is assigned to a skeletal torsional mode, associated with the isomerization reaction coordinate[2].

5.5.2 Longer Time Scales

Figure 5.5 displays the pump-probe transients for TPE in cyclohexane and ethanol on longer time scales. All transients show a pronounced solvent dependence, which relates to twisting around and charge separation across the central carbon-carbon bond. The time scale of the twisting motion is most apparent in the decay of the excited state absorption at

650 nm. In this spectral region the signals do not depend very much on the relative orientation of the pump and probe polarizations, but a marked dependence on solvent viscosity is observed. Note that in cyclohexane after about 15 ps a plateau is reached.

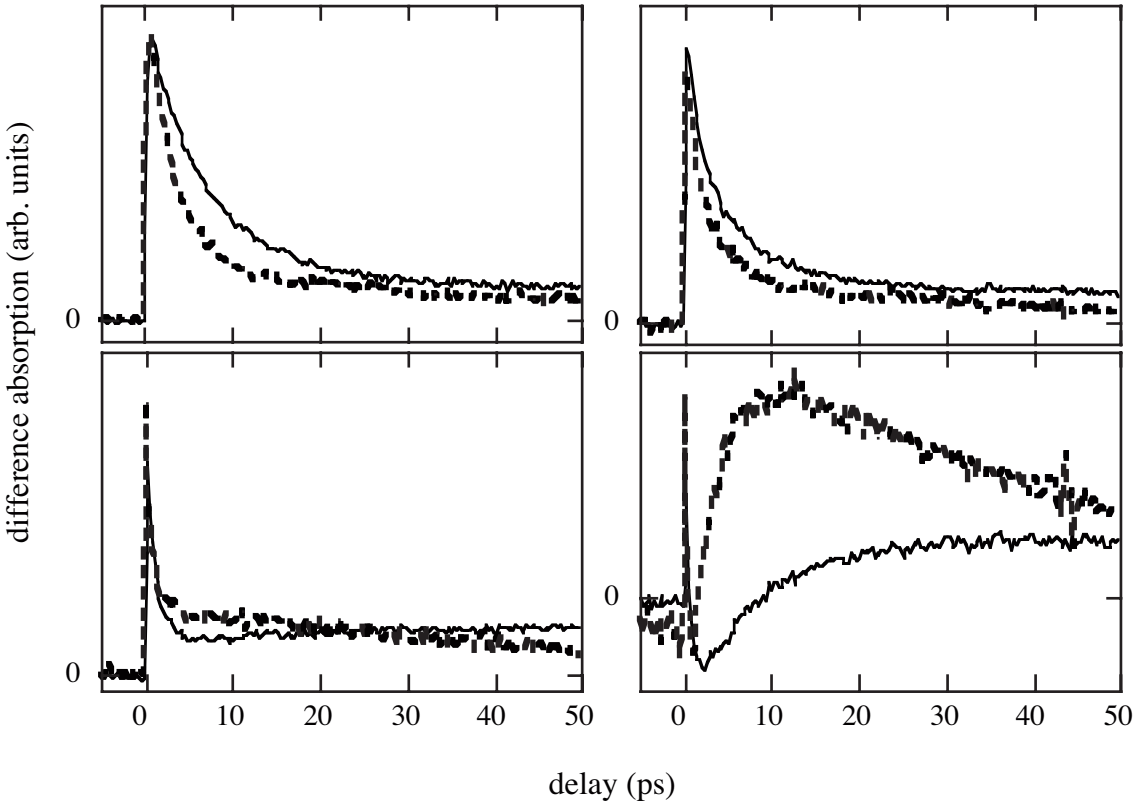

Figure 5.5 Comparison between the ps pump-probe transients of TPE in cyclohexane (solid line) and ethanol (dashed line). The probe wavelengths are 500, 550 (bottom right and left panel), 600 and 650 nm (top right and left panel). For all alcohols, the decay in the red part of the spectrum is related to the rise of the signal in the green. For cyclohexane, no such relation is found.

In alcohols the 650 nm transient shows a faster decay, reaching a plateau within 10 ps. On a longer time scale this "plateau" decays with a lifetime which strongly depends on solvent polarity. Evidently, phenyl twisting in TPE proceeds on a time scale of several picoseconds instead of a few hundred femtoseconds as originally concluded[23]. This is about the same time scale as observed for trans-stilbene but a factor of ten slower than for cis-stilbene. Replacement of an ethylenic hydrogen atom in stilbene by a phenyl ring in TPE decreases the electron pair repulsion due to some delocalization, while increasing the solvent drag. The isomerization rate in any of these alkenes is determined by a subtle balance between electrostatic and steric factors, making it difficult to compare these molecules.

The most dramatic solvent dependence on the ps transients is observed in the 500-550 nm region. In this spectral region the transients are not only sensitive to solvent viscosity but also to solvent polarity. Figure 5.6 displays these transients for three different alcohols and cyclohexane. This figure clearly shows that the ps transients for ethanol and cyclohexane are very different, even though their viscosities are similar. For

the longer alcohols the buildup and decay become progressively slower, by the increase of viscosity and the decrease of polarity. We further note that for alcohols a direct relation is found for the decay of the 650 mn band and the buildup time of the 500 nm absorption, that follows after the stimulated emission signal at this wavelength (figures 5.5 and 5.6).

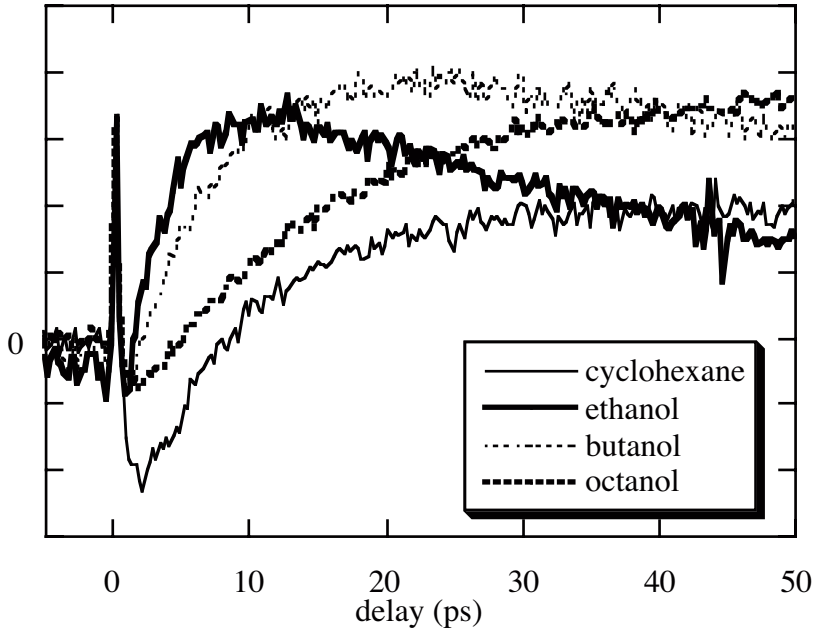

Figure 5.6 The picosecond dynamics of TPE at 500 nm in ethanol, 1-butanol, 1-octanol and cyclohexane. In this part of the spectrum, the pump-probe transients are strongly dependent on the polarity and the viscosity of the liquid, as discussed in the text.

These observations suggest that the 500 nm transient is connected to a species, directly generated from the Franck-Condon relaxed excited state. Because of the strong polarity dependence of the rise and decay of the 500 nm transient, which is strongest for perpendicular polarizations, this species is suggested to be the zwitterionic state of TPE. Apparently, the Franck-Condon relaxed excited state is converted into a zwitterionic state by motion along the twist coordinate.

In order to characterize the dynamics, a simple kinetic analysis of all transients observed at the various wavelengths was performed. In this way the various time scales of the overall dynamics are determined, which facilitates the construction of the quantum mechanical picture presented in the next section.

It was found that a two-state model excellently fits the ps excited state dynamics of TPE in alcohols, and most likely in all polar solvents. A satisfactory fit to each set of transients was obtained, using a global fitting routine. Herein, all transients for a given alcohol are fitted simultaneously, with the same rate constants but different spectral amplitudes. In this fitting procedure the 500, 550, 600 and 650 nm transients have been included using a simple two-state consecutive reaction scheme. Figure 5.7 displays the resulting fits for ethanol; the quality of the fits for butanol and *n*-octanol is equally good. A careful look at the 550nm transient reveals a small discrepancy between the data and the fit at a delay of about 4 ps. As will be discussed below for the case of TPE in cyclohexane,

this small discrepancy is indicative of the presence of a third state in the dynamics. However, since in polar solvents this state apparently is hardly populated, the two-state model provides an adequate fit to the data.

For cyclohexane, the decay of the 650 nm transient is not directly related to the buildup of the 500 nm transient. Consequently, the results can not be fitted within a two-state model, as shown in figure 5.8. However, a three-state model, in which a dynamic equilibrium exists between two product states, works well. The reaction scheme covering the dynamics in both polar and nonpolar solvents therefore is the following:

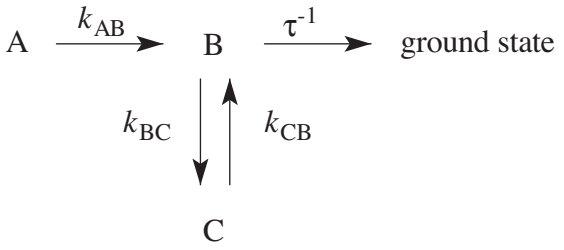

(5.9)

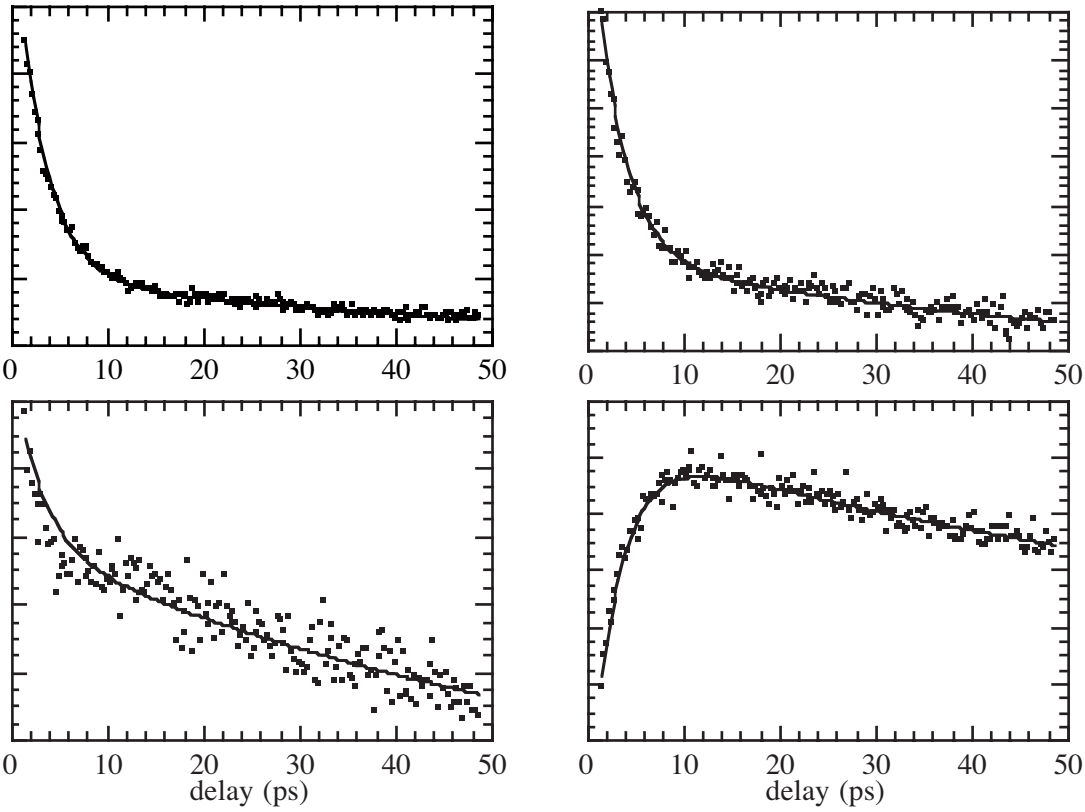

Figure 5.7 Fits (solid lines) of the 500, 550 (bottom right and left panels), 600 and 650 (top right and left panels) nm transients of TPE in ethanol (dots). For simplicity, the solvent independent ultrafast part of the response (<2 ps) was excluded from the fitting. A two-state model suffices to explain the data at all wavelengths with the same set of dynamic parameters. These are given in Table 5.2.

Excellent fits for the transients at all wavelengths are obtained for TPE in alcohols and cyclohexane as well, when the equilibrium with the third level is taken into account. In

principle, there could also be some direct transfer from A to C, involving k_{AC} as yet another kinetic parameter. The present data are not accurate enough to either exclude or identify this reaction path.

All parameters obtained from fitting the pump-probe transients to the two- and three-state models are given in Table 5.2. For the alcohols no values can be given for the kinetic parameters of the equilibrium between B and C, since C is not, or hardly, populated ($k_{BC} \ll k_{CB}$). These data show that the reaction rate out of state A is strongly influenced by the viscosity of the solvent, while state B has a lifetime that is directly related to the solvent polarity.

At this point it is noted that an interpretation of the transients, just discussed, in terms of vibrational relaxation phenomena is ruled out. Although the time scale for the observed effects is right, the excellent correspondence between the rise and fall times of these transients at different wavelengths in alcoholic solutions, but not for cyclohexane, is a very strong point for the interpretation given. Of course, effects of vibrational cooling should be present, for instance, in the spectral width of the transients involved. This is outside the scope of the present study.

When these results are considered in the light of the qualitative discussion presented above, the identification of states A, B and C seems clear. State A is suggested to be the vibrationally relaxed planar S_1 state, which is formed on a subpicosecond time scale from the vertically excited state. This state predominantly absorbs in the red part of the spectrum, while at 500 nm stimulated emission to the ground state occurs.

solvent	k_{AB} (ps^{-1})	k_{BC} (ps^{-1})	k_{CB} (ps^{-1})	τ (ps)
ethanol	0.32			60
1-butanol	0.15			350
1-octanol	0.07			$\sim 10^3$
cyclohexane	0.46	0.042	0.082	$>>10^3$

Table 5.2 Kinetic parameters for the dynamics of excited state TPE. A is the Franck-Condon relaxed planar configuration, B the zwitterionic (dipolar) state, and C is the charge resonance twisted state with an approximately symmetric charge distribution across the C-C bond. The k's are the rate constants for the transitions, and τ is the lifetime of the excited state.

This planar configuration subsequently decays on a ps time scale through a twist around the central C-C bond, accompanied by charge separation across this bond. Hence, B is the zwitterionic form of TPE, which has distinct polar character. Its main spectral feature is the strong absorption at 500 nm. This state subsequently decays to a twisted conformation on the ground state potential surface, or establishes an equilibrium with state C, the charge-resonance form of perpendicular geometry, which weakly absorbes over a large frequency range.

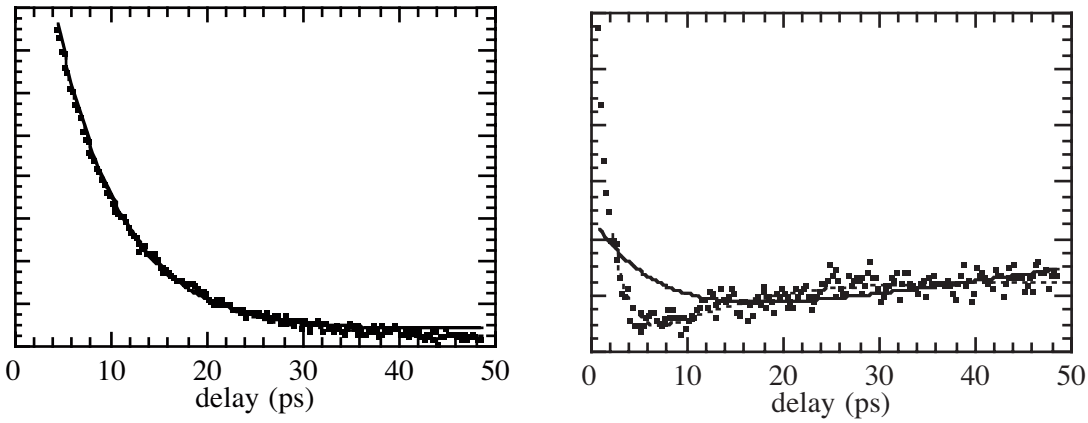

Figure 5.8 Fits of the 650 nm (left panel) and 550 nm (right panel) transients of TPE in cyclohexane. The fits to the data (dots) of the two-state model (solid lines) are clearly not as good as those of the three-state model (dashed lines). In nonpolar solvents, the transients at all wavelengths can only be simulated consistently, with the same dynamic parameters, when (at least) three states are involved in the dynamics. The parameters of the fits are given in Table 5.2.

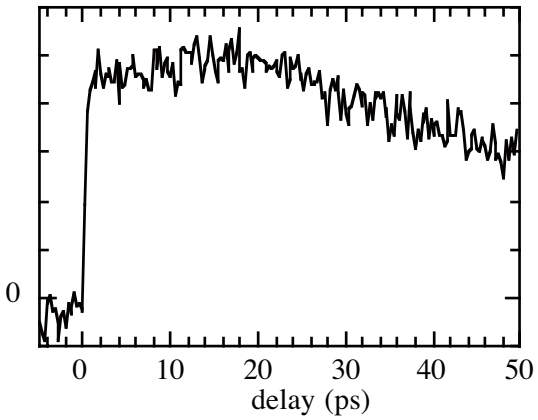

Figure 5.9 The picosecond dynamics of TPE in ethanol for probing at 450 nm. Apart from a small rise, due to the wing of the 500 nm band, only the overall decay of the excited state population is observed. Twisting and charge separation do not significantly influence this part of the spectrum.

In cyclohexane, both the charge-resonance state and the zwitterionic form are populated appreciably. In alcohols, the equilibrium is strongly shifted towards the zwitterionic state; in fact the charge-resonance form in these solvents is hardly detected at all. The small discrepancy in the two-state fit of the 550 nm transient of figure 5.8 is due to the very limited and short-lived population of this state. The stabilization of the zwitterionic state in polar solvents is caused by the interaction between the induced dipole of the zwitterion and the dipoles of the solvent. As a result, the charge-resonance state is largely bypassed and/or its lifetime in polar solvents is so short that its transient

population can hardly be detected at all. This analysis is supported by the observation of a broader transient spectrum in the 500-550 nm range in cyclohexane compared to alcohols, which suggest that the red flank of this transient may be due to absorption of the charge-resonance excited state of TPE. In fact, a weak build-up of the signal at 550 nm is observed, which is absent in the alcoholic solutions. This absorption resembles the weak band at 520 nm in the diphenylmethylradical[35], making it plausible that the charge-resonance form of TPE absorbs here.
This interpretation leads also to the conclusion that the delayed fluorescence[18] of TPE in alkanes around 560 nm must be attributed to emission from the charge-resonance form of TPE. Previously, this emission was assigned to the relaxed S_1 state[17, 19, 20]. The absence of this band in polar liquids is then immediately explained as well. A further consequence of this line of reasoning is that the so-called "prompt" fluorescence[36], peaked near 500 nm, must be due to emission from the relaxed S_1 state, and not from the vertically excited state, as suggested hereto.

Greene[21] suggested in his ps pump-probe study of TPE that transient absorption of the zwitterionic state is located at 420 nm. Pump-probe measurements at the red flank of this band (at 450 nm, dictated by available interference filters) provide no support for this assignment. These data are shown in figure 5.9. Obviously, no dynamics occur other than a slow decay similar to the 500 nm band. Since the absorption is induced instantaneously, and only weakly responds to ethylenic bond twisting, this 420 nm band is assigned to an excitation localized at the phenyl rings. Of course, when excitation pulses of about 30 ps are being used for pump-probe measurements, all dynamics occurring prior to population of the zwitterionic state go unnoticed and this band can perfectly be used as a marker for the lifetime of the zwitterionic state of TPE[22].

5.6 Avoided Crossing and Charge Separation

Now that the states participating in the isomerization process of TPE have been identified, the question arises whether a coherent picture of the isomerization and charge separation dynamics can be generated. A model for this reaction where the avoided crossing between the π-π^* and π^*-π^* potential surfaces plays a crucial role[32] is suggested. Figure 5.10 shows the level scheme that explains all results. After initial relaxation from the Franck-Condon excited state, the system proceeds along the isomerization pathway towards the avoided crossing region. While this is, most likely, a barrierless process for isolated, gas phase TPE molecules, in solvents considerable friction occurs. This phenomenon is taken into account as potential barrier along the twisting coordinate. The energy levels in figure 5.10 thus represent dressed potential energy surfaces.

As discussed in the introduction, near the avoided crossing the surfaces interact strongly by, for instance, a combination of vibronic coupling and solvation dynamics, and new adiabatic states are formed. Landau and Zener have calculated the transition probability for nonadiabatic crossing between two surfaces at an avoided crossing, using a semiclassical description. Their result for the transition probability P_{LZ} between two states that are strongly coupled is[37]:

$$P_{LZ} = \exp\left[-\frac{(\pi\Delta)^2}{h\theta v}\right] \qquad \textbf{(5.10)}$$

where Δ is the smallest gap between the two states, θ is the difference between the slopes of the unperturbed surfaces at the crossing, and v is the classical velocity of the system at the crossing point.

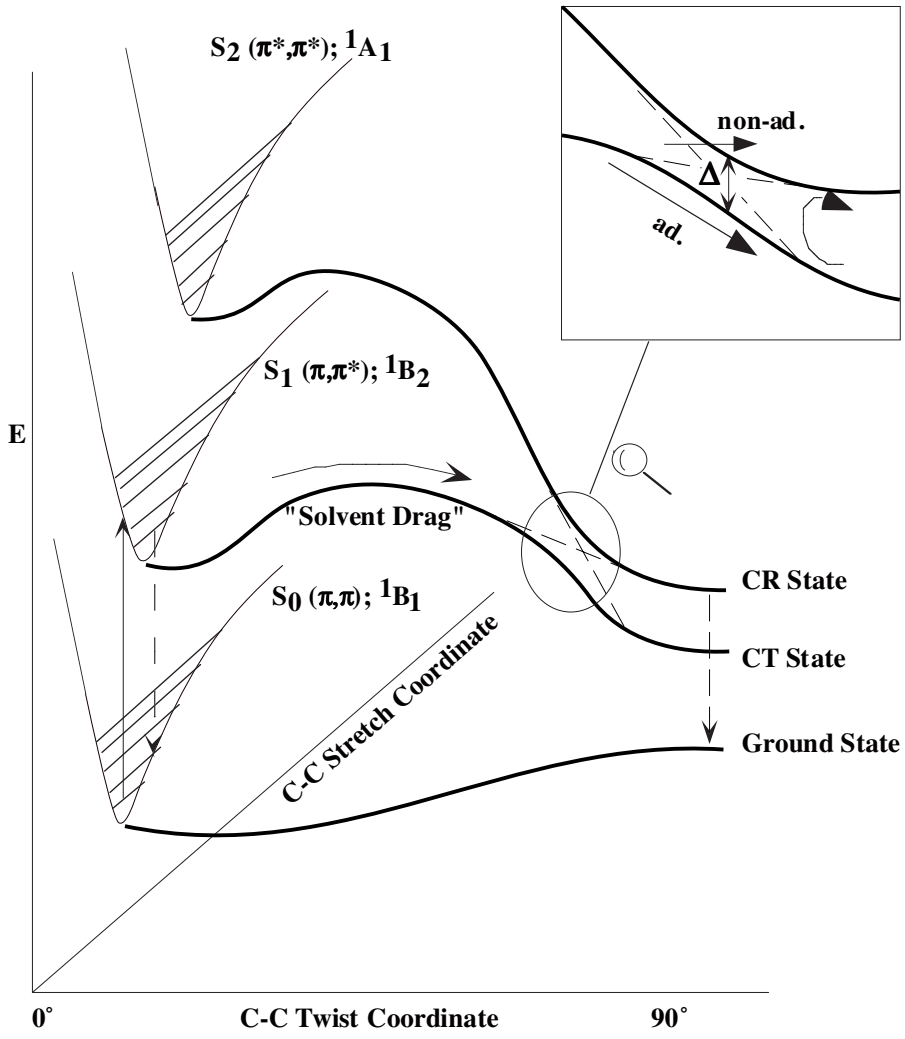

Figure 5.10 Impression of the excited state dynamics of TPE.

It is very difficult to evaluate this expression quantitatively, since the coupling involves dynamic rearrangements of many solvent molecules. In addition, the energy levels themselves depend on the speed of solvent rearrangement when dressed potential energy surfaces are considered. However, it is clear that when the gap at the avoided crossing is large, the reaction proceeds adiabatically to the lower surface. In our case this is the zwitterionic state, carrying a large induced dipole. Nonadiabatic crossing leads to the charge-resonance state, which subsequently relaxes to a state with a minimal induced dipole. The here presented experiments show that in alcohols the zwitterionic state is formed almost exclusively, with only a very small fraction crossing to the upper potential curve. This implies that the charge separation proceeds nearly completely adiabatically through the twisting motion, which is the rate-limiting step in this reaction as well. The

zwitterionic state, thus formed, is stabilized further by solvation. This increases the energy gap with respect to the avoided crossing region so much, that solvent-induced recrossing becomes an improbable event. In addition, radiationless decay to the ground state is a very efficient and competing process. Therefore, in polar solvents the charge-resonance state is not populated by a recrossing process and, consequently, delayed fluorescence from this state is not observed. In nonpolar solvents the reaction proceeds also adiabatically, as can be concluded from the very low efficiency for prompt emission at 560 nm, compared to the steady state quantum yield for this process. However, in this case the zwitterionic state is only stabilized by induced dipoles of the nonpolar solvent, which reduces the gap between the zwitterionic and charge-resonance states such that solvent-induced recrossing to the upper potential is an effective process. Furthermore, radiationless decay to the ground state is slow. Therefore, in nonpolar solvents the charge-resonance state is in thermal equilibrium with the zwitterionic state and delayed fluorescence is observed with a lifetime determined by the lifetime of the zwitterionic state.

This is displayed in figure 5.10, where an impression of the TPE excited state dynamics is given. Subpicosecond relaxation occurs along the C-C stretch coordinate, leading to a large Stokes shift between the excitation wavelength (310 nm, solid arrow), and the probed stimulated emission (500 nm, dashed arrow). The subsequent twist around the central bond is strongly hindered by the surrounding solvent. This is indicated as "solvent drag". The twist leads to adiabatic electron transfer to a zwitterionic state, through an avoided crossing between two excited state potential surfaces. This is designated by ad(iabatic) in the enlarged crossing region of the inset. The resultant charge transfer (CT) state is stabilized by solvent reorganisation. A very small fraction may cross directly to the upper potential curve (non-ad(iabatic) in the inset), which leads to the symmetric charge resonance (CR) state. In nonpolar solvents thermal activation of this nonpolar state is possible, and a dynamic equilibrium between the CT- and CR-states is established.

5.7 Conclusion

From polarization dependent femtosecond pump-probe studies it is concluded that a four state model provides an adequate description for the excited state dynamics of TPE. The four states involved are the Franck-Condon excited state, the relaxed excited state, the charge-resonance state and the zwitterionic state. The sub-picosecond dynamics is attributed to vibrational cooling of the central C-C stretching mode, by strong intramolecular anharmonic mode coupling. The observed 12000 cm^{-1} Stokes shift can be explained by a C-C bond lengthening of about 0.3 Å. The vertically excited state also comprises a wavepacket along the phenyl torsion mode, possibly by coupling to the C-C stretch mode of the ethylenic bond**.** Along the twist coordinate charge-separation occurs near the avoided crossing region in an adiabatic electron-transfer process. Solvent drag limits the speed of twisting, which is the rate limiting step in the reaction. In polar solvents the zwitterionic state, thus formed, is stabilized such that solvent-induced nonadiabatic crossing to the upper potential hardly occurs at all. In nonpolar solvents the energy gap between the two states is less, leading to a thermal equilibrium between the zwitterionic and charge-resonance state. It is this latter state that is responsible for delayed fluorescence.

Crucial in the identification of the various processes is a transient absorption at about 500 nm, which is attributed to the zwitterionic state of TPE. A transient at 450 nm is assigned to a local π-π^* excitation on a $C(Ph)_2$ fragment of the molecule.

5.8 References

1. G. Wald, Science, **162**, 230-239 (1968).
2. Q. Wang, R.W. Schoenlein, L.A. Peteanu, R.A. Mathies and C.V. Shank, Science, **266**, 422-424 (1994).
3. A.A. Heikal, J.S. Baskin, L. Banares and A.H. Zewail, J. Phys. Chem. A, **101**, 572-590 (1997).
4. R.J. Sension, S.T. Repinec, A.Z. Szarka and R.M. Hochstrasser, J. Chem. Phys., **98**, 6291-6315 (1993).
5. A.Z. Szarka, N. Pugliano, D.K. Palit and R.M. Hochstrasser, Chem. Phys. Lett., **240**, 25-30 (1995).
6. T. Ikeda and O. Tsutsumi, Science, **268**, 1873-1875 (1995).
7. N.P.M. Huck, W.F. Jager, B. de Lange and B.L. Feringa, Science, **273**, 1686-1688 (1996).
8. J. Saltiel, J. D'Agostino, D. Megarity, L. Metts, K.R. Neuberger and O.C. Zafiriou, Org. Photochem., **3**, 1-113 (1973).
9. J. Saltiel, J. Am. Chem. Soc., **89**, 1036-1037 (1967).
10. R.J. Buenker, V. Bonacic-Koutecky and L. Pogliani, J. Chem. Phys., **73**, 1836-1849 (1980).
11. R.W.J. Zijlstra, A.H. de Vries and P.Th. van Duijnen, Chem. Phys., **204**, 439-446 (1996).
12. V. Bonacic-Koutecky, P. Bruckmann, P. Hiberty, J. Koutecky, C. Leforestier and L. Salem, Angew. Chem., Int. Ed. Engl., **14**, 575-576 (1975).
13. R.A. McGill, J.K. Rice, A.P. Baranovski, J.C. Owrutsky, A.H. Lowrey, K.K. Stavrev, T. Tamm and M.C. Zerner, Int. J. Quant. Chem. Symp., **30**, 383-394 (1996).
14. K.C. Hasson, F. Gai and P.A. Anfinrud, Proc. Natl. Acad. Sci. U.S.A., **93**, 15124-15129 (1996).
15. A. Stolow, B.A. Balko, E.F. Cromwell, J.-S. Zhang and Y.T. Lee, J. Photochem. Photobiol. A. Chem., **62**, 285-300 (1992).
16. D.B. Toublanc, R.W. Fessenden and A. Hitachi, J. Phys. Chem., **93**, 2893-2896 (1989).
17. W. Schuddeboom, S.A. Jonker, J.M. Warman, M.P. de Haas, M.J.W. Vermeulen, W.F. Jager, B. de Lange, B.L. Feringa and R.W. Fessenden, J. Am. Chem. Soc., **115**, 3286-3290 (1993).
18. J. Morais, J. Ma and M.B. Zimmt, J. Phys. Chem., **95**, 3885-3889 (1991).
19. J. Ma, G. Bhaskar Dutt, D.H. Waldeck and M.B. Zimmt, J. Am. Chem. Soc, **116**, 10619-10629 (1994).
20. P.F. Barbara, S.D. Rand and P.M. Rentzepis, J. Am. Chem. Soc., **103**, 2156-2162 (1981).
21. B.I. Greene, Chem. Phys. Lett., **79**, 51-53 (1981).
22. C.L. Schilling and E.F. Hilinski, J. Am. Chem. Soc., **110**, 2296-2298 (1988).
23. E. Lenderink, K. Duppen and D.A. Wiersma, J. Phys. Chem., **99**, 8972-8977 (1995).
24. E. Lenderink, *Femtosecond Chemistry in Solutions*, Ph.D. thesis, University of Groningen, 1995.

25. R.W.J. Zijlstra, P. Th. van Duijnen, B.L. Feringa, T. Steffen, K. Duppen and D.A. Wiersma, J. Phys. Chem. A, **101**, 9828-9836 (1997).
26. S. Mukamel, *Principles of Nonlinear Optical Spectroscopy*, Oxford University Press, New York, 1995.
27. S. Mukamel, C. Ciordas-Ciurdariu and V. Khidekel, *Time-Frequency and Coordinate-Momentum Wigner Wavepackets in Nonlinear Spectroscopy*, in: Advances in Chemical Physics, Ed: P. Gaspard and I. Burghardt, John Wiley and Sons, Inc., New York, 1997.
28. M.D. Levenson and S.S. Kano, *Introduction to Nonlinear Spectroscopy*, Academic Press, San Diego, 1988.
29. C.J. Bardeen, Q. Wang and C.V. Shank, Phys. Rev. Lett., **75**, 3410-3413 (1995).
30. Y.J. Yan, L.E. Fried and S. Mukamel, J. Phys. Chem., **93**, 8149-8162 (1989).
31. G.R. Fleming, *Chemical Applications of Ultrafast Spectroscopy*, Oxford University Press, New York, 1986.
32. L. Salem, Science, **191**, 822-830 (1976).
33. P. Piotrowiak, G. Strati, J. Warman and W. Schuddeboom, J. Am. Chem. Soc., **118**, 8981-8982 (1996).
34. K. Duppen, F. de Haan, E.T.J. Nibbering and D.W. Wiersma, Phys. Rev. A, **47**, 5120-5137 (1993).
35. A. Bromberg and D.J. Meisel, J. Phys. Chem., 2507-2513 (1985).
36. J. Ma and M.B. Zimmt, J. Am. Chem. Soc., **114**, 9723-9724 (1992).
37. C. Zener, Proc. Roy. Soc. London, A, **137**, 696-702 (1932).

Solvent Dependent Excited State Dynamics and Charge Separation of *Para*-Substituted TPEs

6.1 Introduction

As reported in the introduction of the previous chapter, tetraphenylethylene (TPE) has been widely used as a model alkene in a large number of spectroscopical investigations with the aim to study the sudden polarization effect in the condensed phase[1-11]. In these investigations, the solvent dependent TPE excited state lifetimes and dynamics as well as its electronic nature have been studied by various techniques. It has been established that a polar form (i.e. a CT state) of the twisted TPE excited state does exist,[3-7, 9, 11] even though evidence has been provided that this is not the only state present at this geometry, especially in nonpolar solvents. These findings have been confirmed by the femtosecond pump-probe measurements presented in the previous chapter, where a dramatic difference in the TPE excited state lifetime and absorption spectrum was observed between polar and nonpolar solvents. Especially an absorption band around 500 nm, which was intense in polar solvents only and which was formed after several picoseconds, could be assigned to the twisted CT state of TPE. However, the much weaker intensity of this absorption in cyclohexane strongly suggested a less populated CT state in this medium. This was confirmed by fitting the various data sets to a kinetic model, which revealed the existence of another twisted excited state in cyclohexane. This second twisted excited state was assumed to be non-absorbing at 500 nm and of a nonpolar nature.

The main reason for the (D_2-symmetrical) TPE being the popular choice in the aforementioned studies is the fact that, apart from it meeting the symmetry requirements to study the sudden polarization effect, TPE is a commercially available compound which is soluble in a large number of organic solvents. Unsurprisingly, much less is known about the impact of the addition of substituents to the TPE phenyl rings on both the twisting dynamics and the charge separation process, not in the least because such compounds are not as readily available as TPE itself. This is unfortunate, since the availability of such information could provide valuable insights on, for instance, the tunability of the CT states in symmetrical alkenes by means of the introduction of electron directing substituents at the phenyl rings.

Only a few studies have been reported on *para*-substituted TPE's[4, 6, 9] (figure 6.1). First of all, Ma and Zimmt published a study[9] in which they investigated four different compounds (**I** to **IV**) by means of picosecond optical calorimetry in methylcyclohexane.

It was observed that for all compounds except for **II** an equilibrium exists between two conformationally relaxed states and that an intense long-lived fluorescence could be detected with an emission maximum at $\lambda = 542$ nm[4]. Between compounds **I**, **III** and **IV**, only small differences where observed even though **III** and **IV** showed a slight increase in both fluorescence quantum yield and excited state decay rate.

These observations did not apply to compound **II**, however, which barely showed any steady state fluorescence and had a much shorter excited state lifetime. This was explained by assuming more explicit CT nature for the excited state of **II**, which prevented recrossing to the other conformationally relaxed state held responsible for the observed fluorescence.

Albeit not unexpected, this latter finding is still intriguing, since the non-symmetrical substitution of the two halves of the molecule in the case of compound **II**

apparently provides the necessary (intramolecular) symmetry breaking which might very well be solely responsible for effectively polarizing the twisted excited states, without requiring an external symmetry lowering perturbation (i.e. a solvent shell). This observation is a clear indication that minor modifications to the molecule structure already can have a dramatic effect on the CT behaviour of such compounds.

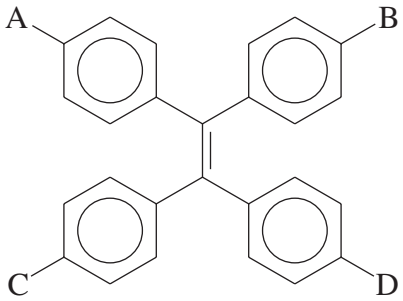

Figure 6.1

I A-D = H;
II A, B = H, C, D = CH_3;
III A≠B = (H, CH_3), C = H, D = CH_3;
IV A-D = CH_3

Another investigation involving a *p*-substituted TPE has been reported by Schuddeboom et al.[6] In this work, *para*-methoxy-TPE (A=B=C=D=OCH_3 in figure 6.1) as well as TPE itself have been studied by means of time-resolved microwave conductivity studies using cyclohexane and benzene as a solvent. It was established that the conformationally relaxed excited states of both TPE as well as its *p*-methoxy-subsituted analogue exhibited zwitterionic behaviour in cyclohexane. The nanosecond timescale of the experiments prohibited the detection of such behaviour in benzene, which is likely to be indicative of a shorter excited state lifetime in that particular solvent.

It is obvious that on the basis of the limited amount of information present no definite conclusions can be drawn regarding the role of the substituents on the TPE excited state behaviour, and that additional investigations are required. In order to gain more insight in the possible role of substituents on the TPE excited state shape and dynamics, this chapter will be dedicated to the investigation of a number of *p*-substituted TPE's by means of time resolved dual colour pump probe spectroscopy as described in chapter 5. The *p*-substituted TPE's presented in this chapter have been synthesized and characterized by means of ^{13}C NMR by Anne-Marie Schoevaars, for which she is gratefully acknowledged.

In the pump-probe experiments, the same experimental setup as described in chapter 5 has been used with one important modification. In the experiments reported in this chapter, the relative pump and probe beam polarizations have been oriented under a 45° angle with respect to each other. With a polarizing beam splitter, both the parallel (∥) and perpendicular (⊥) oriented signals have been separated behind the sample and detected simultaneously with two photodiodes of identical type. This is an important improvement, since it provides additional information regarding orientation of transition

dipoles and rotational diffusion[12]; topics which could only be briefly addressed in the previous chapter due to the separate detection of these signals there.
The following compounds have been investigated and compared:

1 A-D = H (see chapter 5 for more elaborate data)
2 A-D = CH_3
3 A-D = OCH_3
4 A-D = F
5 A-D = NO_2

The motivation for the selection of these particular components is that their substituents both exhibit electron donating (**2**, **3**) as well as electron withdrawing (**4**, **5**) behaviour in terms of the Hammett equation[13]. In this chapter, the interesting question is treated whether it is possible to utilize such effects in the 'tuning' of the charge separation in the excited states of the functionalized TPE's.
The excited state dynamics of all compounds has been investigated in the nonpolar solvent cyclohexane and the polar solvent ethanol. The only exception is compound **5**, which proved to be almost insoluble in the former. Solubility problems also prohibited the investigation of phenyl- and amino-substituted TPE's.

The outline of this chapter will be very similar to that of the previous one: first the excited state behaviour in the first two picoseconds will be described, followed by the dynamics at a longer timescale (~50 ps). The latter transients will be fitted to the same kinetic model as described in chapter 5 in order to compare the various results.

6.2 Results and Discussion

6.2.1 The First Two Picoseconds

For compounds **2-4**, the excited state behaviour in the first two picoseconds closely resembles that of TPE itself. The transients recorded in cyclohexane of **2-4** are compared in figure 6.2. Compound **5** showed anomalous behaviour which will be discussed later.

As in the case of **1** (TPE), the pump probe response of **2-4** is largely solvent independent over the first 2 ps. In the 650 nm transients, the same vibrational coherence can be observed as reported for **1**, even though the oscillations are somewhat less pronounced here. The main reason for this difference in amplitude is that the 650 nm pump pulse in the experiments described here was somewhat longer (~80 ps) than in the case of the experiments reported in chapter 5 (~65 ps). This pulse broadening was caused by a slight modification in the alignment of the quartz prisms used for the wavelength selection in front of the sample. This adjustment was made to allow inclusion of the blue part (400-450 nm) of the continuum. This resulted in a slight increase of prism material in the probe beam, thus altering the (non-linearity of the) chirp of the continuum pulse. Even though this chirp was compensated for by adjusting the positioning of the grating pair, the slightly longer pulse widths at the red part of the spectrum could not be avoided.

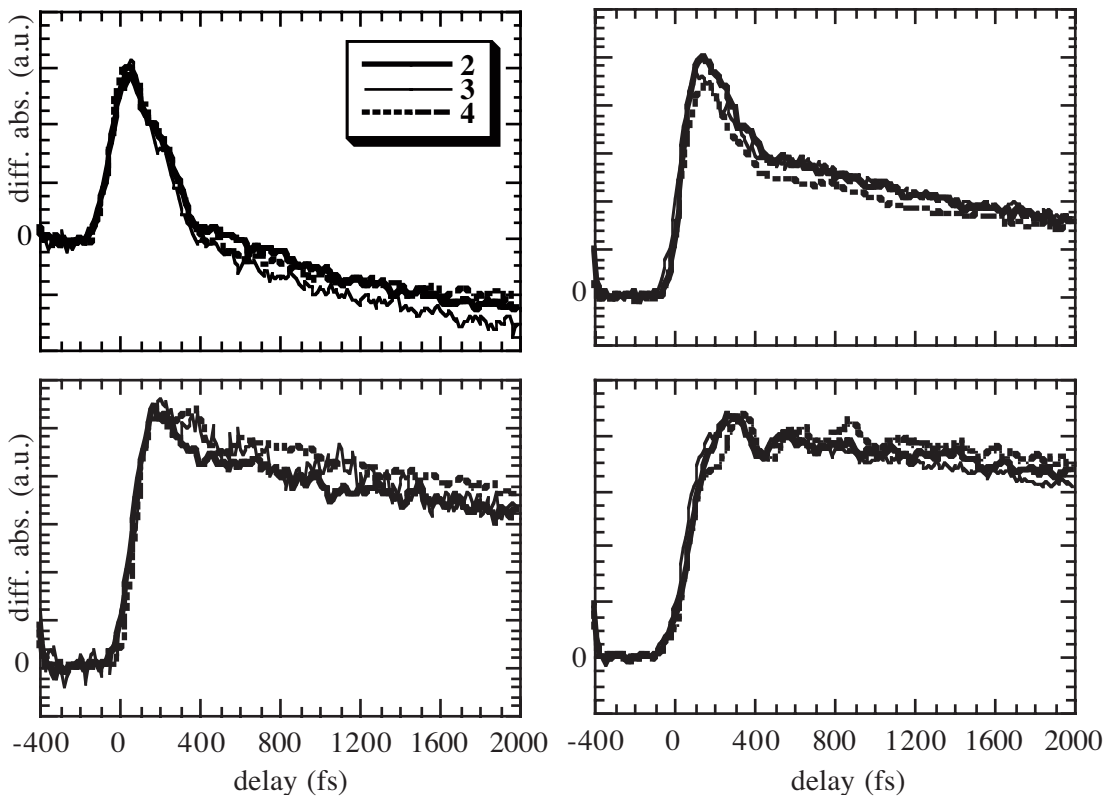

Figure 6.2 Pump probe spectra (|| polarization; difference absorption in arbitrary units) at 500 nm (top left), 550 nm (top right), 600 (bottom left) and 650 nm (bottom right plot) of the first 2 ps of **2**-**4** in cyclohexane.

It is apparent from figure 6.2 that the spectral evolution of **2**-**4** is quite similar in the first 2 ps.

However, some subtle differences can be observed when comparing them with **1**. This can be observed in figure 6.3, where the transients at 500 nm and 650 nm of **1** and **2** in cyclohexane are compared. The main difference is that the buildup of the stimulated emission at 500 nm as depicted in the top plot of figure 6.3 is somewhat slower in the case of the functionalized TPE's than in the case of TPE itself. Apparently the elongation of the C-C central bond, which in chapter 5 was held responsible for the large Stokes shift of this stimulated emission, appears to be somewhat delayed by the introduction of functional groups on the phenyl rings.

This is somewhat surprising especially in the case of **4**, since the small fluorine is only fractionally larger than a hydrogen atom[14] and much smaller than for instance a methyl group. The stimulated emission build-up rates of **2** and **4** are, however, comparable as can be seen from figure 6.2.

In figure 6.4 the pump-probe transient at 500 nm of tetrafluoroderivative **4** is compared to that of TPE itself. It appears that in the case of **1** and **4** the transients at 500 nm are more alike even though the build-up of the stimulated emission is still somewhat quicker (~ 50-100 fs). The most likely explanation for this small delay in the buildup of the stimulated emission in the case of **2**-**4** in comparison to **1** is that the C-C central bond elongation is accompanied by some initial twisting around this bond. The latter component of the dynamics can be responsible for the slower buildup, since it has been reported

before that the introduction of *p*-substituents on the phenyl rings introduces additional solvent drag, which slows down the twisting process[9]. These findings will be supported by the transient behaviour at longer time scales (*vide infra*).

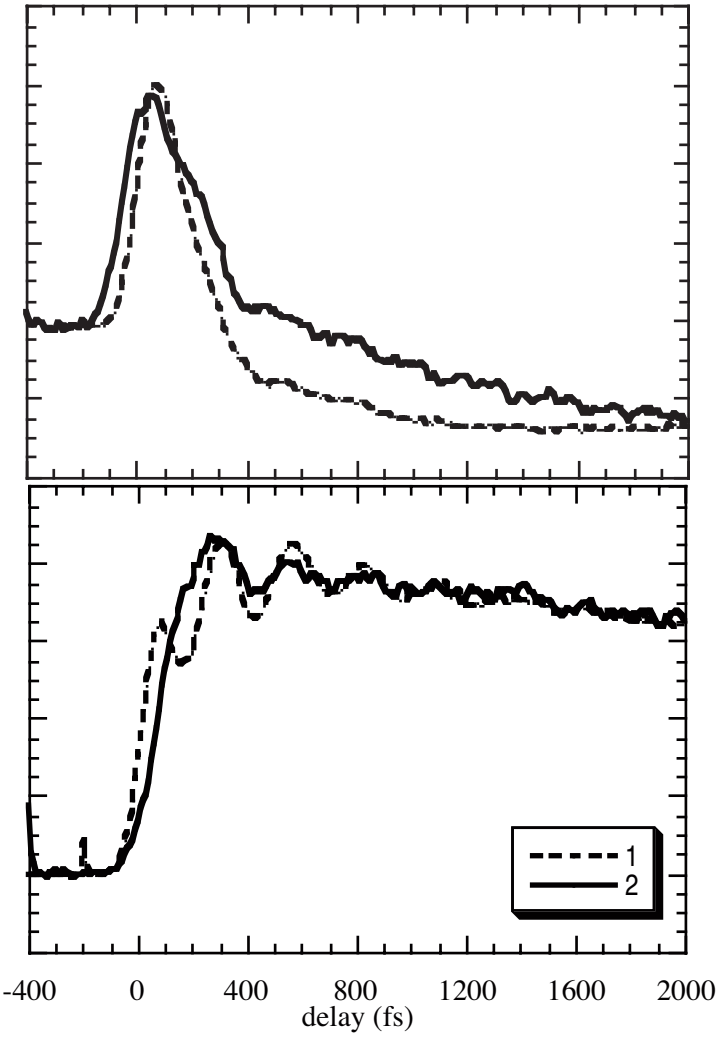

Figure 6.3 Pump probe spectra at 500 nm (top plot) and 650 nm (bottom plot) of the first 2 ps of **1** and **2** in cyclohexane.

Another observation that can be made from figure 6.3 is that the vibrational coherence observed at the 650 nm transient is more or less the same for both **1** and **2**, apart from amplitude of the beats and the behaviour in the first 100 fs. As already mentioned in chapter 5, the pulse shape of the 650 nm probe pulse has a distinct influence on the transient response[15] and the somewhat broader pulse used in the experiments reported here can be held responsible for the missing beat in the first 150 fs in the spectrum of **2**. Apart from that, the periodicity of the oscillations (124 cm^{-1}) is the same between **1** and **2.** These were attributed[10,11] to wavepacket dynamics in the scissoring motions of the geminal phenyl rings[16], which resembles the correlated motion of two interlocking ratchets. Apparently, these are unmodified for the *p*-substituted TPEs, which can be expected since the *p*-subtituents are situated on the axis of rotation of the phenyl

groups involved in these motions. This will drastically limit their influence on the rotation dynamics.

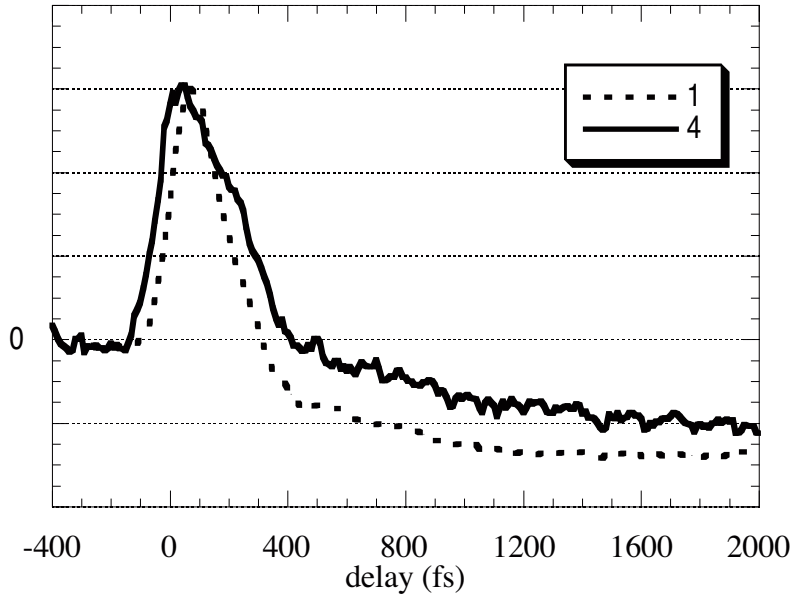

Figure 6.4 500 nm transients (|| orientation of pump and probe) of **1** and **4** in cyclohexane.

A validation of this assumption could be obtained by repeating these experiments with *o*- or *m*-substituted TPE's in which case the substituents are expected to have a more pronounced effect on the scissoring motions. This is beyond the scope of the present study though.

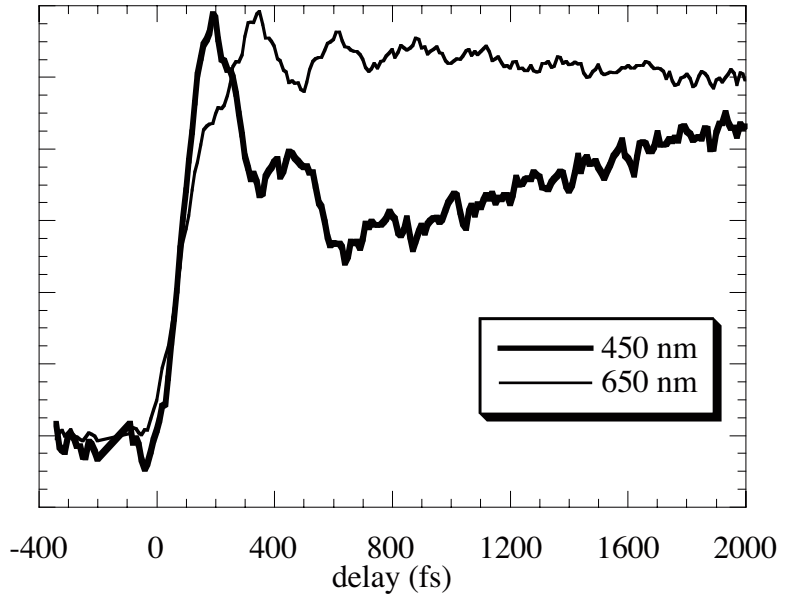

Figure 6.5 450 nm (bold line) and 650 nm (thin line) transients of **2** in cyclohexane (|| pump probe polarization orientation)

A highly relevant observation supporting the assignment of the oscillations to these scissoring motions is made in the absorption spectra of **2**-**4** at 450 nm (figure 6.5).
A complication of measuring at 450 nm is that the t=0 fs point, i.e. the point where pump and probe pulse coincide, could not be determined by the routine autocorrelation technique[12] due to the fact that the difference frequency of the pump and probe pulses lies well within the infrared part of the spectrum. At the time of these experiments, no appropriate detection was available. The t=0 point has been estimated by mapping the rising flank of the probe response at 450 nm on that of 650 nm.

Figure 6.5 clearly shows the 450 nm oscillations to be in almost perfect counterphase with that observed at 650 nm. As explained in the theoretical description in chapter 5 (see also figure 5.2), this is fully consistent with what one would expect for wave packet dynamics on a bound potential, where the transients at the inner and outer probe frequencies exhibit oscillations in counterphase with respect to each other[17-20]. Since this wavelength was not available on the original experimental setup used in the case of **1**, the oscillations at 450 nm were not detected in the experiments reported in chapter 5.

Finally, the excited state behaviour of **5** has to be discussed. Figure 6.6 shows the excited state behaviour of **5** probed at 650 nm. Quite surprisingly, within 500 fs the 650 nm transient transforms into a 'steady state' absorption lacking any significant decay dynamics, even after hundreds of picoseconds. The same behaviour is also observed at the other probe wavelengths. On the basis of the sub-nanosecond dynamics, it is estimated that the lifetime of **5** extends towards the μs domain, which is indicative of the existence of a triplet excited state. It is well documented that triplet states can be formed effectively in the presence of NO_2-groups[21-23]. Therefore, the most likely explanation for this phenomenon is that a rapid avoided crossing between the originally populated S_1 surface and a localized excitation on the NO_2 groups takes place, after which the observed triplet state is formed by highly efficient intersystem crossing. In conclusion, the excited state behaviour of **5** is completely different from that of the other TPE's and will therefore be excluded from further discussions.

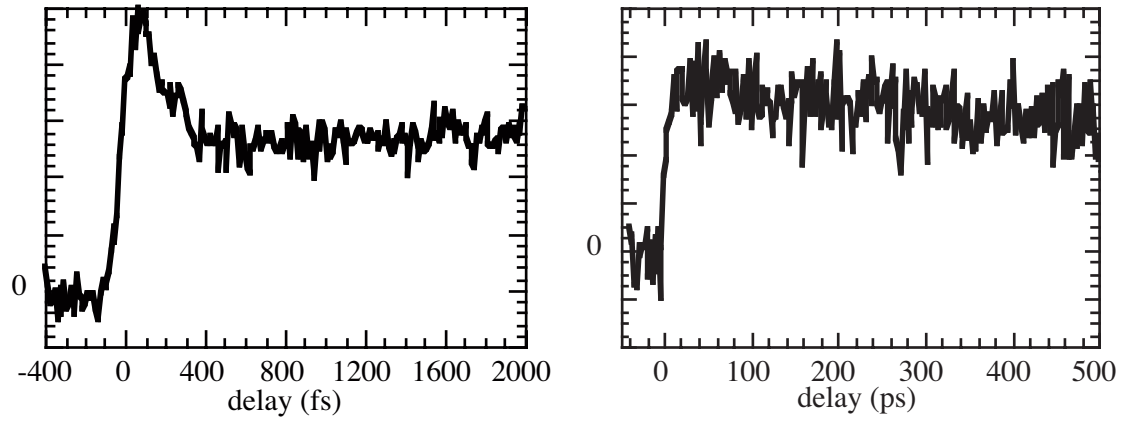

Figure 6.6 650 nm transients of **5** in ethanol. Left panel depicts the first 2 ps, right panel depicts the behaviour on sub-ns time scales.

6.2.2 Longer Time Scales in Cyclohexane

Figure 6.7 depicts the pump probe transients (‖ orientation) of **2**, **3** and **4** at longer time scales in cyclohexane. From figure 6.7 it becomes clear that all three compounds show roughly the same behaviour within the investigated timeframe, especially for the red part of the spectrum. At the green part some more substantial, albeit still minor, differences occur. Two observations can be made: first of all, the intensity of the stimulated emission of **4** appears to be weaker than that of **2** and **3**. Furthermore, **2** and **4** show a buildup of an absorption at 550 nm (similar to **1** in this solvent), which appears to be somewhat weaker for **3**.

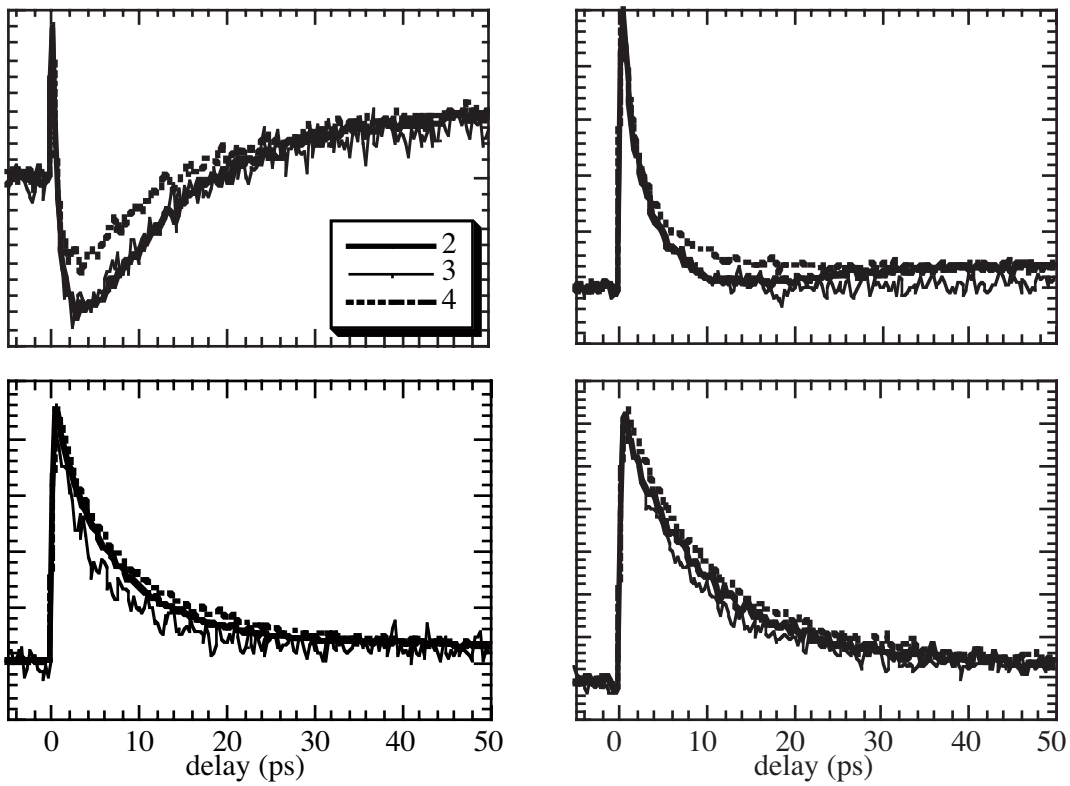

Figure 6.7 Pump probe spectra (‖ pump probe polarization orientation) up to 50 ps at 500 (top left), 550 (top right), 600 (bottom left) and 650 nm (bottom right panel) of **2**, **3** and **4** in cyclohexane.

At this stage, it becomes relevant to focus on the polarization dependent behaviour of the various transients[12]. Figure 6.8 shows the ‖ versus ⊥ polarization orientation of the 600 and 500 nm transients of **2**-**4** in cyclohexane. The data prove to be rather puzzling and difficult to interprete. First of all, the 600 nm transients show comparable behaviour for **2**-**4**, in which the depolarization of the transients occurs on a timescale of 10-20 ps. The 550 and 650 nm transients behave similarly. The depolarization rate of **3** is the highest (10 ps), followed by **2** and **4** (20 and 25 ps respectively). Since the rate of twisting dynamics for **2**-**4** appears to be roughly the same, another explanation has to be found for this difference in depolarization rates. It is likely that this is somehow connected to the freely

rotating out-of-plane local dipoles associated with the methoxy groups of **3**, a feature absent in compounds **2** and **4**.

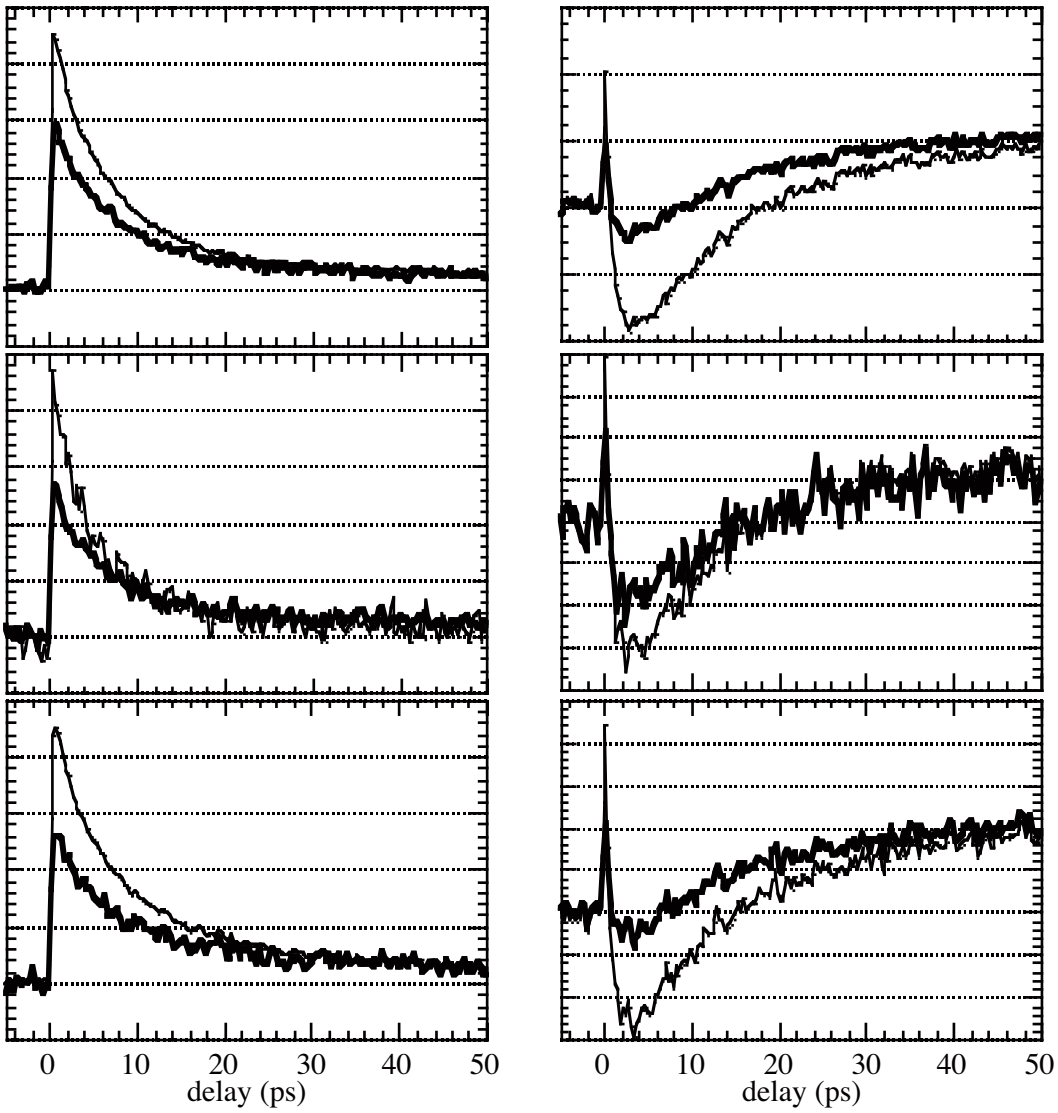

Figure 6.8 ∥ (thin line) and ⊥(bold line) pump probe orientations at 600 (left panels) and 500 nm (right panels) of **2**-**4** (from top to bottom) in cyclohexane.

When comparing the depolarization rates at the red part of the spectrum to the polarization dependent behaviour at 500 nm, it becomes clear that the rotational diffusion (i.e. the randomization of molecule orientation in the solvent) cannot be responsible for the observed decay in anisotropy. These transients show some complex behaviour. At first, when focussing on the lifetime of the stimulated emission occurring in the ∥ polarized spectrum at 500 nm, it appears to be roughly the same as the depolarization rates of the 600 nm transients. But at 20 ps, a substantial difference in transient intensity of the two polarization directions still exist in the case of **2** and **4**, and in fact this difference is still partly present at 50 ps in the case of **2**. This proves that the depolarization of the red part of the spectrum cannot be assigned to rotational diffusion, due to the fact that this would also cause complete depolarization at other wavelengths such as the 500 nm transients

examined here. Therefore, we have to conclude that two (or more) different modes of motion are being monitored. This can be explained in the following manner.

It has been reported before that the red part of the spectrum of the TPE excited state is connected to the twisting dynamics[1, 3, 11]. On the basis of this information and on the more intense absorption for the || oriented probe channel in the first picoseconds, it can be concluded that the orientation of the transition dipole moment with the probe at 600 nm is more or less parallel to that of the $S_1 \leftarrow S_0$ excitation, which exhibits a perpendicular orientation relative to the central double bond. The rotation of this bond randomizes the orientation of this transition dipole moment, which leads to the observed decay of the anisotropy at 600 nm. This can be regarded as an intramolecular reorganization which requires only a partial reorganization of the solvent cage.

The lifetime of the emission part of the spectrum at 500 nm is the same as that of the intramolecular rearrangement, responsible for the depolarization at the red part of the spectrum. This is another justification of the assumption that the observed transition at 600 nm has a transition dipole parallel to that of the $S_1 \leftarrow S_0$ transition as, for obvious reasons, the stimulated $S_0 \leftarrow S_1$ emission will also be polarized that way.

In addition, at 500 nm a second transition is probed. Due to the fact that this transition is more intense at the perpendicular pump probe orientation (see figure 6.8), it can be concluded that the transition dipole moment is oriented perpendicular to that of the $S_1 \leftarrow S_0$ excitation. Moreover, it appears to be unconnected to the central bond rotation, which must mean that the central bond rotation has no influence on the depolarization of this transition. Therefore, the orientation of the transition dipole moment of this excitation must be parallel to the axis of rotation of the central bond, hence (more or less) parallel to the central bond itself (figure 6.9).

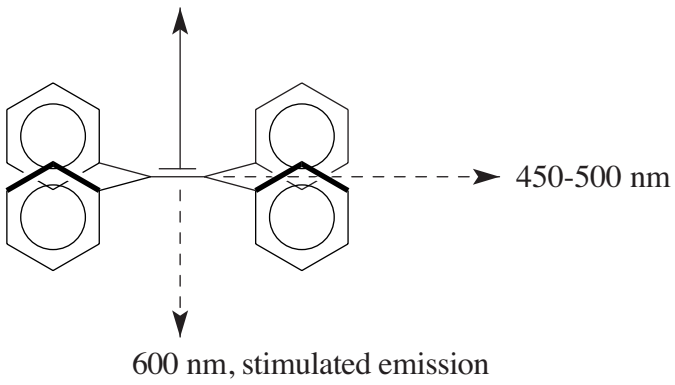

Figure 6.9 Schematic orientation of the proposed transition dipole moments of $S_1 \leftarrow S_0$ (solid arrow) and various $S_n \leftarrow S_1$ transitions (dashed arrows) of TPE. The 600 nm transition dipole is oriented anti-parallel to the $S_1 \leftarrow S_0$ transition for reasons of clarity only.

This picture is, of course, schematic and it is very well possible that the transition dipole of the 450-500 nm absorption will, for instance, be parallel to the C-C phenyl bond. But even then, central bond rotation will only partly depolarise the orientation of the

transition dipole moment and larger motions involving the whole molecule will have to take place to complete this process. Therefore, the complete depolarization of the 500 nm transient is ultimately caused by the (solvent dependent) rotational diffusion.

Confirmation for this theory can be found in the behaviour of the 450 nm transient. Figure 6.10 shows the 450 nm probe signal of **4** in cyclohexane. Intriguingly, at the perpendicular pump probe polarization, the absorption is immediately present upon excitation and the only dynamics observed are connected to the excited state lifetime of the molecule. For the parallel polarization however a buildup takes place which matches the perpendicular intensity at similar time scales as observed for the 500 nm transient. This is strong evidence for an orientation of the transition dipole moment perpendicularly to that of the $S_1 \leftarrow S_0$ for this particular excitation.

Additional evidence for the observation of two rather than one transition at 500 nm can be gained from analyzing the intensities of the ∥ and ⊥ channels (figure 6.8). For a probed transition with a transition dipole moment parallel to that of the initial excitation by the pump pulse, the intially observed ratio in the transient intensities of the two probe directions (∥ /⊥) should roughly be 3:1[12]. However, the stimulated emission at 500 nm, especially in the case of **2** and **4**, clearly exceeds this ratio. This can only be explained by assuming a simultaneous polarized absorption along the perpendicular channel which increases the aforementioned ratio. Compound **3** does not seem to exhibit this behaviour, the ratio observed in the stimulated emission between the respective probe orientations appears to be in accordance with a single transition with parallel transition moment. In addition, the complete depolarization of the 500 nm transient already takes place within 20 ps, much faster than in the case of **2** and **4**.

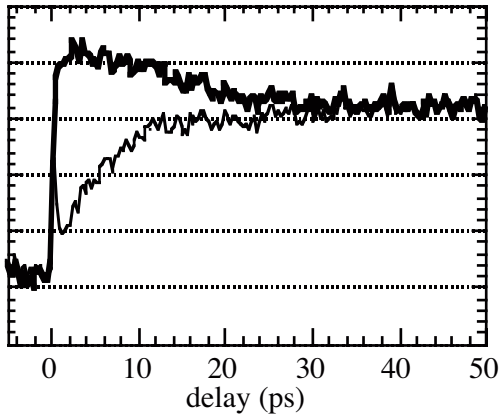

Figure 6.10 Pump probe spectrum (∥ thin line; ⊥ bold line) at 450 nm of **4** in cyclohexane.

There is a definite buildup of the 500 nm absorption in the spectrum of **3**, as was also observed for 2 and 4, but this absorption is already strongly depolarized over the first few picoseconds. Even though not yet fully understood, this must again be connected to the out-of-plane local dipole associated with the methoxy substituents of **3**. This considerable out-of-plane local dipole near the phenyl rings, which can shift quickly by the simple rotation of the C-O bond, is absent in **2** and **4**. If the fast randomization of the out-of-plane dipoles due to the rotation of the methoxy groups alters the direction of the

transition dipole of interest, this effect may be responsible for the rapid depolarization of the 500 nm probe signal of **3**. This depolarization decay then is not related at all to the rotational diffusion time of compound **3**.

6.2.3 Longer Time Scales in Ethanol

Next, the behaviour of **2**-**4** in ethanol will be analyzed. In figure 6.11 the pump probe spectra of **2**-**4** in ethanol are shown.Two remarkable observations were made. First of all, the behaviour at 500 nm is completely different for **2**, **3** and **4**. In the case of **1**, this absorption was assigned to its charge separated twisted excited state[11] (see also chapter 5), which would indicate significant differences in charge separation behaviour of **2**-**4**. This will be addressed in more detail later (*vide infra*).

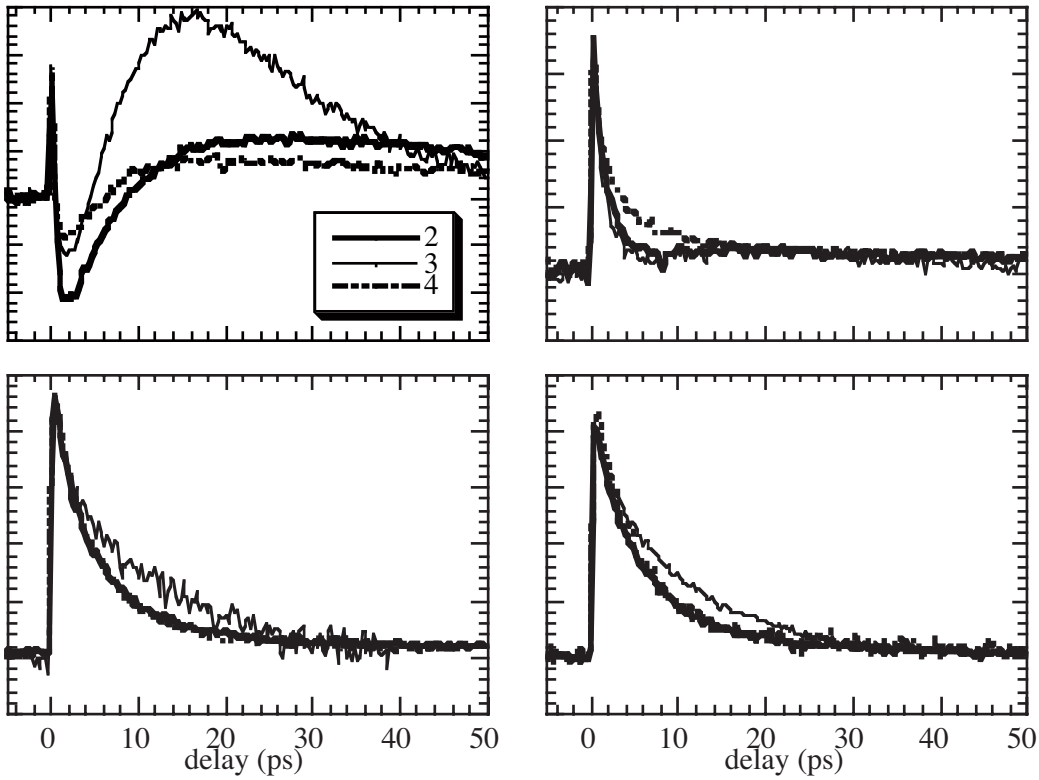

Figure 6.11 Pump probe spectra (|| pump probe orientation) at 500 (top left), 550 (top right), 600 (bottom left) and 650 nm (bottom right panel) of **2**-**4** in ethanol.

The second remarkable feature occurs in the red part of the spectrum. In contrast to the situation in cyclohexane (see figure 6.7), the central bond twisting dynamics of **3** are slower than those of **2** and **4** in ethanol. The most likely explanation is the fact that the methoxy groups of **3** are capable of forming hydrogen bonds with ethanol[13], which leads to an increase in the solvent drag for **3**, thus effectively slowing down the phenyl motions.

Figure 6.12 shows the polarization dependent transient behaviour in ethanol. At the red part of the spectrum, similar behaviour as in cyclohexane was observed. The

depolarization of **3** takes slightly longer than that of **2** and **4**, which is indicative of the slower twist in ethanol as just discussed.

More interestingly, the behaviour at 500 nm is somewhat different when compared to cyclohexane. Clearly, the depolarization of the 500 nm transients for **2** and **4** in ethanol is considerably faster. Confirmation of this observation can again be obtained from analyzing the 450 nm transient. Figure 6.13 shows this transient of **2** in ethanol. While the anisotropy in the first few ps is comparable to that in cyclohexane, the depolarization is already complete in 30 ps or less.

Apparently, rotational diffusion takes place much faster in ethanol. This leads to the conclusion that both solvent polarity and solvent viscosity have a distinct effect on the dynamics of such systems, an effect that also has been observed for the dynamics of *cis*- and *trans*-stilbenes[22, 24].

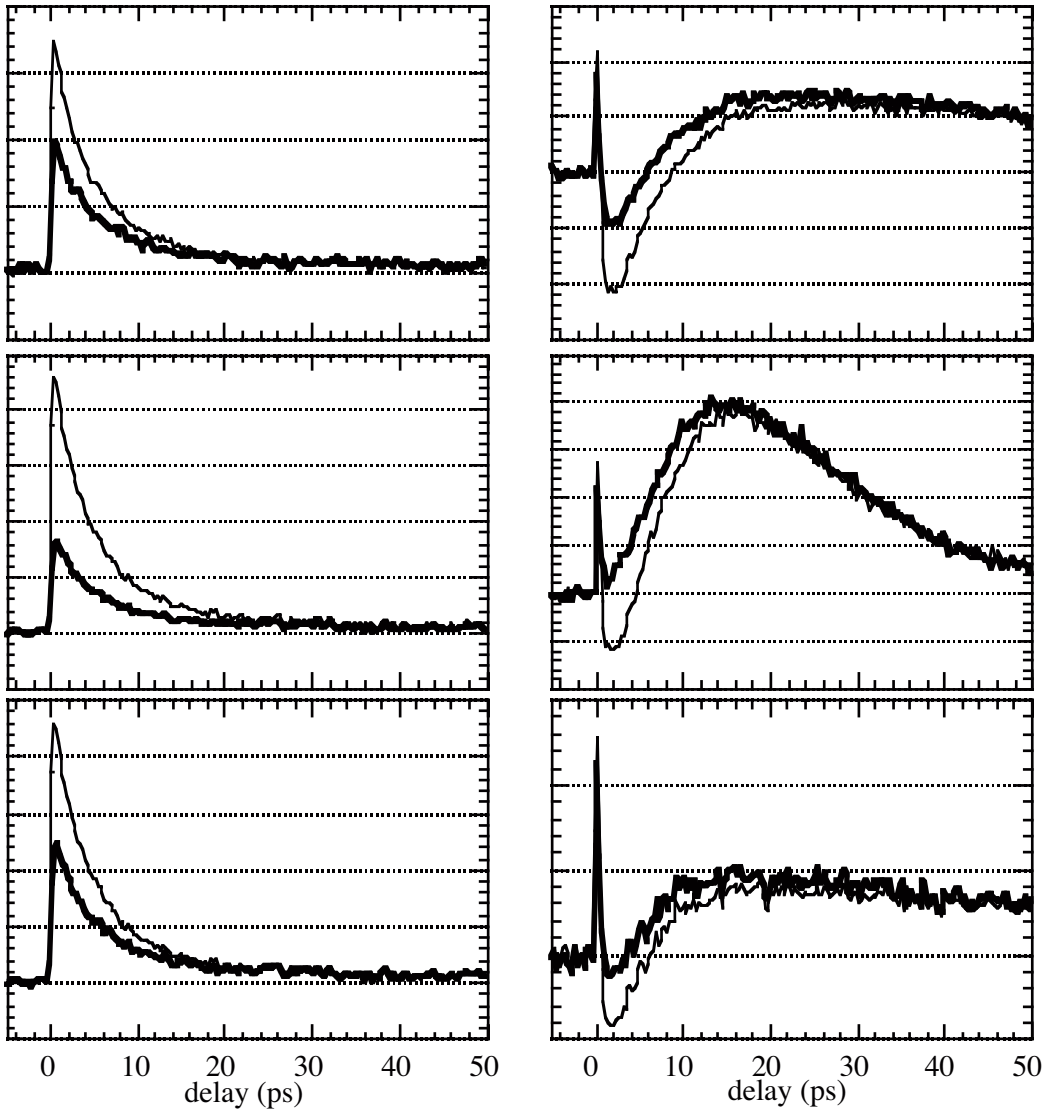

Figure 6.12 600 nm (left panels) and 500 nm (right panels) transients of **2**-**4** (top to bottom) at parallel (thin line) and perpendicular (bold line) pump probe orientation in ethanol.

In figure 6.14 the transients at 500 nm and 600 nm of the substituted TPEs **2**-**4** in cyclohexane and ethanol are compared to those of TPE itself. These two transients are indicative of the behaviour at the blue flank of the spectrum (450-500 nm) and the yellow-red flank of the spectrum (550-650 nm).
The latter transients show little solvent dependence. The shape of the transients is the same in both cyclohexane and ethanol, and the differences in decay dynamics are subtle.

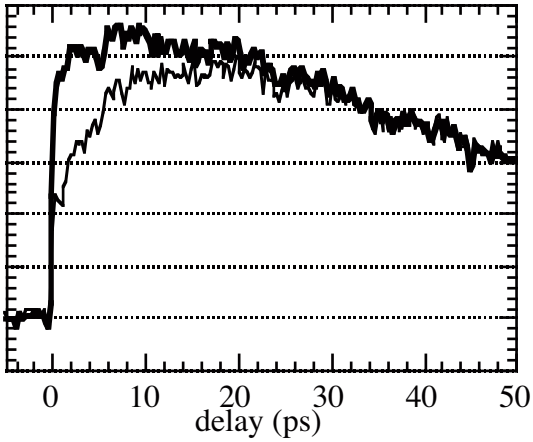

Figure 6.13 Pump probe spectrum (∥: thin line, ⊥: bold line) of **2** at 450 nm in ethanol.

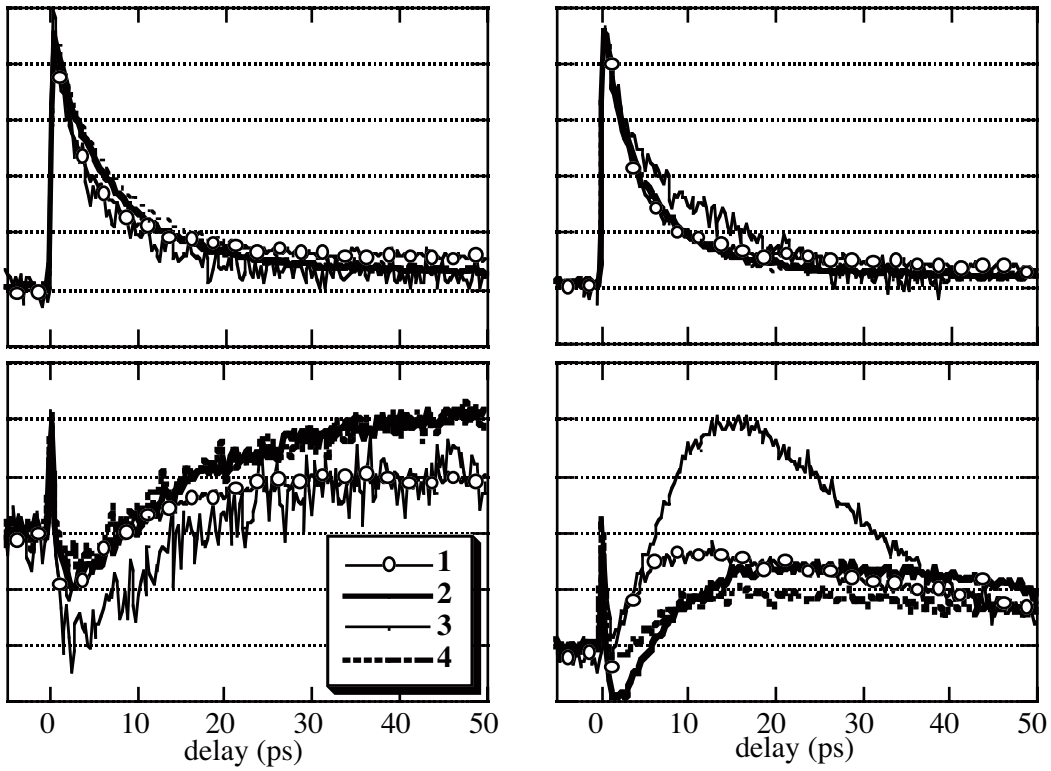

Figure 6.14 Pump probe spectra of **1**-**4** at 600 (∥; top panels) and 500 nm (⊥;bottom panels) in cyclohexane (left panels) and ethanol (right panels).

Apparently, the central bond twisting dynamics that are held responsible for the decay of the red flank of the spectrum are largely solvent independent.

Larger differences can be detected in the green-blue part of the spectrum. Relevant solvatochromic effects can be observed and even in cyclohexane some differences occur between the different compounds even though the overall behaviour appears the same: after 50 ps all transients have reached some sort of steady state which appears to extend into the nanosecond domain. Compounds **2** and **4** show a more intense long-lived absorption at 500 nm than **1** and **3** in cyclohexane. However, care has to be taken with such observations. Even though the intensity of **3** in comparison to **2** and **4** is much smaller, analysis of the data in figure 6.7, which displays the parallel pump probe polarization orientation at 500 nm in cycohexane, shows no significant difference in intensity between **2**-**4**. Therefore, the depolarization rate appears to play a significant role here as well. This topic will be addressed in more detail when the results of the fitting procedure are being discussed (*vide infra*).

A complicating fact is that these transients have been recorded without quantifying the difference absorption in an absolute way. In both chapter 5 and 6, data are scaled with respect to each other by assuming similar response to the pump pulse. In other words, the intensities of the probe transients around t=0 fs are assumed to be similar for the various transients at mutual wavelength and polarization orientation. Even though not unreasonable, this obviously is a somewhat crude scaling method which can easily introduce errors in the relative transient intensities. As a result, comparison of transients from different measurements has to be handled with care especially when (small) differences in intensities are concerned. It should be emphasized, however, that differences in transient shape and decay dynamics as well as large differences in intensities obviously remain highly relevant for the analysis of molecular dynamics.

The behaviour at 500 nm of **1**-**4** exhibits large differences. The most remarkable observation is the intense absorption of **3** and its rapid decay. A possible explanation may be based on the fact that the methoxy groups are capable of special interactions with ethanol, e.g. the formation of hydrogen bonds with the solvent. This can cause increased stabilization of a charge separated state. The rapid decay in ethanol supports this theory, because a short lifetime is indicative of a narrow gap between excited and ground state potential energy surfaces, implying excited state stabilization[5].

Compounds **1** and **2** behave similarly in the later stages of the measurement, but the build-up of **2** is much slower than that of **1**. Finally, the absorption of **4** is surprisingly weak, even though its dynamics appear to roughly resemble those of **1**-**2**. At this point it is interesting to compare the behaviour of **2** and **4** at the blue part of the spectrum in both cyclohexane and ethanol (figure 6.15).

The overall behaviour of **2** and **4** in terms of lifetimes resembles that of **1** in cyclohexane and ethanol (see chapter 5). However, the intensity of especially the 500 nm transients can be regarded as puzzling. Both **1** and **3** have shown a strong increase of the absorption at 500 nm when the polarity of the solvent is increased, but **2** and **4** do not obey this trend. In fact, the buildup at 500 nm is more intense in cyclohexane for **4**, even though its lifetime is much shorter in ethanol.

This is confirmed by the decay dynamics of the 450 nm transient, which decays more rapidly in ethanol for both **2** and **4**, even though the sample time of 50 ps is almost too

short to observe this in the case of **2**. The differences in absorption intensity between **1**-**4** remain difficult to explain, however.

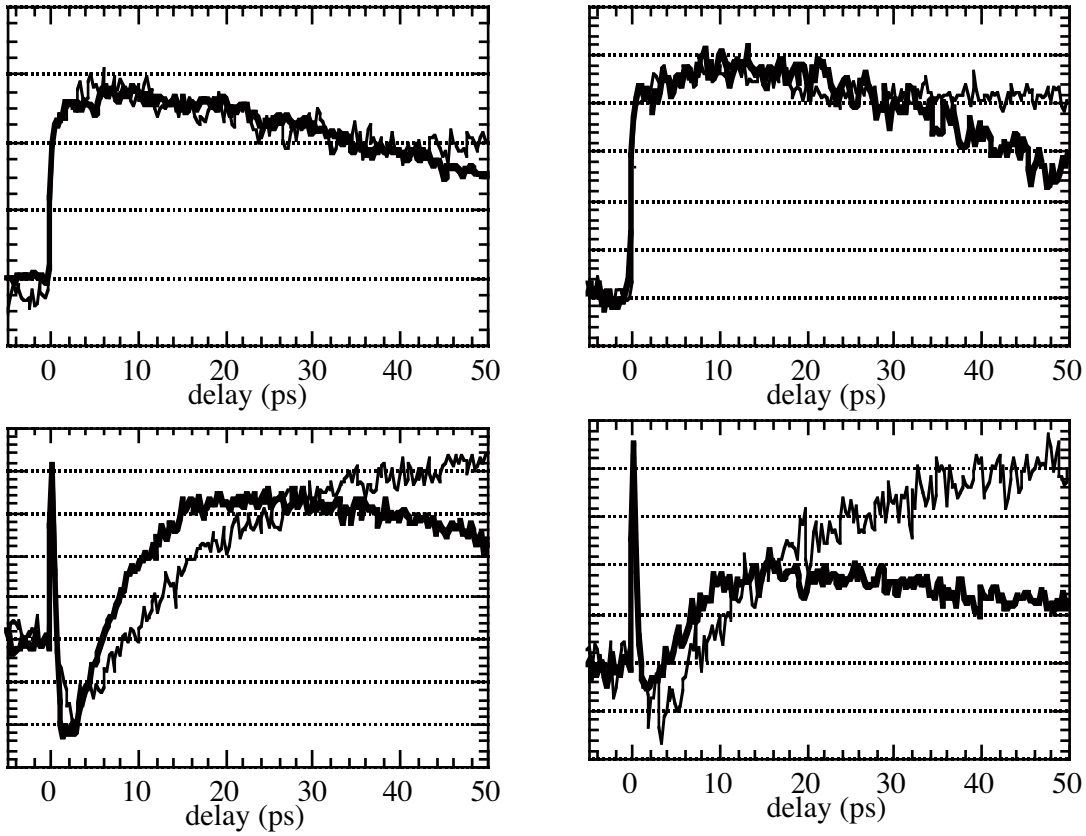

Figure 6.15 Pump probe spectra (⊥) of **2** (left panels) and **4** (right panels) in cyclohexane (thin line) and ethanol (bold line) at 450 nm (top panels) and 500 nm (bottom panels)

In chapter 5, the 500 nm absorption was assigned to the charge separated (CS) state of **1** at the (near) perpendicular geometry. For **3**, this assignment still appears to be valid, but **2** and especially **4** are more difficult to fit in this picture. For instance, this would suggest that for **2** and **4** the CS state is more effectively populated in cyclohexane (see figure 6.15 at 20 ps time scale). It is therefore likely that in this case the scaling of the data to the instantenous response has introduced a margin of error which causes this anomalous difference in intensities.

In order to create more insight in the overall potential energy landscape and the states involved, the global fitting routine as applied to TPE in chapter 5 has been repeated for **2**-**4** (equation 6.1). In this model, A is the Franck-Condon relaxed planar geometry whereas B and C are the perpendicular charge separated and charge resonant states. In the procedure, the 450-650 nm transients from 3-50 ps have been fitted according the kinetic model in equation 6.1, first with assuming K_{bc} and K_{cb} equal to zero. The ∥ oriented signals have been used, except in the case of 450 and 500 nm, for which the transients at both polarization orientations have been included. The first 3 ps have been removed from the fit to exclude the influence of ultrafast dynamics (see section 6.2.1) and vibrational cooling from the data. In cases where the fit to this model proved unsatisfactory, K_{bc} and

K_{cb} were included in the fit. The quality of the fits of **2**-**4** proved to be similar to those of **1** presented in chapter 5. The results are shown in table 6.1.

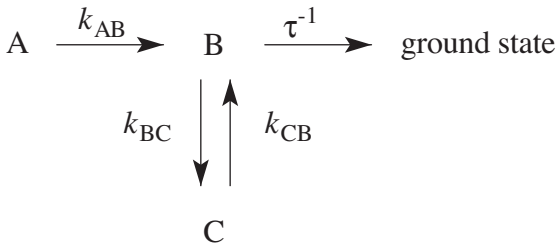

(6.1)

	k_{AB} (ps^{-1})	k_{BC} (ps^{-1})	k_{CB} (ps^{-1})	τ (ps)
cyclohexane				
1	0.46	0.042	0.082	$>10^3$
2	0.25	0.087	--	$>10^3$ a)
3	0.21	0.045	0.060	$>10^3$ a)
4	0.27	0.078	--	$>10^3$ a)
ethanol				
1	0.32			60
2	0.14			70
3	0.10			16
4	0.18			60

Table 6.1 Kinetic parameters for the dynamics of the excited state of **1**-**4**
a) all estimated to be similar to that of **1**

With regard to the twisting from the Franck Condon relaxed excited state to the twisted geometry (i.e. A→B), the fitted data clearly show the increase of solvent drag by the substituents as indicated by the significantly smaller values ofk_{AB} for **2**-**4** with respect to **1**. Intriguingly, the faster central bond rotation of **3** in cyclohexane in comparison to **2** and **4** as suggested by the transients at the red part of the spectrum (as depicted in figure 6.8), is not reproduced by the fit results. No definite explanation for this discrepancy can be provided even though the electronic nature of the methoxy groups must be connected to it. It is likely that the rotation of these groups is seriously hampered in ethanol as a result of the hydrogen bonding which can explain why the depolarization of the red part of the spectrum is in better agreement with the estimated k_{AB}.

The most remarkable finding is that for **2** and **4** in cyclohexane quite excellent fits could be obtained without including k_{CB}.This suggests a three state system for **2** and **4**, which shifts towards the third state without effective repopulation of the second one. This can explain the more intense 'perpendicular' absorption at 500 nm of **2** and **4**, an absorption assigned to the CS state in the case of **1**.

Even though the difference in 500 nm absorption intensity of **4** has already been discussed in terms of transient scaling, it still remains that some dramatic differences in intensity occur especially at the 500 nm transient in ethanol which cannot be explained this way. These remarkable differences in intensity can indicate that the oscillator strength of

the transition is sensitive to a combination of substituent and solvent effects which complicates comparisons between transients in different solvents.

Another possibility is that the λ_{max} of the absorption assigned to the twisted geometry shows solvatochromic behaviour. If, for instance, electron donating substituents cause a red shift whereas electron withdrawing substituents cause a blue shift in polar solvents, the behaviour at 500 nm in ethanol can also be easily explained. In that case, the absorption maximum of **4** will be shifted towards 450 nm. The transient at this wavelength provides hardly any evidence of twisting, as shown in both this as well as the previous chapter. So if the latter assumption is correct, it is impossible to establish an accurate estimate of the quantum yield of the CS state in compounds with electron withdrawing substituents on the basis of this data. This would imply that the weaker intensity of the 500 nm transient of **4** in ethanol is relevant. Unfortunately, at this point no definite evidence supporting either of the two theories is present and, for instance, more extensive DRF studies[25] extending those presented in chapter 4, can be helpful in providing answers to these questions.

The fits clearly show solvatochroic behaviour on the excitated state features. Many lifetimes in nonpolar solvents appears to extend into the nanosecond domain, whereas in ethanol lifetimes are limited to several tens of picoseconds. In cyclohexane, **2** and **4** appear to exhibit more pronounced CS behaviour than **1** and **3** on the basis of the 500 nm transient behaviour, as indicated by the global fits. This seems to indicate that both solvent as well as substituent effects can be the driving force behind the required symmetry breaking in the formation of long-lived CS intermediates. This cannot be fully explained on the basis of the work presented in this and previous chapters, which underlines the complexity of the phenomenon studied here.

In polar solvents like ethanol, the charge separation process appears to be less governed by subtle intramolecular effects. The interaction with the solvent governs this process completely. Especially the short lifetime of **3** indicates additional solvent stabilization of the CS state. This has been attributed to the role of hydrogen bonding between the ethanol acidic proton and the methoxy oxygens of **3**. The other investigated compounds all exhibit CS state lifetimes of 60-70 ps, which supports the theory that solvent rather than the substituent effects govern the electronic processes involved here.

6.3 Summary and Conclusion

In this chapter, time-resolved dual colour femtosecond pump probe studies of **2**-**4** in cyclohexane and ethanol have been presented. It has been shown that the dynamics at the first 2 ps are solvent independent and very similar to that of **1**, even though the elongation of the central bond appears to be slowed down a bit by the introduction of *para*-substituents. These substituents were shown to have a negligible influence on the frequency of the vibrational coherence observed at the 650 nm transient. The recording of the 450 nm probe transient revealed oscillations with the same frequency as those observed at 650 nm, but with the prefect counterphase. This is indicative of wave packet dynamics in a bound potential.

At longer timescales, explicit solvatochromic effects have been observed.

First of all, it has been established that rotation around the central olefenic bond as monitored at the red part of the spectrum, is mainly governed by solvent viscocity. In addition, it has been demonstrated by means of fitting the data to a kinetic model, that the introduction of substituents increase the solvent drag of the phenyl groups leading to a slower central bond twist in comparison to **1**. In the case of **3** this effect has been amplified in ethanol, due to the possible formation of hydrogen bonds with the solvent which introduces additional drag.

The separate detection of probe signals at both parallel and perpendicular orientation relative to the pump polarization has revealed that solvent polarity plays a significant role in the rotational diffusion rate for **2**-**4**. In ethanol, this process takes place much faster than in cyclohexane. It is likely that the polar solvent molecules induce local out-of-plane dipole moments at the (*para*-substituted-)TPEs, which accelerate the reduction of the initial polarization anisotropy. Furthermore, the difference in the depolarization rates at the red and blue flanks of the spectrum has demonstrated the observation of two different depolarization processes: the rotation of the central bond as well as the motion of the complete molecule in the solvent. The most remarkable solvent dependent differences have been observed at the 500 nm transient (⊥), which has been assigned to the CS state of such compounds in chapter 5. In cyclohexane, these transients exhibit lifetimes extending into the nanosecond domain in the case of **1**-**4**. However, the transients of **2** and **4** are more intense than those of **1** and **3**, indicative of a more effective CS state formation in the case of the former two compounds if this state can be held solely responsible for the spectral features of this transient. This is supported by the outcome of the fitting routine, which suggested an equilibrium between two states at the perpendicular geometry for **1** and **3** in this solvent, whereas this equilibrium almost completely shifted to one state in the case of **2** and **4**. Apparently, the *p*-substituents have a distinct influence on the charge separation process, even though no direct correlation with the electronic nature of the subtituents seems to be present. In order to be able to establish such a correlation, a more extensive study including a larger number of *p*-substituted TPE analogues is required. It can be concluded though that both intramolecular and intermolecular (i.e. the solvent) symmetry lowering effects play an important role in the formation of charge separated states.

In ethanol, the lifetimes τ of the probed (*p*-)TPE excited states are drastically shortened in comparison to cyclohexane, indicative of the more effective CS formation and stabilization for **1**-**4**. This appeared to be especially the case for **3** (τ=15 ps), whereas the other three compounds exhibited lifetimes of approximately 60 ps. Possibly, formation of hydrogen bonds plays an important role in the stabilization of the CS state. Another remarkable finding has been the strong differences in absorption intensity at 500 nm in ethanol. On the basis of the results of the global fitting procedure it could not be established whether or not the CS state was less effectively populated in cases where the 500 nm absorption was weak. It is possible that the λ_{max} of the CS excitation probed here is subject to solvatochromic influences and that this is the main reason for the observed differences in intensity at 500 nm.

6.4 References

1. B.I. Greene, Chem. Phys. Lett., **79**, 51-53 (1981).
2. P.F. Barbara, S.D. Rand and P.M. Rentzepis, J. Am. Chem. Soc., **103**, 2156-2162 (1981).
3. C.L. Schilling and E.F. Hilinski, J. Am. Chem. Soc., **110**, 2296-2298 (1988).
4. J. Ma and M.B. Zimmt, J. Am. Chem. Soc., **114**, 9723-9724 (1992).
5. J. Morais, J. Ma and M.B. Zimmt, J. Phys. Chem., **95**, 3885-3889 (1991).
6. W. Schuddeboom, S.A. Jonker, J.M. Warman, M.P. de Haas, M.J.W. Vermeulen, W.F. Jager, B. de Lange, B.L. Feringa and R.W. Fessenden, J. Am. Chem. Soc., **115**, 3286-3290 (1993).
7. Y-P. Sun and C.E. Bunker, J. Am. Chem. Soc., **116**, 2430-2433 (1994).
8. T. Tahara and H. Hamaguchi, Chem. Phys. Lett., **217**, 369-374 (1994).
9. J. Ma, G. Bhaskar Dutt, D.H. Waldeck and M.B. Zimmt, J. Am. Chem. Soc, **116**, 10619-10629 (1994).
10. E. Lenderink, K. Duppen and D.A. Wiersma, J. Phys. Chem., **99**, 8972-8977 (1995).
11. R.W.J. Zijlstra, P. Th. van Duijnen, B.L. Feringa, T. Steffen, K. Duppen and D.A. Wiersma, J. Phys. Chem. A, **101**, 9828-9836 (1997).
12. G.R. Fleming, *Chemical Applications of Ultrafast Spectroscopy*, Oxford University Press, New York, 1986.
13. S.H. Pine, *Organic Chemistry*, McGraw-Hill Book Company, New York, 1987.
14. R.C. Weast, M.J. Astle and W.H. Beyer, *Handbook of Chemistry and Physics*, CRC Press Inc., Boca Raton, Fl., USA, 1985-1986.
15. C.J. Bardeen, Q. Wang and C.V. Shank, Phys. Rev. Lett., **75**, 3410-3413 (1995).
16. Z. Rappoport and S.E. Biali, Acc. Chem. Res., **30**, 307-314 (1997).
17. M. Dantus, R.M. Bowman, M. Gruebele and A.H. Zewail, J. Chem. Phys., **91**, 7437-7450 (1989).
18. U. Banin, A. Waldman and S. Ruhman, J. Chem. Phys., **96**, 2417-2419 (1992).
19. U. Banin and S. Ruhman, J. Chem. Phys., **98**, 4391-4403 (1993).
20. Q. Wang, R.W. Schoenlein, L.A. Peteanu, R.A. Mathies and C.V. Shank, Science, **266**, 422-424 (1994).
21. N.J. Turro, *Modern Molecular Photochemistry*, The Benjamin/Cummings Publishing Company, Inc., Menlo Park, CA, 1978.
22. D.H. Waldeck, Chem. Rev., **91**, 415-436 (1991).
23. C.T. Lin, H.W. Guan, R.K. McCoy and C.W. Spangler, J. Phys. Chem., **93**, 39-43 (1989).
24. R.A. McGill, J.K. Rice, A.P. Baranovski, J.C. Owrutsky, A.H. Lowrey, K.K. Stavrev, T. Tamm and M.C. Zerner, Int. J. Quant. Chem. Symp., **30**, 383-394 (1996).
25. P. Th. van Duijnen, A.H. Juffer and H.P. Dijkman, J. Mol. Struct. (THEOCHEM), **260**, 195-205 (1992).

Samenvatting

Alkenen zijn koolwaterstoffen welke een koolstof-koolstof (C-C) dubbele binding bevatten. De aanwezigheid van deze dubbele binding zorgt ervoor dat alkenen een beperkte intramoleculaire beweeglijkheid hebben. De rotatie rond de dubbele binding kost namelijk zoveel energie dat de ruimtelijke structuur van alkenen bij kamertemperatuur grotendeels bevroren is in een vlakke vorm.

Dit beeld verandert echter als de dubbele binding onder invloed van licht met een geschikte golflengte tijdelijk wordt gereduceerd tot een enkele binding (foto-excitatie). Hierbij is het molecuul vanuit zijn grondtoestand naar een zogenaamde electronisch aangeslagen toestand gebracht, waarbij een electron uit de dubbele binding zich in een hogere electronische baan bevindt. In deze aangeslagen toestand is de energiebarrière voor de rotatie rond de koolstof-koolstof binding veel lager, en de vlakke vorm van het alkeen verandert razendsnel in een vorm waarbij de fragmenten van het alkeen die aan weerszijden van de C-C binding zitten onder een hoek van ongeveer 90° komen te staan, in plaats van de hoek van 0° in de oorspronkelijke vlakke geometrie.

Een eigenaardig fenomeen dat optreedt tijdens deze rotatie van 0° naar 90° is dat vlakbij het 90° punt twee electronisch aangeslagen toestanden elkaar 'tegenkomen'. Hierbij kunnen de twee electronen die eerder de dubbele binding vormden in principe 'kiezen' in welke van deze twee toestanden ze willen zitten. Deze keuze is echter niet willekeurig; in een symmetrisch molecuul zullen ze gelijkmatig over beide toestanden verdeeld worden, waarbij de totale ladingsverdeling van het molecuul dientengevolge ook symmetrisch blijft. Als de symmetrie van het moleuul echter op een of andere wijze verstoord wordt, verhuizen beide electronen broederlijk naar één zijde van het molecuul. Dit heeft als gevolg dat er zich aan één kant van het molecuul ineens veel meer electronen bevinden; de ladingsverdeling is 'plotseling gepolariseerd'. Dit fenomeen wordt ook wel ladingsscheiding genoemd, omdat de ene helft van het molecuul positief geladen is geraakt, terwijl de andere helft negatief geladen is.

Het onderzoek dat beschreven staat in dit proefschrift heeft zich bezig gehouden met dit soort ladingsscheiding in symmetrische alkenen, waarbij het zich heeft toegespitst op de vraag welke symmetrieverstoring verantwoordelijk gehouden moet worden voor het optreden van de ladingsscheiding. De motivatie voor dit onderzoek is tweeledig.

Ten eerste bestaat de mogelijkheid dat de ladingsscheiding een belangrijke rol speelt in vele foto-excitatie processen waarbij alkenen betrokken zijn, zoals het proces van het zien door mensen en andere zoogdieren. Dit proces begint doordat een foton in het oog wordt geabsorbeerd door het alkeen retinal dat een onderdeel van het oog-eiwit rhodopsine is. De eventuele ladingsscheiding in retinal kan een belangrijke rol spelen bij het doorgeven van het signaal aan de hersenen hetgeen uiteindelijk leidt tot het waarnemen van beelden.

Ten tweede bestaat er een zekere mate van controverse over de oorzaak van het optreden van ladingsscheiding in met name symmetrische alkenen. Eind jaren zeventig zijn er een aantal quantumchemische berekeningen verricht aan het kleinste basisalkeen etheen (C_2H_4). Deze berekeningen lieten zien dat een selectieve vervorming van één helft van het molecuul in de buurt van het 90° punt leidt tot een sterke ladingsscheiding in de aangeslagen toestand van etheen, waarbij deze vervormde toestand zelfs stabieler bleek te

zijn dan de onvervormde geometrie. Deze resultaten hebben ertoe geleid dat dergelijke intramoleculaire symmetrieverstoringen als de algemene drijvende kracht achter de ladingsscheiding worden beschouwd. Het is belangrijk om op te merken dat, indien dit inderdaad zo is, alkenen in hun aangeslagen toestand in de buurt van de 90˚ altijd een dergelijke ladingsscheiding moeten laten zien.

Experimenten waarbij de gedragingen van deze aangeslagen toestand van aanmerkelijk grotere alkenen, zoals tetraphenyletheen (TPE), in oplossing zijn geregistreerd, laten echter een ander beeld zien. Deze experimenten tonen aan dat de ladingsscheiding zeer sterk optreedt in polaire oplosmiddelen; dit zijn oplosmiddelen waarvan de moleculen zelf ook een enigszins gepolariseerde elektronenverdeling hebben. In apolaire, zeg maar ladingssymmetrische oplosmiddelen, lijkt het effect van de ladingsscheiding in de symmetrische alkenen veel minder sterk op te treden. Deze metingen suggereren dus dat het oplosmiddel een rol speelt in het induceren van ladingsscheiding in dit soort alkenen. Dit is in tegenspraak met de conclusie van de eerdergenoemde quantummechanische berekeningen aan etheen, waarbij voorspeld werd dat de ladingsscheiding altijd zal optreden omdat het een intramoleculair proces is waar het oplosmiddel in principe geen rol speelt.

Het doel van het in dit proefschrift beschreven onderzoek is geweest te ontdekken wat nu de werkelijke algemene drijvende kracht achter de ladingsscheiding in symmetrische alkenen is. Hierbij zijn verschillende quantumchemische rekenmethoden gebruikt, welke beschreven zijn in de hoofdstukken 2-4, en is er gebruik gemaakt van een ultrasnelle spectroscopische techniek (time resolved femtosecond pump-probe spectroscopy) om de gedragingen van een aantal symmetrische alkenen in verschillende oplosmiddelen te bestuderen. De resultaten hiervan staan beschreven in de hoofdstukken 5 en 6.

In hoofdstuk 2 is middels CASPT2 berekeningen (een bepaalde quantummechanische rekenmethode) een vergelijk gemaakt tussen de selectieve vervorming van etheen en het wat grotere tetramethyletheen (TME). Alhoewel de CASPT2 methode niet bij uitstek geschikt is voor het bestuderen van dergelijke ladingsscheidingsprocessen, werd bij gebrek aan alternatieven toch voor deze methode gekozen. Het bleek dat de resultaten van de eerdergenoemde quantummechanische studies aan etheen goed gereproduceerd konden worden; inderdaad leverde een selectieve vervorming in het geval van etheen een stabielere, ladingsgescheiden aangeslagen toestand in de buurt van de 90˚ op. Dit bleek echter niet het geval voor TME; de grotere methylgroepen bleken door de selectieve vervorming van TME zoveel hinder van elkaar te ondervinden dat de ladingsgescheiden toestand juist gedestabiliseerd werd. Deze resultaten suggereren dus dat voor grotere alkenen de symmetriebreking door intramoleculaire vervorming energetisch juist ongunstig is, waardoor dat proces zeker niet algemeen verantwoordelijk kan zijn voor het optreden van ladingsscheiding in symmetrische alkenen.

Met deze wetenschap is gepoogd middels quantumchemische berekeningen vast te stellen of oplosmiddelen in staat zijn om de symmetrie van de alkenen dusdanig te verstoren dat ladingsscheiding kan optreden. Hierbij is gebruik gemaakt van het Direct Reaction Field (DRF) model dat in Groningen is ontwikkeld in de groep van Van Duijnen.

In hoofdstuk 3 staat een exploratieve studie met dit model beschreven, waarbij de C-C binding van onvervormd etheen over een traject van 70-90˚ is gedraaid in een niet-symmetrische omgeving van puntladingen. Deze berekeningen laten zien dat een grote mate van ladingsscheiding optreedt in de buurt van de 90˚ (bij circa 81˚ is deze maximaal), maar dat in het geval van kleine puntladingen deze ladingsscheiding voorbij dit punt weer snel verdwijnt.

In hoofdstuk 4 is vervolgens een uitgebreidere DRF studie gedaan waarbij het onvervormde (symmetrische) etheen op de rotatiehoek van 81˚ is vastgezet en omringd is door een oplosmiddel bestaand uit 50 moleculen, waarbij ervoor gezorgd is dat het oplosmiddel in evenwicht is met een symmetrische ladingsverdeling op het etheen. Op deze wijze zijn 20 oplosmiddelconfiguraties gegenereerd, waarbij voor elke configuratie berekend is wat de door het oplosmiddel geïnduceerde ladingsscheiding in het etheen is. Deze procedure is herhaald voor een vijftal verschillende oplosmiddelen met uiteenlopende polariteit. De uitkomsten van deze studie bleken bijzonder interessant. Beide apolaire oplosmiddelen ethaan en tetrachloromethaan waren niet in staat tot het induceren van significante ladingsscheiding in het symmetrische etheen. Dit in tegenstelling tot het zwak polaire chloroform en het sterk polaire koolstofdioxide en aceton, welke alle drie een grote ladingsscheiding in de aangeslagen toestand van etheen teweeg brachten. Hierbij dient wel opgemerkt te worden dat de door chloroform geïnduceerde ladingsscheiding kleiner was dan die geïnduceerd door koolstofdioxide en aceton. Tevens wisten de polaire oplosmiddelen de ladingsgescheiden toestand significant te stabiliseren.

De in dit proefschrift gepresenteerde theoretische studies suggereren dus dat het waarschijnlijker is dat de symmetriebreking, die noodzakelijk is voor het ontstaan van de plotselinge polarisatie in de aangeslagen toestanden van symmetrische alkenen, wordt veroorzaakt door een (polair) oplosmiddel in plaats van door een intramoleculaire vervorming, hetgeen in tegenspraak is met eerdergenoemde theoretische bevindingen.

Om deze nieuwe inzichten te toetsen is een spectroscopisch experiment op femtoseconde (10^{-15} s) tijdschaal gedaan, waarbij het aangeslagen toestandsgedrag van TPE in een viertal oplosmiddelen is onderzocht. De bevindingen van deze studie staan beschreven in hoofdstuk 5. Deze studies laten zien dat in de eerste picoseconde de C-C binding aanmerkelijk langer wordt, zonder dat het oplosmiddel hier een dramatische invloed op heeft. Op langere tijdschalen blijkt er echter wel degelijk een invloed van het oplosmiddel te zijn; de aangeslagen toestand van TPE blijkt bij 500 nm een sterke absorptie in polaire alcoholen te hebben. In het apolaire cyclohexaan bleek deze absorptie echter veel zwakker. Deze absorptie is toegeschreven aan de ladingsgescheiden aangeslagen toestand van TPE. Tevens bleek, door de experimentele data aan een kinetisch model te 'fitten', dat er in het geval van cyclohexaan een evenwicht bestaat tussen twee toestanden in de buurt van het 90˚ punt van TPE, hetgeen lijkt te duiden op de aanwezigheid van beide electronische toestanden. Deze experimentele resultaten geven dientengevolge een bevestiging van de resultaten beschreven in hoofdstuk 2-4, waarbij een polair oplosmiddel als drijvende kracht achter de ladingsscheiding in symmetrische alkenen werd gesuggereerd.

Tot slot zijn met dezelfde experimentele techniek een aantal *para*-gefunctionaliseerde TPEs onderzocht. De resultaten van dit werk staan beschreven in hoofdstuk 6. Hierbij is gekeken of kleine functionele groepen, bevestigd aan het molecuul, de ladingscheiding zouden kunnen beïnvloeden, zonder dat deze groepen overigens de

symmetrie van het molecuul mogen verbreken. Het gedrag van een viertal verschillende alkenen is onderzocht in cyclohexaan en ethanol. Net als in het geval van ongefunctionaliseerd TPE bleek er in de eerste picoseconde vrijwel geen invloed van het oplosmiddel te zijn. Op langere tijdschalen gedroegen de vier alkenen zich in cyclohexaan hetzelfde als TPE, maar in ethanol, waarbij het oplosmiddel de ladingsgescheiden toestand goed kan vormen, ontstonden er grote verschillen. Niet alleen was de moleculaire mobiliteit sterk verschillend, maar ook de mate van ladingsscheiding vertoonde grote variatie tussen de onderzochte alkenen. Hiermee is aangetoond dat moleculaire modificaties inderdaad een dramatisch effect op het dynamisch gedrag en de mate van ladingsscheiding van dit soort alkenen kunnen hebben, alhoewel een duidelijk verband tussen de electronische aard van de aangebrachte functionele groepen en de mate van ladingsscheiding niet kon worden vastgesteld.

Summary

Alkenes are carbohydrates comprising a carbon-carbon (C-C) double bond. The presence of this double bond causes the majority of alkenes to only have limited intramolecular flexibility. For most alkenes, the rotation around the double bond requires large amounts of energy, causing their primary structure to be caught in a planar form at room temperature.

This picture changes drastically when the double bond is temporarily reduced to a single bond under the influence of light with an appropriate wavelength (photo-excitation). This lifts the molecule from its ground state to a so-called electronically excited state, in which an electron is migrated from the double bond to a higher electronic orbital. The alkene exhibits a much smaller rotation barrier for the aforementioned C-C bond in this excited state, and as a result the planar form of the alkene rapidly changes into a form in which the fragments on either side of the C-C bond approximately adopt a 90˚ (perpendicular) orientation with respect to each other, instead of the original 0˚ angle in the planar form.

A peculiar phenomenon that occurs during the twisting process from 0˚ to 90˚ is that near the 90˚ point two electronically excited states meet each other. In principle, the two electrons previously forming the double bond can choose which of the two states they want to occupy. This choice is not unrestricted, though. In a symmetrical molecule they will be equally devided over both states, thus maintaining the symmetry in the charge distribution of the molecule. However, if the symmetry of the molecule is somehow disturbed, both electrons migrate to one side of the molecule. This causes an excess of electrons on one side of the molecule, i.e. the molecule has become 'suddenly polarized'. This phenomenon is frequently referred to as charge separation as well, since one half of the molecule has become positively charged, whereas the other half has become negatively charged.

The work described in this thesis has focussed on the topic of this charge separation process in symmetrical alkenes, and in particular on what kind of symmetry breaking has to be held responsible for the occurrence of charge separation. The motivation for this investigation has been twofold.

In the first place, there is a distinct possibility that this charge separation plays an important role in many photo-excitation processes involving alkenes, like the process of vision in humans and other mammals. This process is initiated by the absorption of a photon by the alkene retinal, which forms an integral part of the eye protein rhodopsin. It is believed that the occurrence of charge separation in retinal may play an important role in the transfer of the electric signal to the brain that ultimately leads to vision.

In the second place, there exists some controversy about the actual cause of the existence of charge separation in symmetrical alkenes. At the end of the seventies a number of quantum chemical studies have been performed on the parent alkene ethylene (C_2H_4). These calculations showed that selective deformation of one half of the molecule in the vicinity of the 90˚ orientation leads to significant charge separation in the ethylene excited states. In fact, the ethylene proved to be more stable in its charge separated deformed geometry than in its nonpolarized symmetrical form. These findings have led to the belief that such intramolecular deformations are the general driving force behind the

occurrence of charge separation in alkenes. At this point, it is important to stipulate that, if this assumption is correct, the excited states of alkenes should always exhibit charge separation behaviour around the 90˚ orientation.

Experiments, in which the excited state behaviour of significantly larger alkenes like tetraphenylethylene (TPE) in solution has been investigated, show a different picture. These experiments demonstrate that charge separation strongly occurs in polar solvents, i.e. solvents that exhibit a polarized electron distribution themselves. In nonpolar solvents, i.e. solvents with a symmetrical charge distribution, the occurrence of charge separation is much less pronounced. Therefore, these measurements suggest that the solvent plays a role in the induction of charge separation in such alkenes. This is in disagreement with the outcome of the aforementioned quantum chemical calculations on ethylene, which suggested that charge separation will always take place because it is an energetically favourable intramolecular process in which the solvent plays no role.

It has been the goal of the study presented in this thesis to discover the true driving force behind the charge separation in symmetrical alkenes. This has been done by applying several quantum chemical computational methods, which have been described in the chapters 2-4. Furthermore, an ultrafast spectroscopical technique (time resolved femtosecond pump-probe spectroscopy) has been applied to study the excited state behaviour of a number of symmetrical akenes in various solvents. The outcome of these studies can be found in chapters 5 and 6.

In chapter 2, CASPT2 calculations (a particular quantum chemical computation method) have been applied to make a comparison between the selective deformation of ethylene and the somewhat larger tetramethylethylene (TME). Although the CASPT2 method is not the most suitable method to study such charge separation processes, it was still selected because more suitable alternative methods were unavailable. It was found that the results of the aforementioned quantum chemical studies on ethylene could be accurately reproduced; the selective deformation of ethylene indeed yielded a more stable, charge separated excited state in the vicinity of the 90˚ orientation. However, this was not the case for TME; the larger methyl groups proved to introduce such an increase in steric hindrance during selective deformation that it destabilized the charge separated excited states of interest on progressive deformation. These results strongly suggest that for larger alkenes the symmetry breaking by means of intramolecular deformation is an energetically unfavourable process, which implies that this process cannot be held solely responsible for the occurrence of charge separation in symmetrical alkenes.

Having established this, it has been attempted to establish by means of quantum chemical calculations whether solvents are capable to disturb the symmetry of the symmetrical alkenes to such an extent that charge separation can occur. For these studies, the Direct Reaction Field (DRF) Model, which has been developed in Groningen within the group of Van Duijnen, has been used.

In chapter 3 the outcome of an exploratory study using this model has been described. In this study, the C-C bond of undeformed ethylene has been rotated in a stepwise fashion over a range of 70-90˚ in several non-symmetrical surroundings existing of point charges with varying charges. These calculations show that charge separation strongly occurs in the vicinity of the 90˚ orientation with a maximum occurrence at approximately 81˚, but that in the case of small point charges the charge separation in ethylene quickly vanishes beyond this point.

In chapter 4, the findings of a more elaborate DRF study have been reported. In this study, the ethylene has been fixed at its 81˚ twist angle and has been surrounded by a solvent modeled by 50 molecules in such a way that the solvent is in equilibrium with a symmetrical charge distribution of the ethylene. This way, 20 different solvent configurations were generated, and for each configuration the induced charge separation in the ethylene excited states has been calculated. This procedure has been repeated for five different solvents with varying polarity. The findings of this study proved to be highly interesting. Both nonpolar solvents ethane and tetrachloromethane were unable to induce significant charge separation in the ethylene excited states. In contrast, the weakly polar chloroform as well as the strongly polar acetone and carbon dioxide induced large charge separations in the ethylene excited states. However, the charge separation was less pronounced in the case of chloroform than it was in the other two polar solvents. More importantly, all three polar solvents significantly stabilized the charge separated state.

The here presented theoretical studies strongly suggest that it is more likely that the symmetry breaking, which is a prerequisite for the occurrence of the sudden polarazation in the excited states of symmetrical alkenes, is provided by a (polar) solvent rather than an intramolecular deformation, which is in disagreement with aforementioned theoretical findings of the late seventies.

To investigate these new insights, a spectroscopic experiment at femtosecond (i.e.10^{-15} s) time scales has been performed, in which the excited state behaviour of TPE in four different solvents has been studied. The findings of this study can be found in chapter 5. These experiments show that during the first picosecond, the C-C bond is significantly elongated, and that this process is mainly solvent independent. At longer time scales, however, the solvent has a marked influence on the TPE excited state behaviour. Most interestingly, the TPE excited state exhibits a strong absorption at 500 nm in polar alcohols. This absorption is much weaker in the nonpolar cyclohexane. This particular absorption has been assigned to the charge separated state of TPE. In addition, by means of fitting the experimental data to a kinetic model, it has been demonstrated that in cyclohexane an equilibrium exists between two TPE excited states in the vicinity of the 90˚ orientation, which seems to suggest the occurrence of both aforementioned electronic states. Therefore, these experimental findings confirm the outcome of the theoretical studies presented in chapters 2-4, which suggested the solvent to be the driving force behind the occurrence of charge separation in symmetrical alkenes.

Finally, the same experimental technique has been used to study a number of *para*-functionalized TPEs. The outcome of these studies have been reported in chapter 6. In this work, the influence of small functional groups attached to the TPE backbone on the charge separation in the modified molecules is investigated, with the obvious restriction that the addition of these groups did not disturb the overall symmetry of the modified TPEs. The behaviour of four different functionalized TPEs has been studied in both ethanol and cyclohexane. Like in the case of unfunctionalized TPE, hardly any influence of the solvent was observed during the first picosecond. At longer time scales, all four functionalized TPEs showed similar behaviour to TPE in cyclohexane, but in ethanol, wherein the charge separated state can be effectively formed, large differences could be observed. Not only did the investigated functionalized TPEs exhibit large differences in molecular mobility, but the extent of the charge separation also showed large variations between the various compounds. These results prove that molecular modifications are

indeed capable of influencing the dynamic behaviour and the extent of charge separation of such alkenes, although a clearcut correlation between the electronic nature of the substituents and the extent of the charge separation could not be established.